Planetary Spectroscopy & Imaging.

Wesley A. Traub
Smithsonian Astrophysical Observatory

- Introduction.
- Gas giant planets.
- Terrestrial planets:
  - Earth, present;
  - Earth, neoproterozoic;
  - Venus; Mars.
- Terrestrial Planet Finder (TPF, Darwin).
- Terrestrial Planet Imager (TPI).

Exo-planet detection & measurement methods.

1. radial velocity (Latham, Mayor, Marcy + Butler, Noyes, ...)
2. astrometry (SIM, FAME, ...)
3. occultation (Charbonneau, KEPLER, ...)
4. pulsar timing (Taylor, ...)
5. visible-infrared shift (ground-based interferometry, Keck,
6. reflected light
7. transmitted light (Sasselov, ...)
8. auroral emission (Marina Galand, ...)
9. radio emission (Bastien, ...)
10. laser transmission (Horowitz, Townes, ...)
11. gravitational lensing
12. disk: inner hole, annuli, warp, thickness, wakes, asymmetry (Burrows, Dermott, ...)
13. HST or NGST imaging (R. Brown, Trauger, ...)
14. TPF or DARWIN imaging (Angel, Leger, ...)

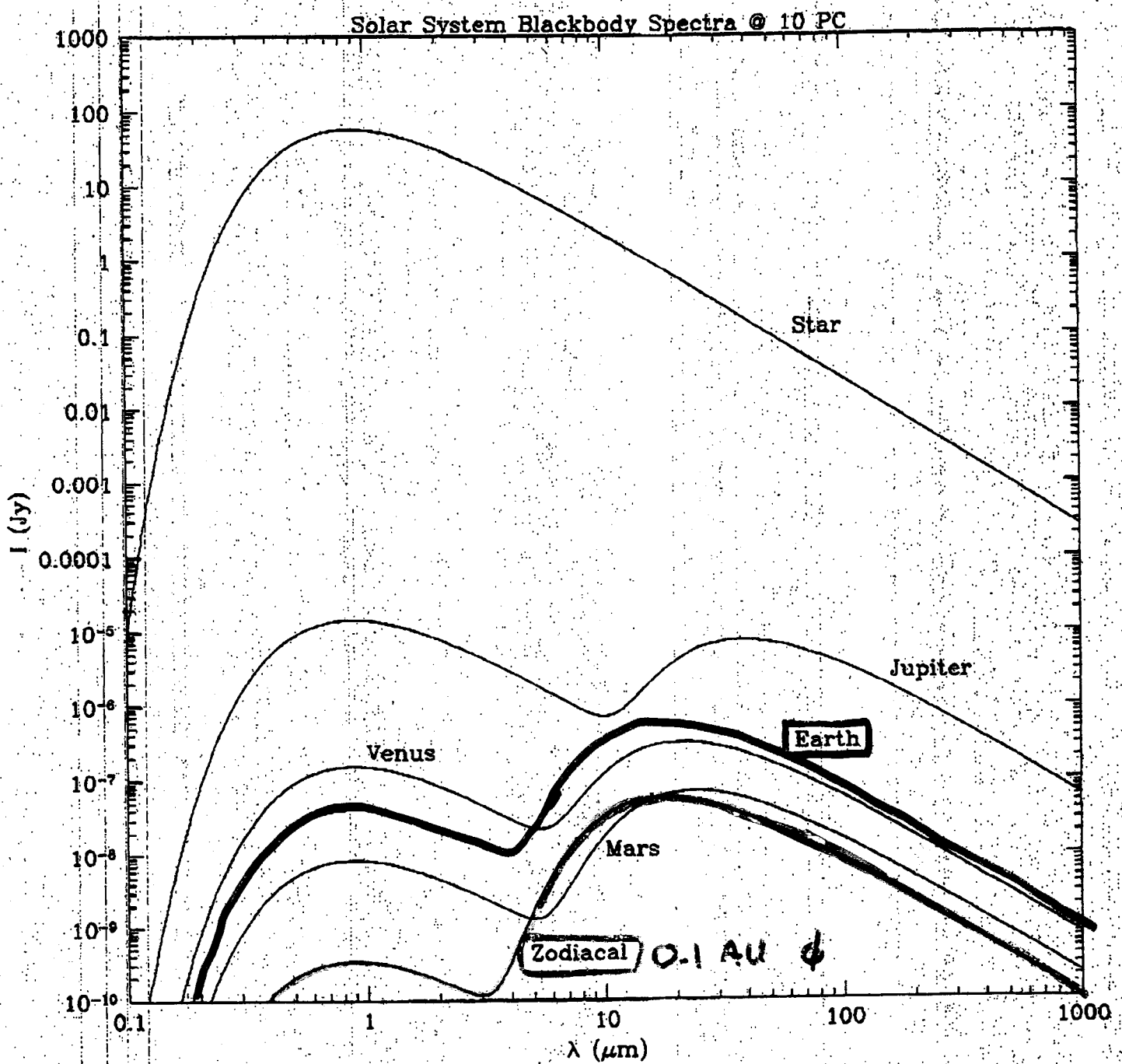
Solar System Blackbody Spectra @ 10 PC
1000
100
10
1
0.1
0.01
0.001
0.0001
10^{-5}
10^{-6}
10^{-7}
10^{-8}
10^{-9}
10^{-10}
I (Jy)
0.1
1
10
100
1000
λ (μm)
Star
Jupiter
Earth
Venus
Mars
Zodiacal
0.1 AU

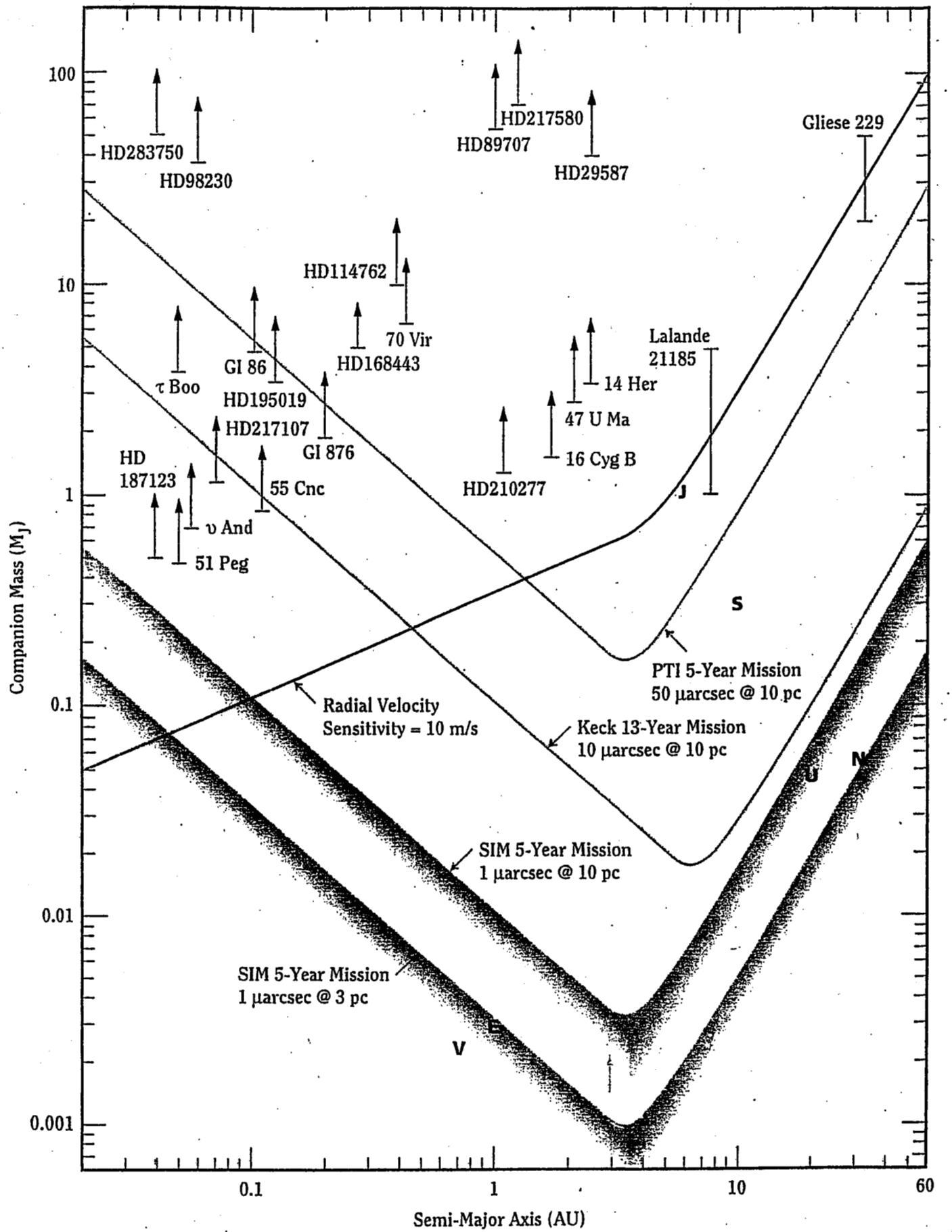
Companion Mass (M_J)
Semi-Major Axis (AU)
100
10
1
0.1
0.01
0.001
0.1
1
10
60
HD283750
HD98230
HD89707
HD217580
HD29587
Gliese 229
HD114762
70 Vir
HD168443
τ Boo
GI 86
HD195019
HD217107
GI 876
55 Cnc
HD 187123
υ And
51 Peg
HD210277
47 U Ma
16 Cyg B
14 Her
Lalande 21185
J
S
U
N
V
E
PTI 5-Year Mission
50 μarcsec @ 10 pc
Radial Velocity
Sensitivity = 10 m/s
Keck 13-Year Mission
10 μarcsec @ 10 pc
SIM 5-Year Mission
1 μarcsec @ 10 pc
SIM 5-Year Mission
1 μarcsec @ 3 pc

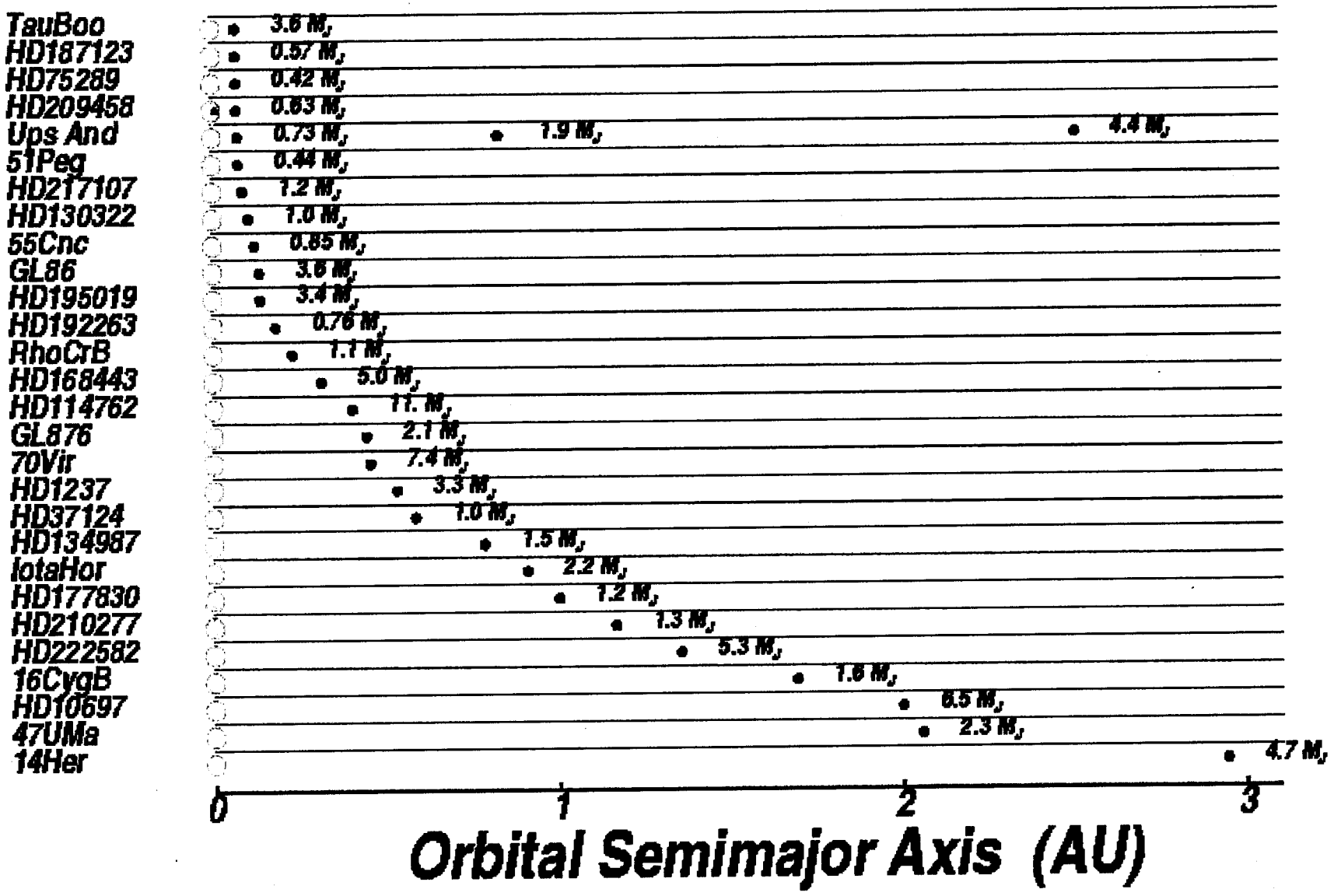
TauBoo
HD187123
HD75289
HD209458
Ups And
51Peg
HD217107
HD130322
55Cnc
GL86
HD195019
HD192263
RhoCrB
HD168443
HD114762
GL876
70Vir
HD1237
HD37124
HD134987
IotaHor
HD177830
HD210277
HD222582
16CygB
HD10697
47UMa
14Her
3.6 M,
0.57 M,
0.42 M,
0.63 M,
0.73 M,
1.9 M,
4.4 M,
0.44 M,
1.2 M,
1.0 M,
0.85 M,
3.6 M,
3.4 M,
0.76 M,
1.1 M,
5.0 M,
11. M,
2.1 M,
7.4 M,
3.3 M,
1.0 M,
1.5 M,
2.2 M,
1.2 M,
1.3 M,
5.3 M,
1.6 M,
6.5 M,
2.3 M,
4.7 M,
0
1
2
3
Orbital Semimajor Axis (AU)

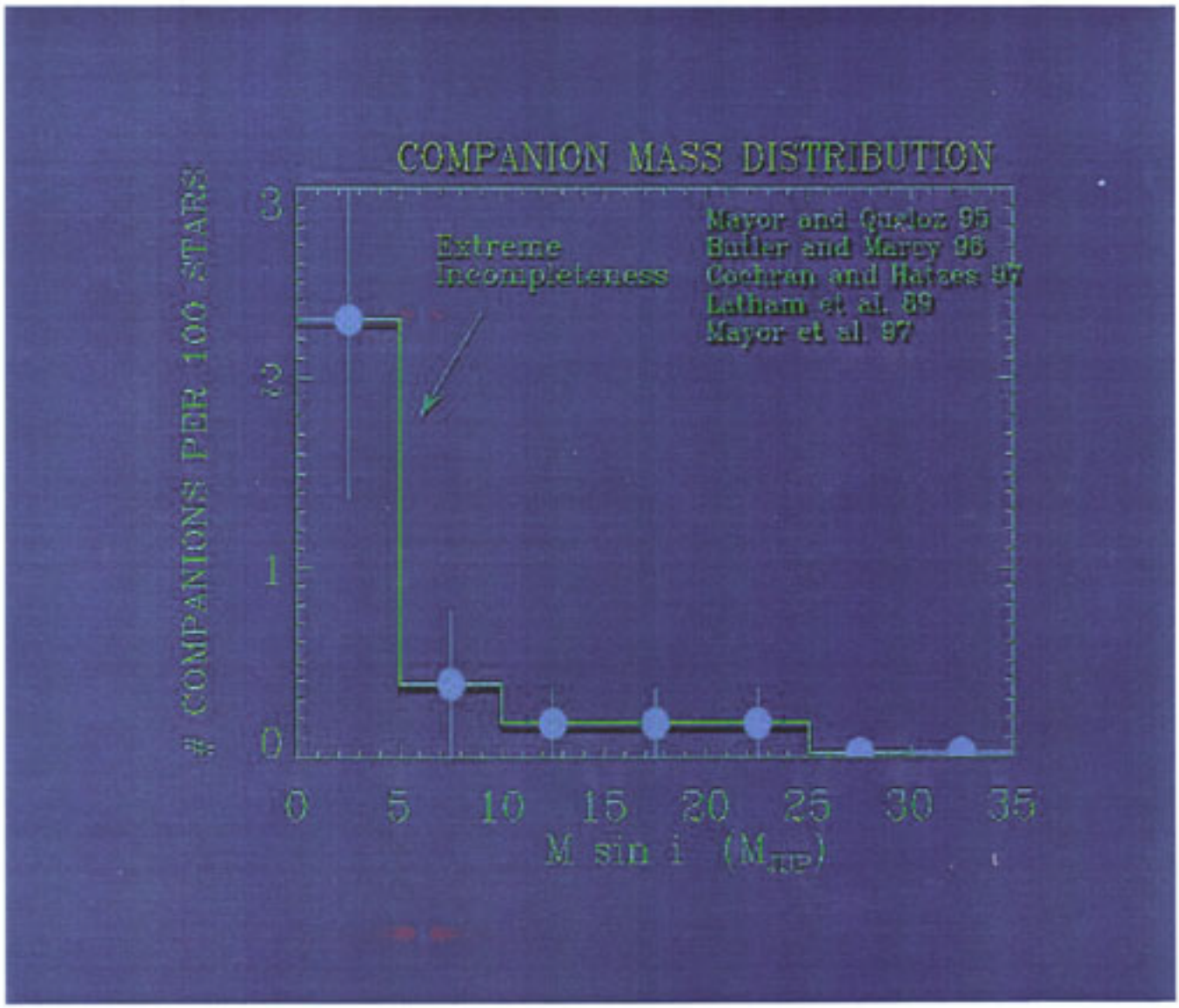
COMPANION MASS DISTRIBUTION
COMPANIONS PER 100 STARS
Extreme
Incompleteness
Mayor and Queloz 95
Butler and Marcy 96
Cochran and Hatzes 97
Latham et al. 89
Mayor et al. 97
0
1
2
3
0
5
10
15
20
25
30
35
M sin i (M_JUP)

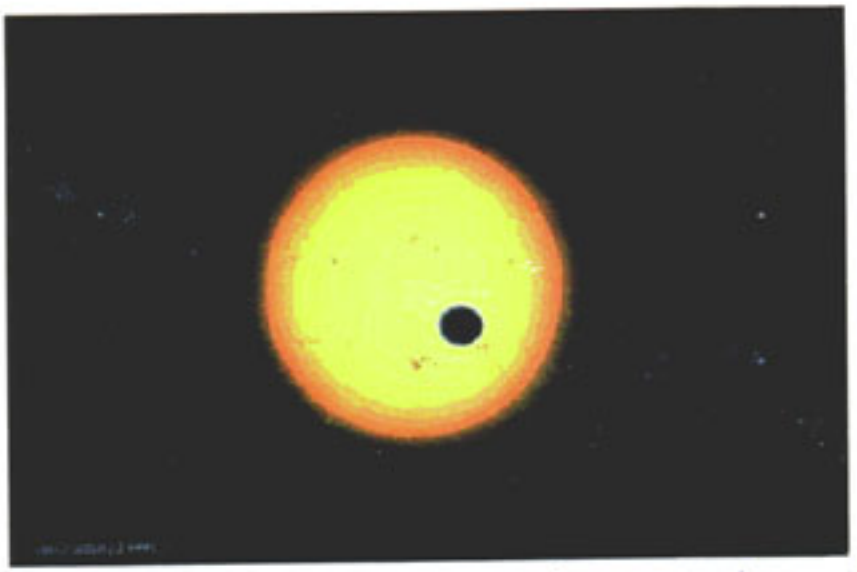

HD 209458 transit 9/99

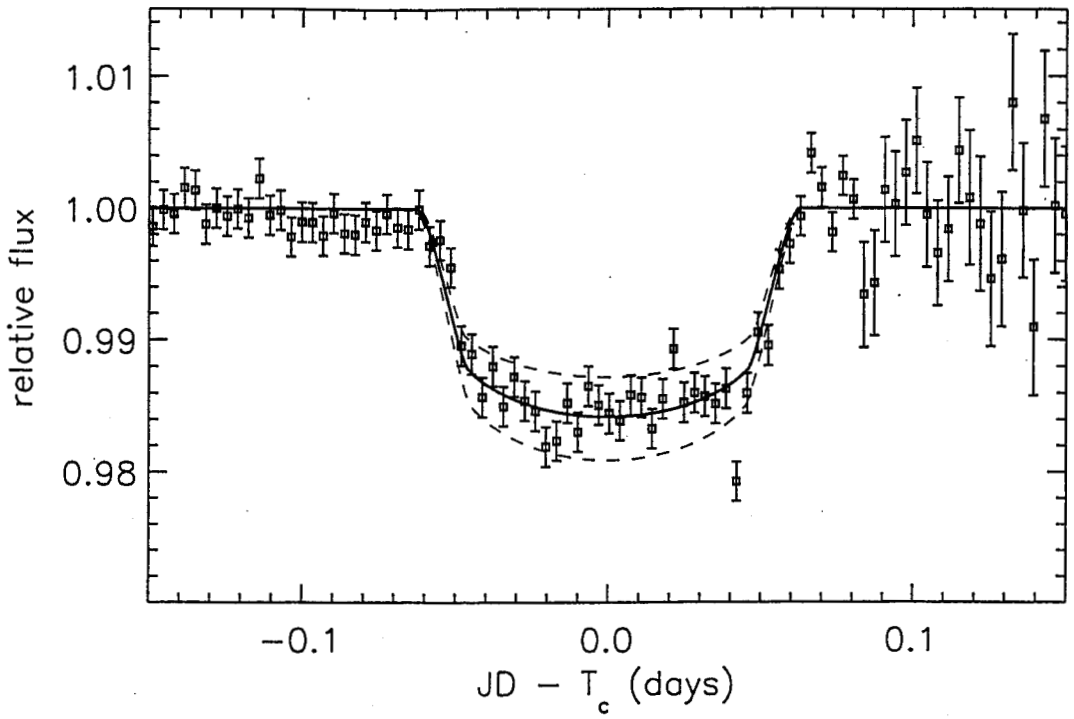

Fig. 2.— Shown are the data from figure 1 binned into 5 m averages, phased according to our best-fit orbit, plotted as a function of time from T_c. The RMS variation at the beginning of the time series is roughly 1.5 mmag, and this precision is maintained throughout the duration of the transit. The increased scatter at the end of the timeseries is due to increasing airmass which occured at roughly the same time for both transits, since the two occured very nearly one week apart. The solid line is the transit shape that would occur for our best fit model, $R_p = 1.27\ R_{\rm Jup}$, $i = 87.1°$. The lower and upper dashed lines are the transit curves that would occur for a planet 10% larger and smaller in radius, respectively. The rapid initial fall and final rise of the transit curve correspond to the times between first and second, and between third and fourth contacts, when the planet is crossing the edge of the star; the resulting slope is a function of the finite size of the planet, the impact parameter of the transit, and the limb darkening of the star. The central curved portion of the transit is the time between second and third contacts, when the planet is entirely in front of the star.

D. Charbonneau et al., 1999.

HST STIS Photometry of HD209458

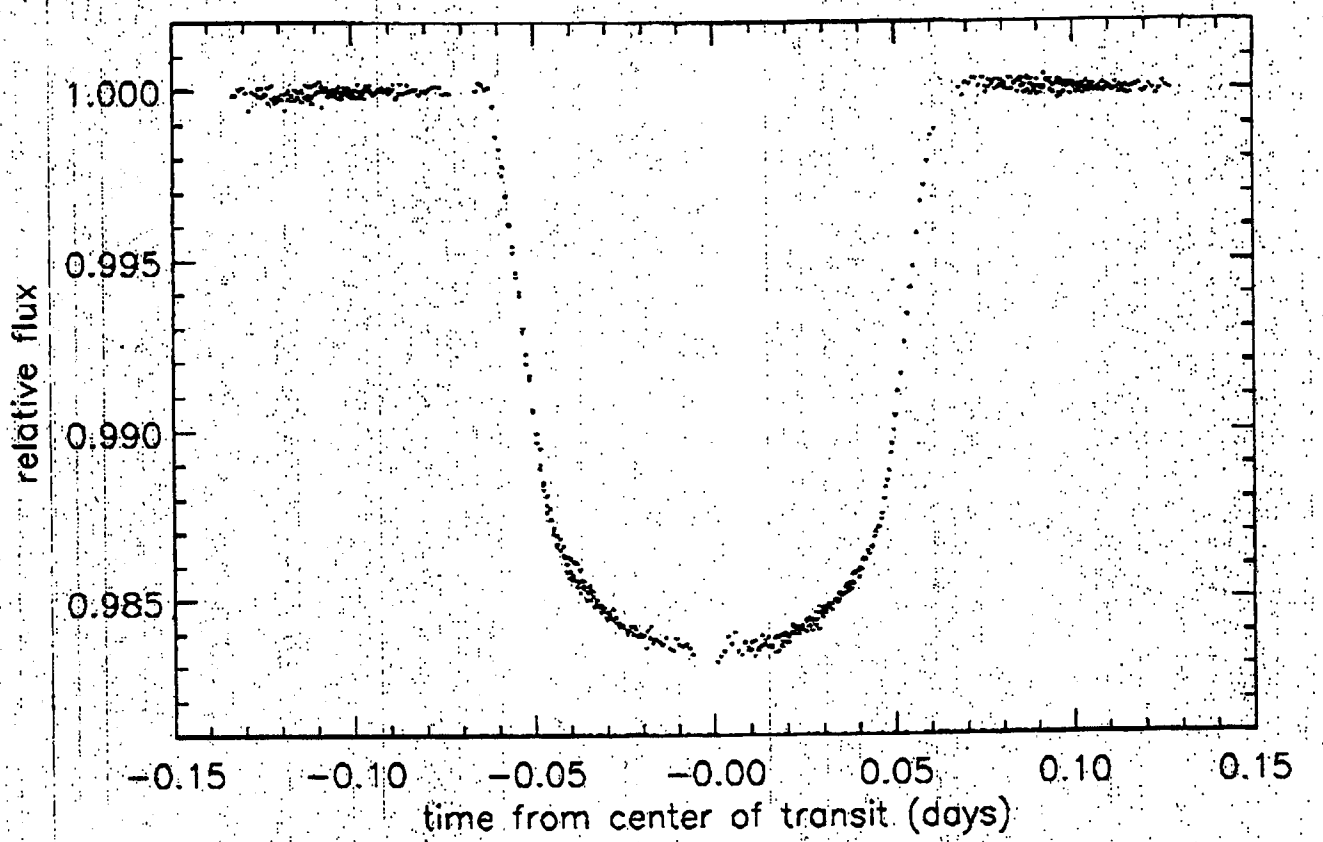

D. Charbonneau, T. M. Brown, R. L. Gilliland,
R. W. Noyes, & A. Burrows (2000)

Radiative transfer.

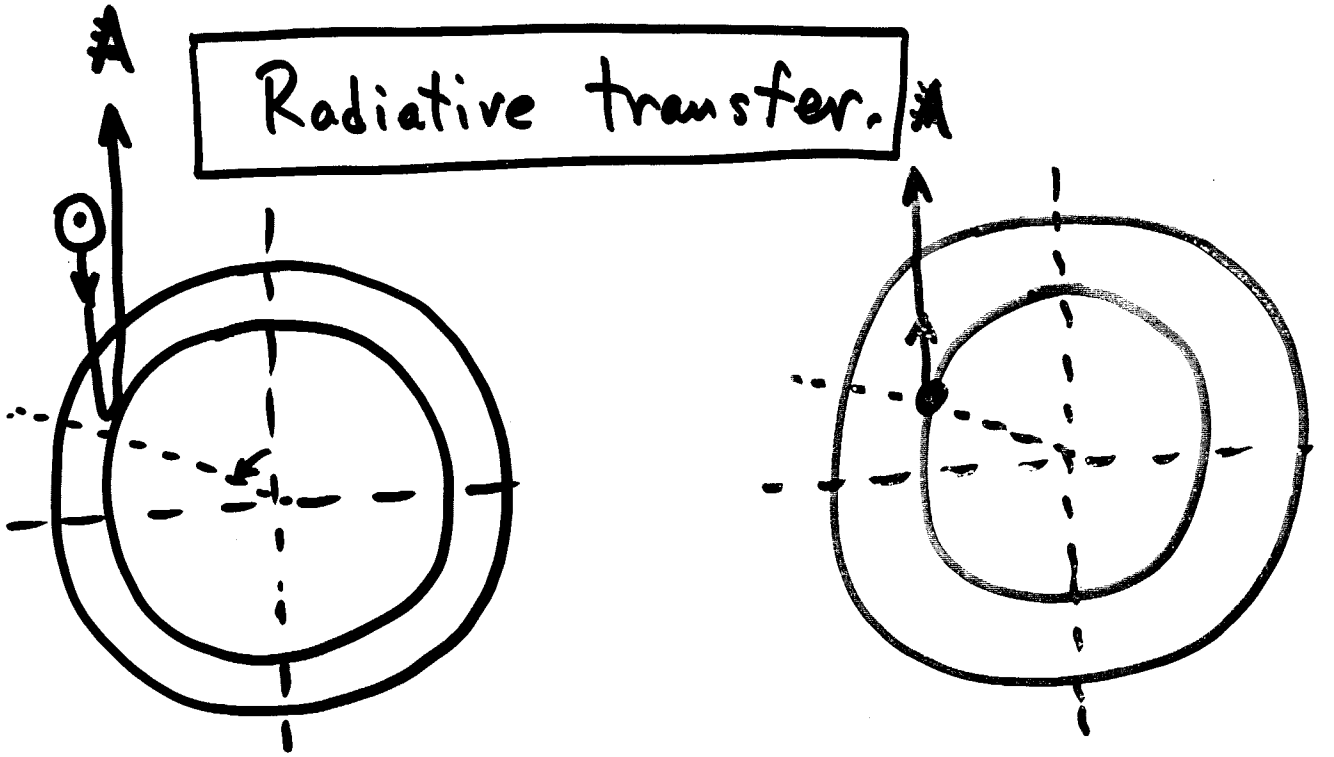

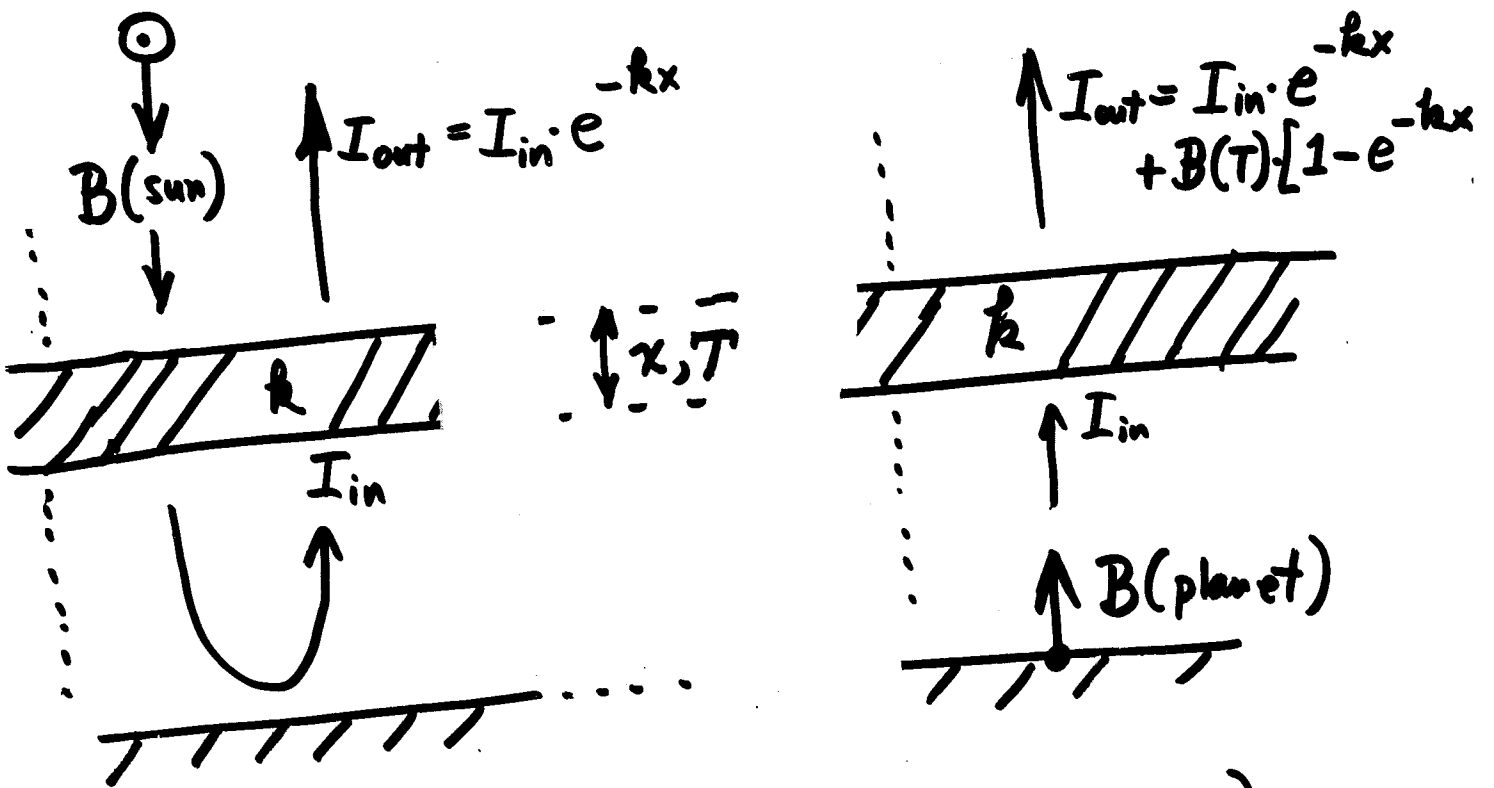

$$k = \sum \left(\begin{array}{c} \text{spectral line profiles} \\ \text{\& continuum} \end{array} \right)$$

MV, $Z_\odot$

Evolution of luminosity with time for different masses

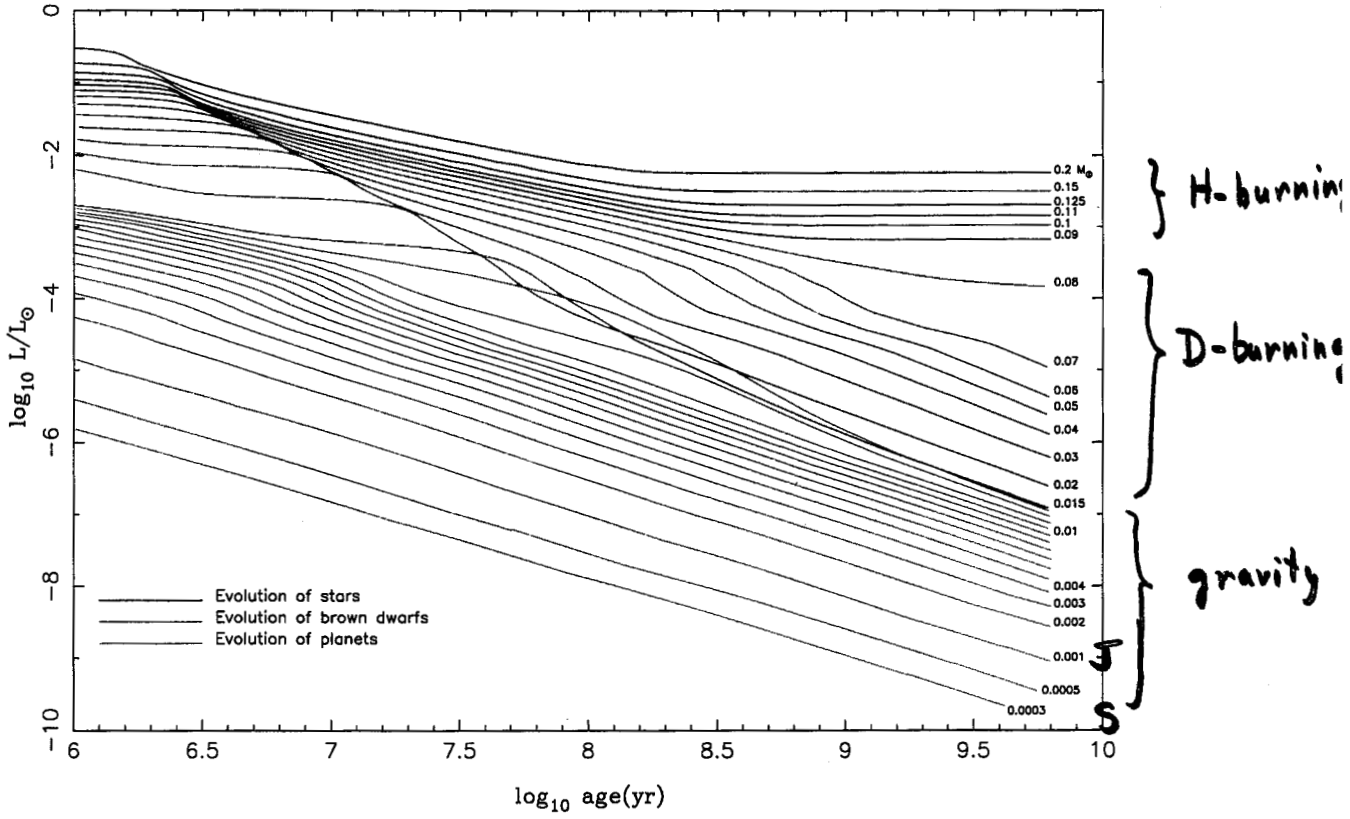

A. Burrows et al. 1997

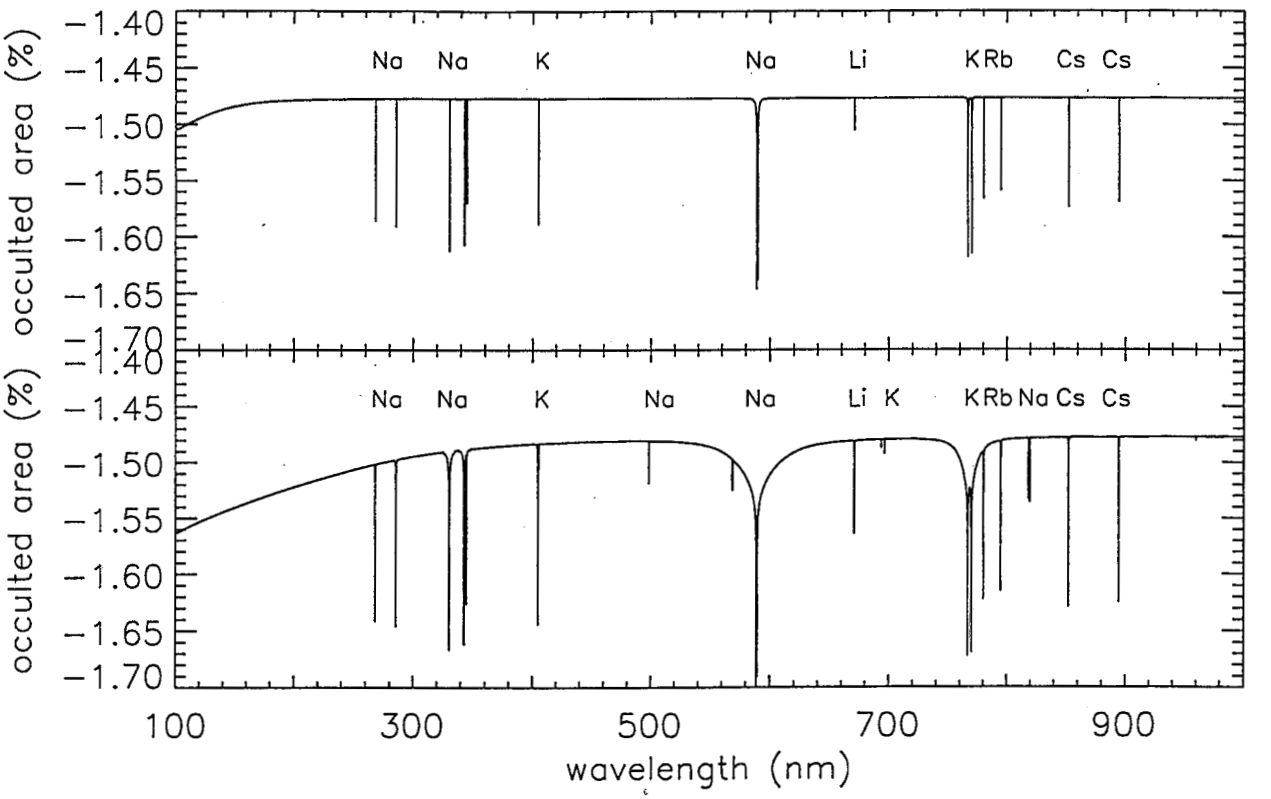

Fig. 2.— Upper plot: the normalized in-transit minus out-of-transit spectra, i.e. percent occulted area of the star. In this model the cloud base is at 2.4×10^{-3} bar. Rayleigh scattering is important in the UV. Lower plot: a model with cloud base at 0.2 bar. The stellar flux passes through higher pressures, densities, and temperatures of the planet atmosphere compared to the model in the upper plot. In addition, a larger transparent atmosphere makes the line depth larger. Observations will constrain the cloud depth. See text for discussion.

S. Seager & D. Sasselov, 2000.

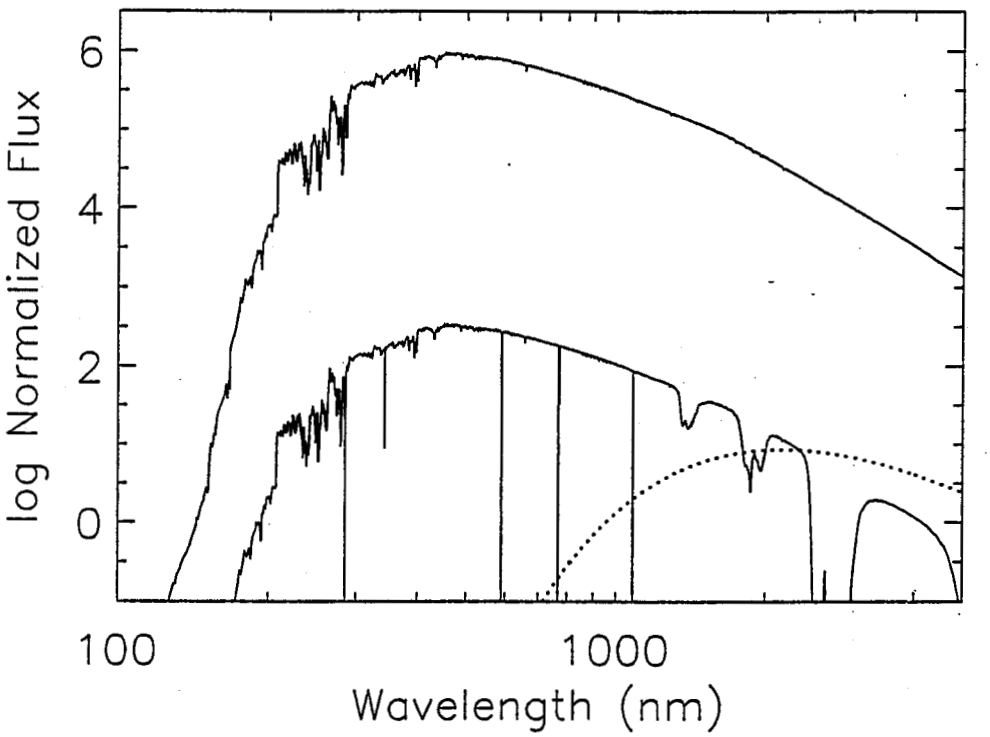

Fig. 1.— The flux of HD 209458 (upper curve) and the transmitted flux through the planet's transparent atmosphere (lower curve). Superimposed on the transmitted flux are the planetary absorption features: Na I resonance lines at 285.4 nm, 342.8 nm, and the doublet at 589.4 nm, the K I resonance doublet at 767.0 nm, and the He I triplet line at 1083 nm. The H_2O and CH_4 molecular absorption dominates in the infrared. The dotted line is a blackbody of 1350 K representative of the CEGP's thermal emission, but the thermal emission can be larger than a blackbody blueward of 2000 nm.

S. Seager & D.D. Sasselov
astro-ph/9912241
13 Dec 1999

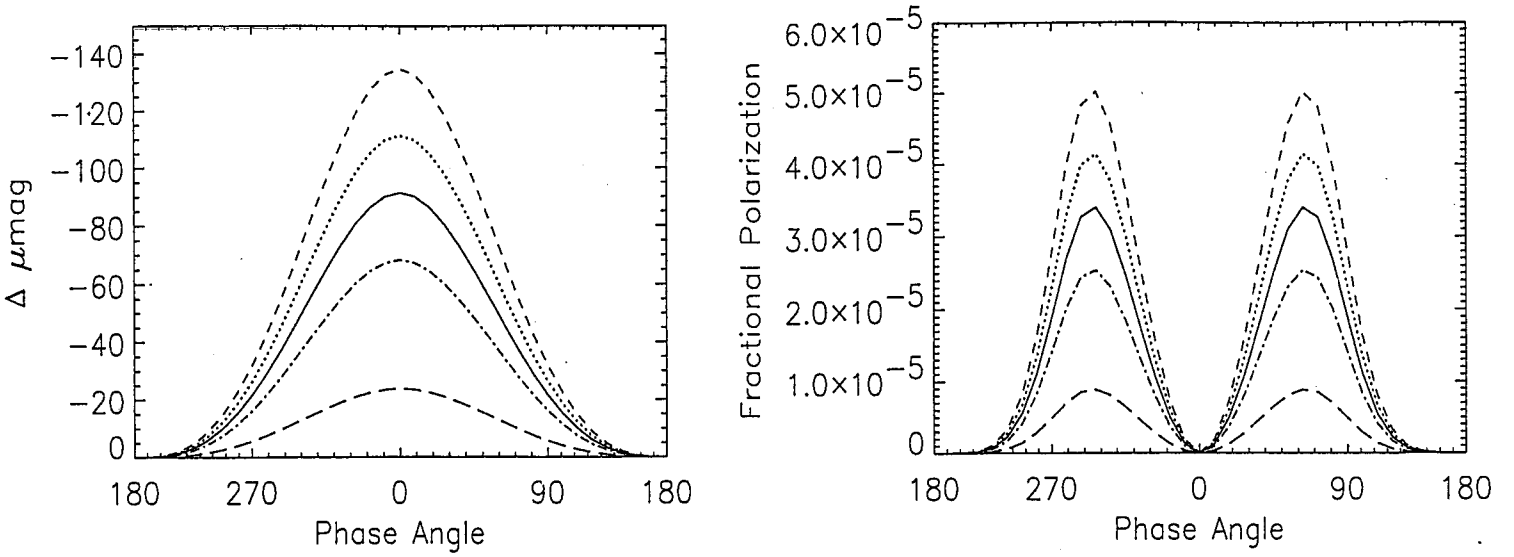

Fig. 1.— Lambert sphere light curves and polarization curves for CEGP systems with different D and $R_P = 1.2R_J$. In descending order the curves are for $D = 0.042$ AU (HD 187123 b), $D = 0.0462$ AU (τ Boo b), $D = 0.051$ AU (51 Peg b), $D = 0.059$ AU (υ And b), and $D = 0.11$ AU (55 Cnc b). For other R_P the curves can be scaled — the light curves approximately and the polarization curves exactly — by the factor $(R_P/1.2R_J)^2$. $\Delta m = 2.5$ μmag corresponds approximatley to a flux ratio of 10^{-6} (see equation (4)).

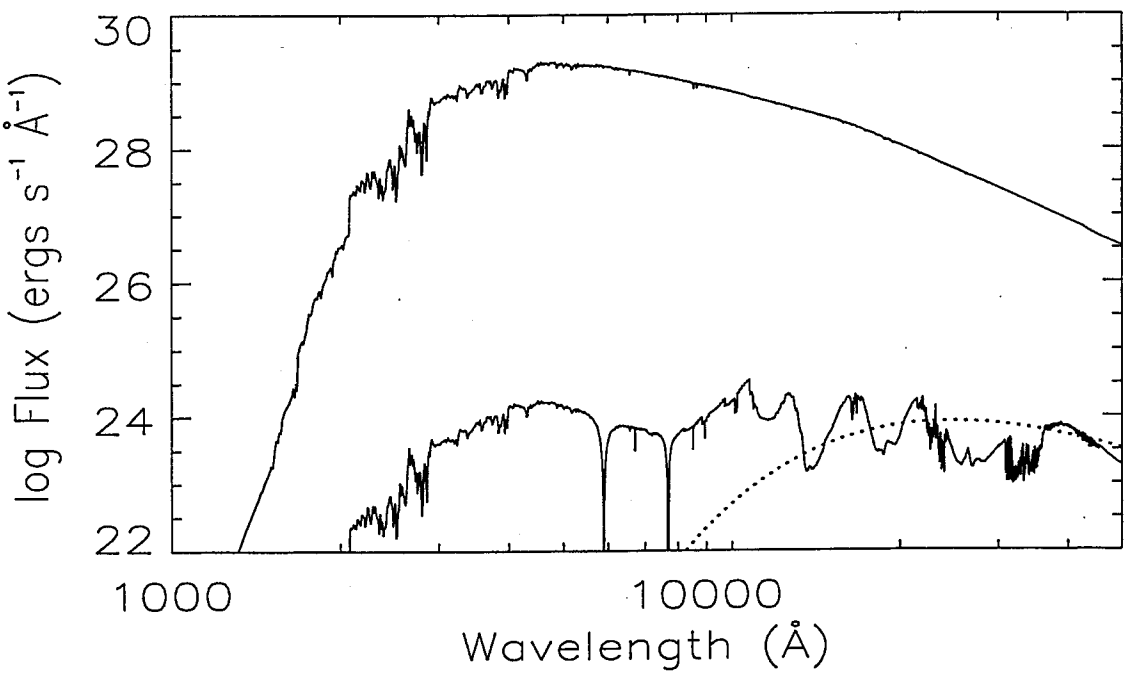

Fig. 2.— Flux of 51 Peg A and b. The upper curve is the model flux of 51 Peg A at the surface of the star, and the lower curve is the model flux of 51 Peg b with a homogenous $MgSiO_3$ cloud with particles of $\bar{r} = 0.01$ μm. The dotted line is a blackbody with the same $T_{\rm eff}$ as the planet model, 1170 K. In 51 Peg b, the features in the blue and UV (< 5000 Å) are reflected stellar features, the absorption features between 5000 Å and 1 μm are alkali metal lines from the planetary atmosphere, and the absorption features > 1 μm are water and methane absorption bands.

S. Seager et al. 2000

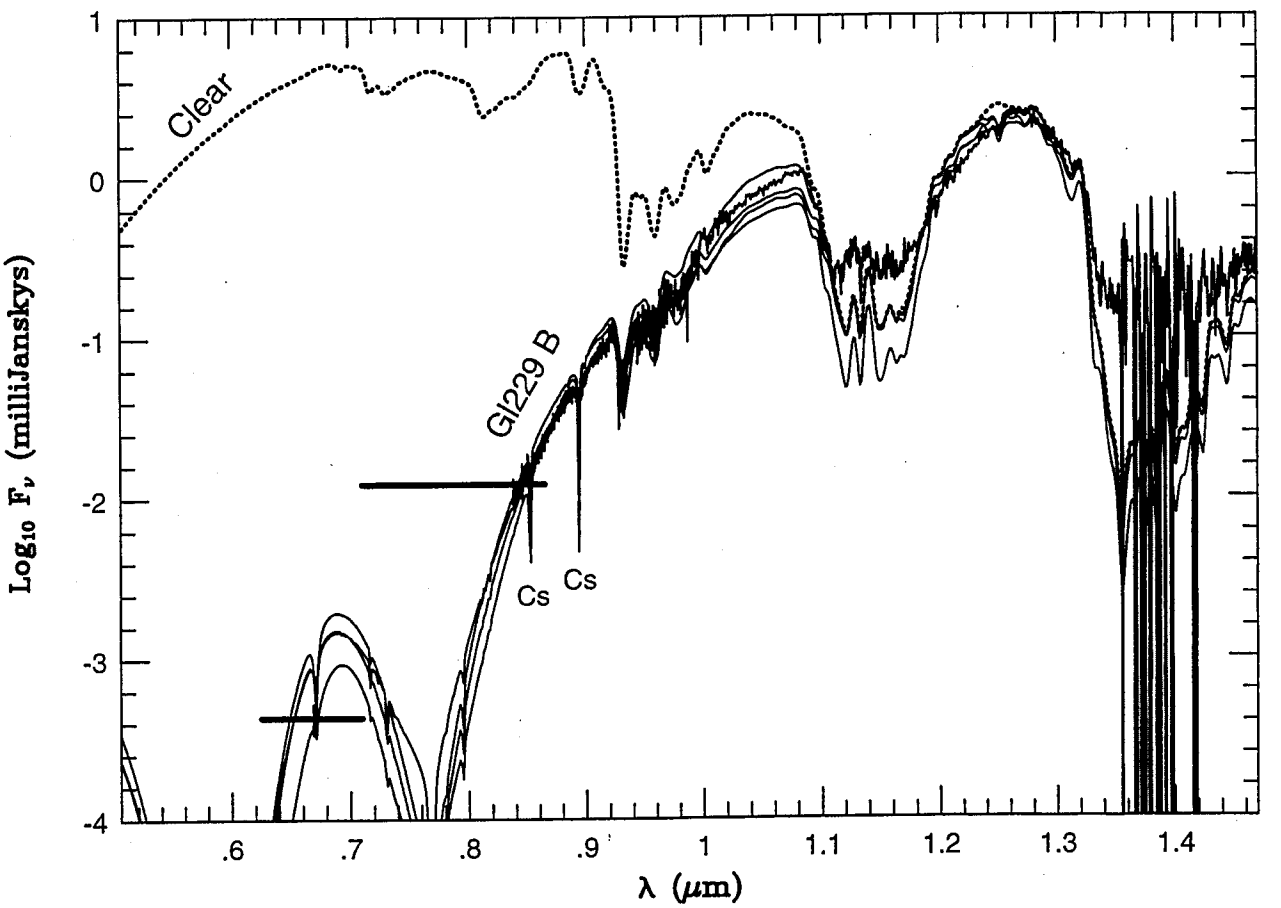

FIG. 1.— The log of the absolute flux (F_ν) in milliJanskys versus wavelength (λ) in microns from 0.5 μm to 1.45 μm for Gliese 229 B, according to Leggett *et al.* (1999) (heavy solid), and for four theoretical models (light solid) described in the text. Also included is a model, denoted "Clear" (dotted), without alkali metals and without any ad hoc absorber due to grains or haze. The horizontal bars near 0.7 μm and 0.8 μm denote the WFPC2 R and I band measurements of Golimowski *et al.* (1998).

A. Burrows et al. 2000.

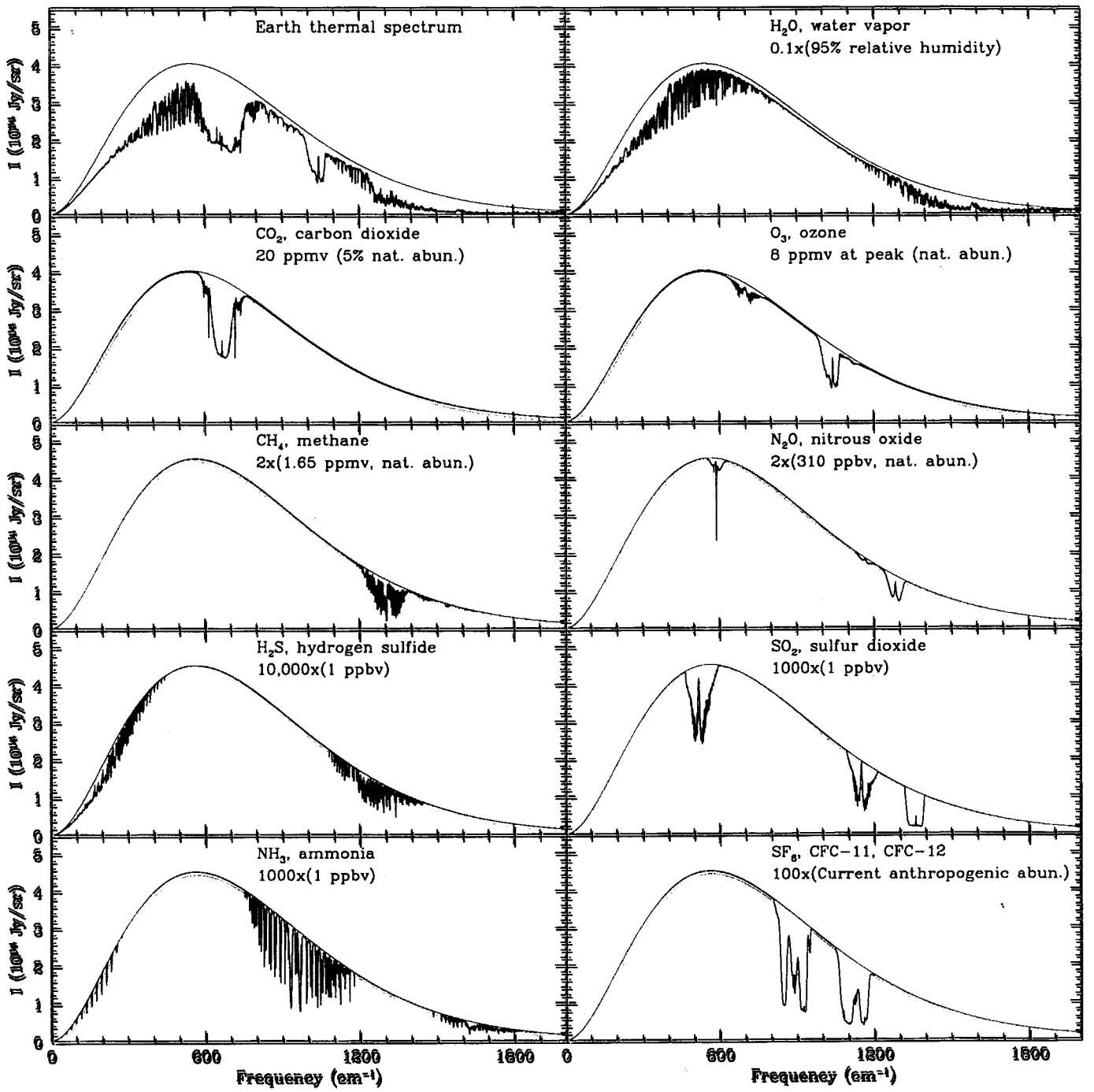
Earth thermal spectrum
H_2O, water vapor
0.1x(95% relative humidity)
CO_2, carbon dioxide
20 ppmv (5% nat. abun.)
O_3, ozone
8 ppmv at peak (nat. abun.)
CH_4, methane
2x(1.65 ppmv, nat. abun.)
N_2O, nitrous oxide
2x(310 ppbv, nat. abun.)
H_2S, hydrogen sulfide
10,000x(1 ppbv)
SO_2, sulfur dioxide
1000x(1 ppbv)
NH_3, ammonia
1000x(1 ppbv)
SF_6, CFC-11, CFC-12
100x(Current anthropogenic abun.)
I (10^{14} Jy/sr)
0
1
2
3
4
5
0
600
1200
1800
Frequency (cm^{-1})

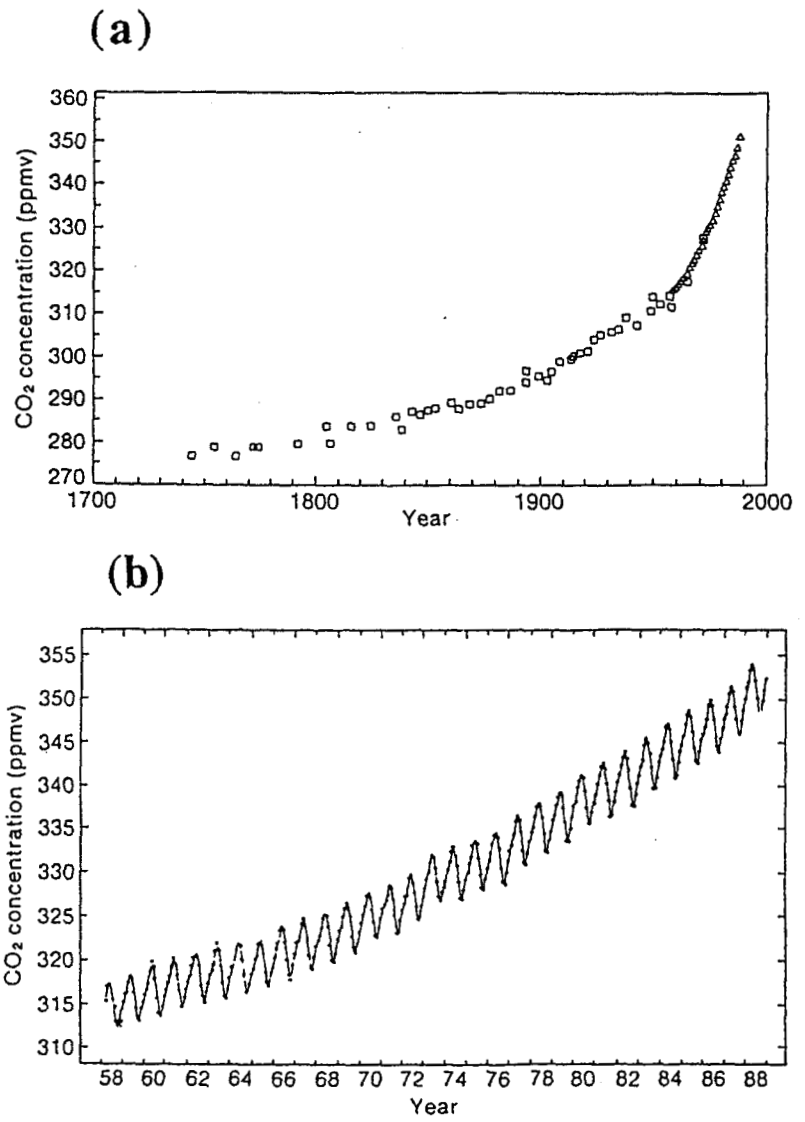

Figure 10.7 CO_2 concentrations for the past 250 years. (a) The early data are from air trapped in ice in Antarctica. The recent data data are from Mauna Loa, Hawaii, taken by Keeling et al. (1989). (b) Recent data (monthly mean) from Mauna Loa. After J. T. Houghton et al., 1991, editor, Intergovernmental Panel on Climate Change, 1990, *Climate Change: the IPCC Scientific Assessment*, and 1992, *Climate Change 1992: Supplement to the IPCC Scientific Assessment* (Cambridge: Cambridge University Press).

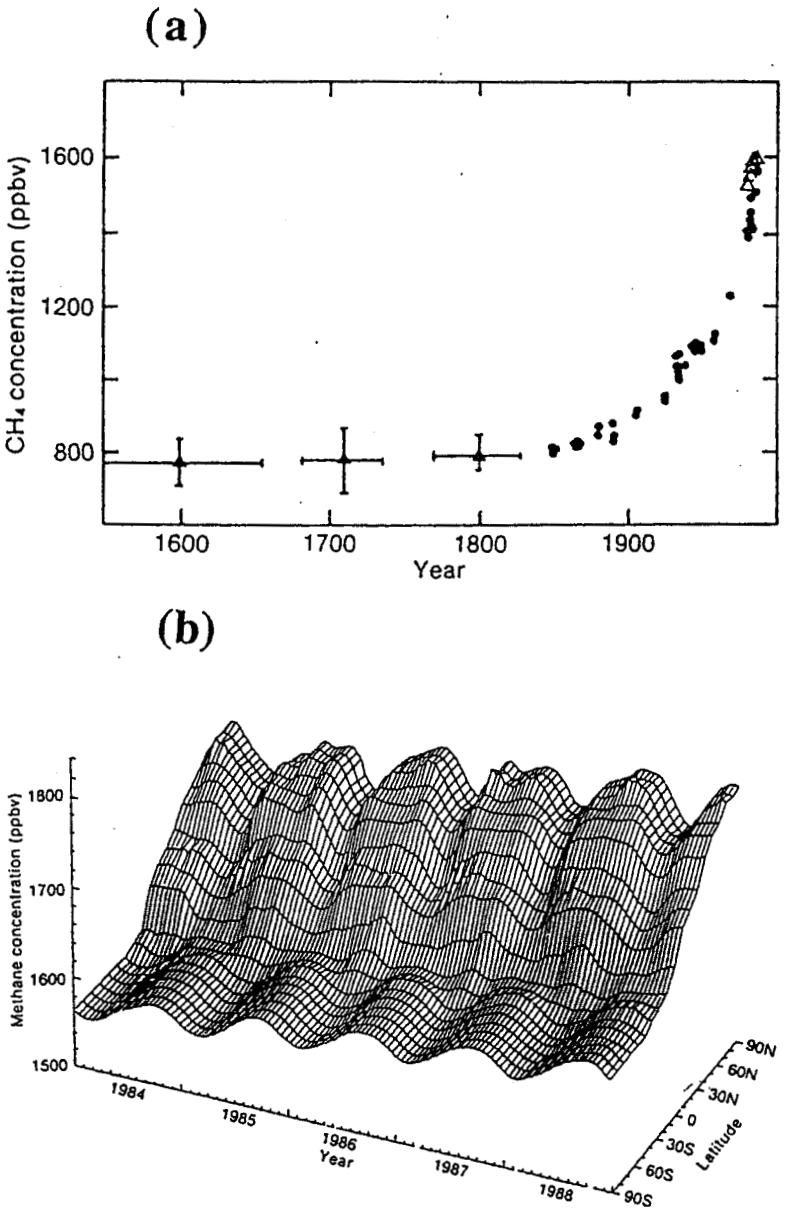

Figure 10.9 CH_4 concentrations in the atmosphere. (a) Variations in the past centuries from air trapped in ice, (b) Global distribution of atmospheric CH_4 and recent trend. After J. T. Houghton et al., 1991, editor, Intergovernmental Panel on Climate Change, 1990, *Climate Change: the IPCC Scientific Assessment*, and 1992, *Climate Change 1992: Supplement to the IPCC Scientific Assessment* (Cambridge: Cambridge University Press).

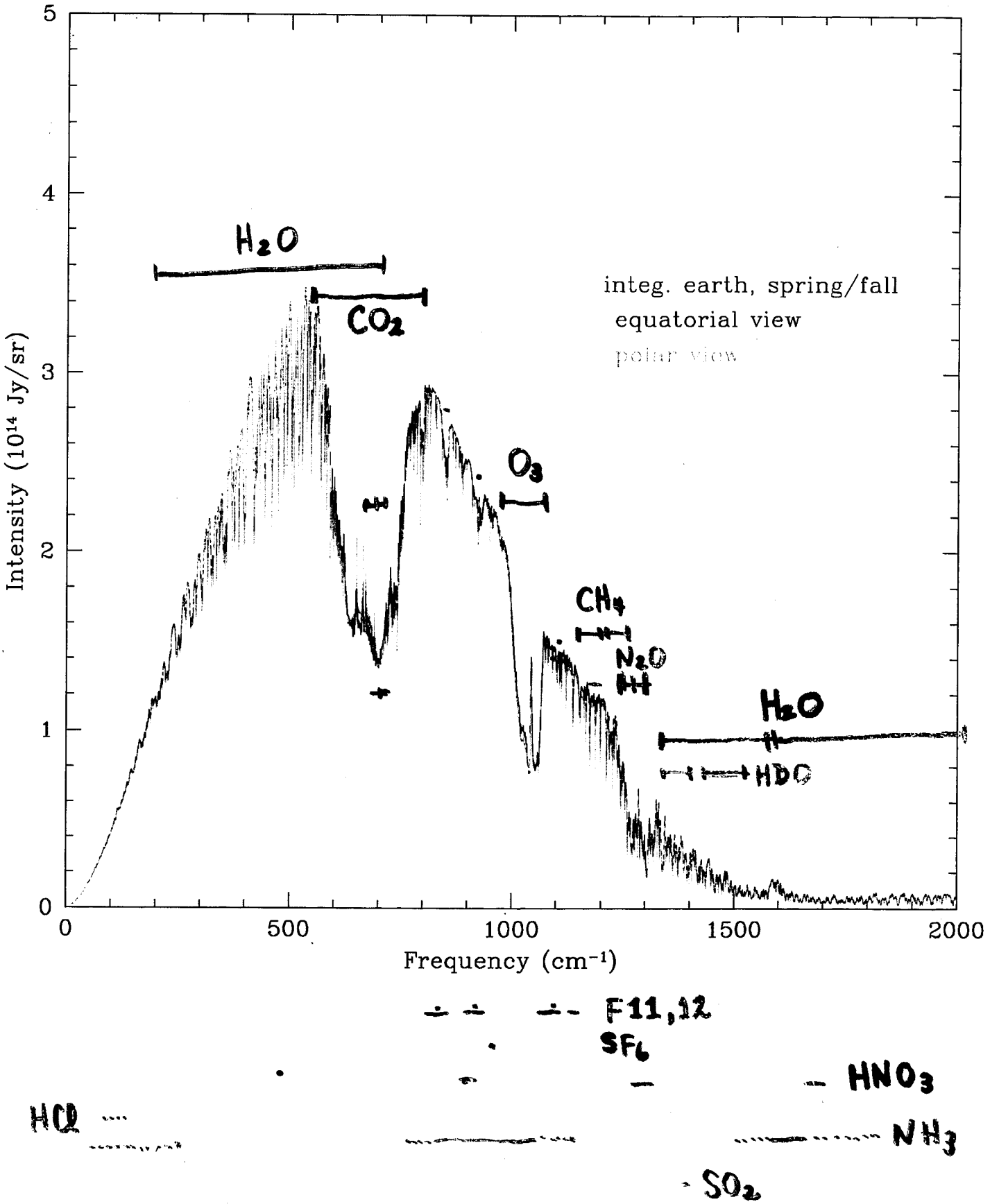
Intensity (10^{14} Jy/sr)
Frequency (cm^{-1})
integ. earth, spring/fall
equatorial view
polar view
H_2O
CO_2
O_3
CH_4
N_2O
H_2O
HDO
F11,12
SF_6
HNO_3
HCl
NH_3
SO_2

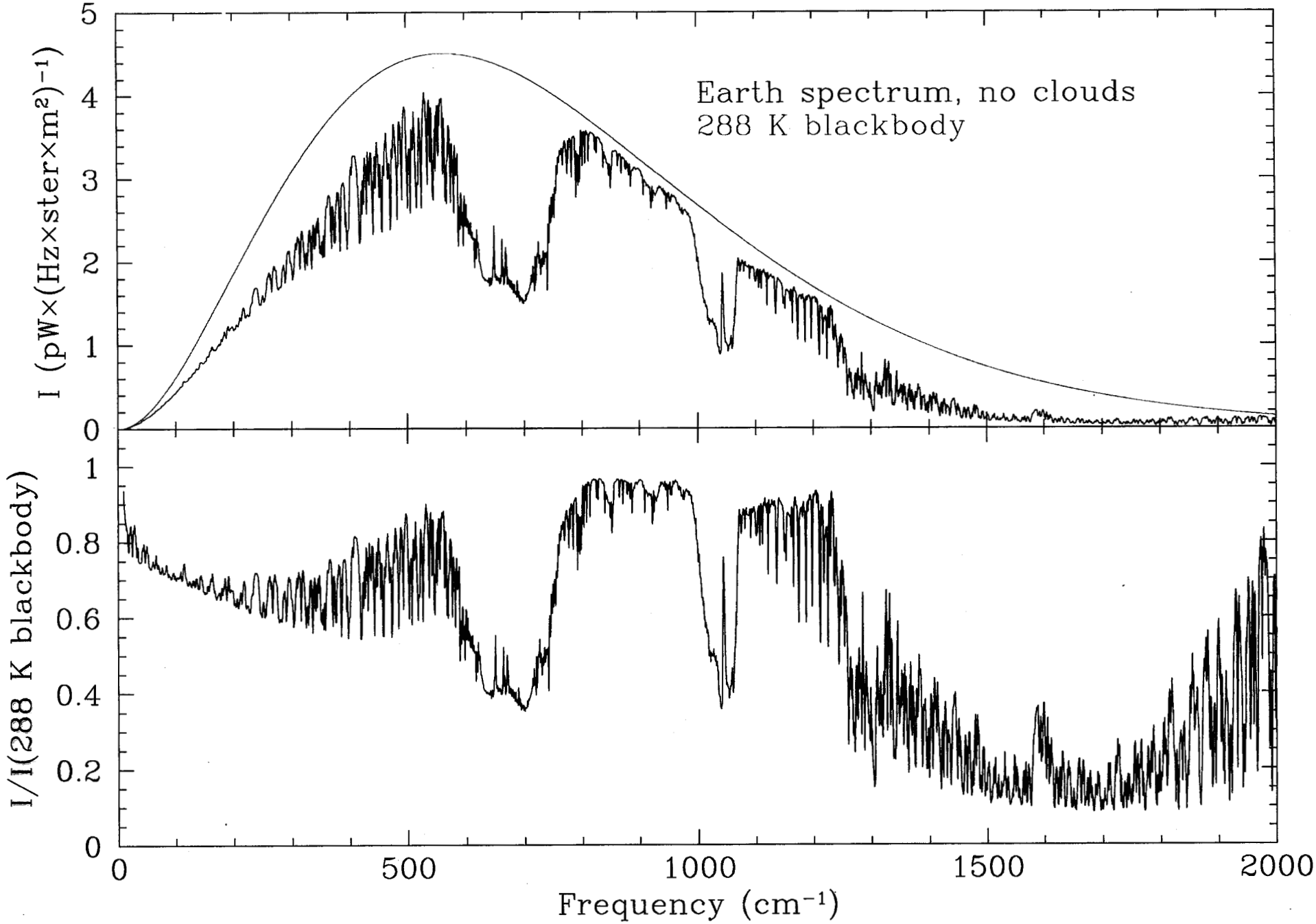
Earth spectrum, no clouds
288 K blackbody
I (pW×(Hz×ster×m²)⁻¹)
I/I(288 K blackbody)
Frequency (cm⁻¹)
0
1
2
3
4
5
0.2
0.4
0.6
0.8
500
1000
1500
2000

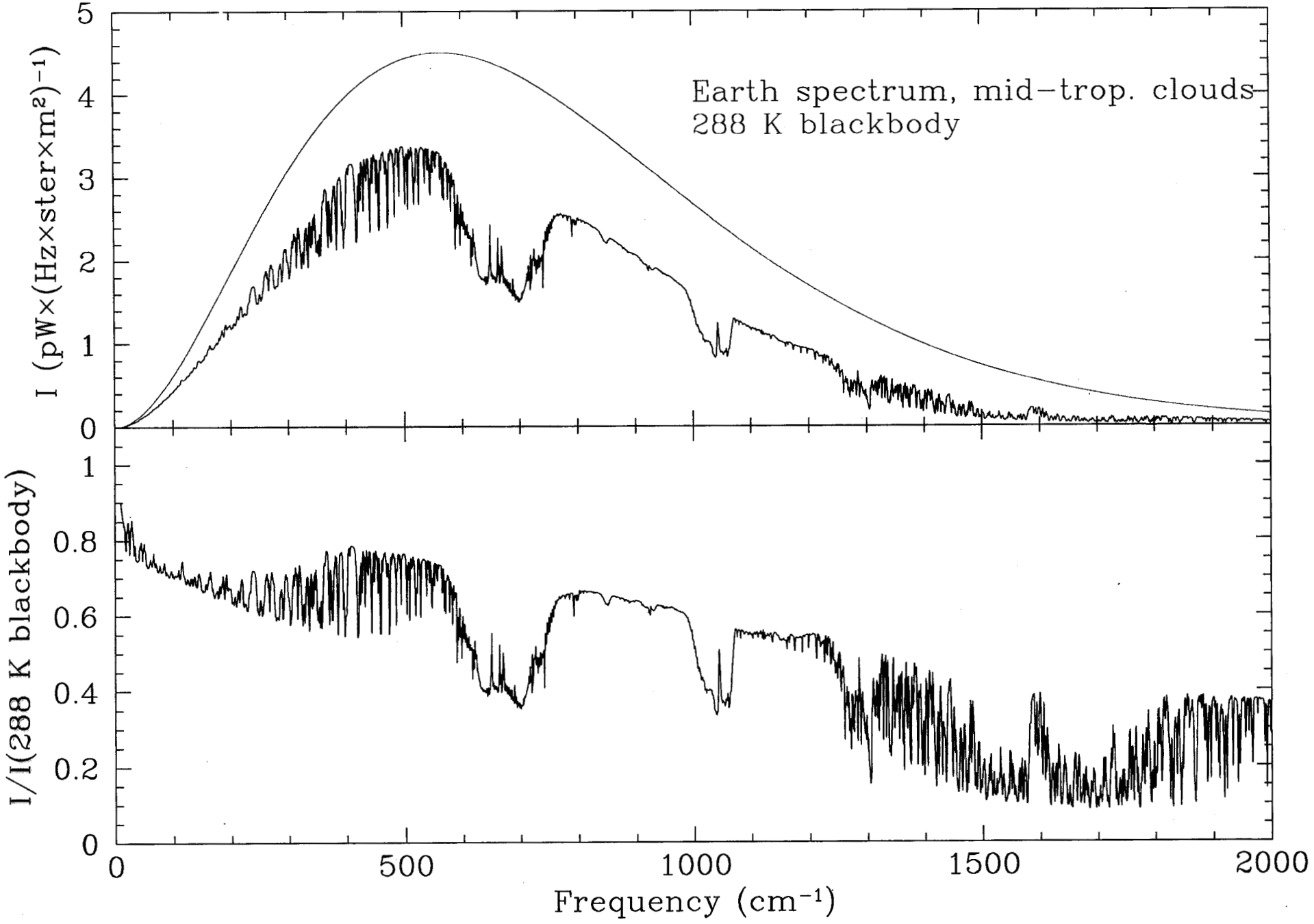
Earth spectrum, mid−trop. clouds
288 K blackbody
I (pW×(Hz×ster×m²)⁻¹)
I/I(288 K blackbody)
Frequency (cm⁻¹)
0
1
2
3
4
5
0.2
0.4
0.6
0.8
500
1000
1500
2000

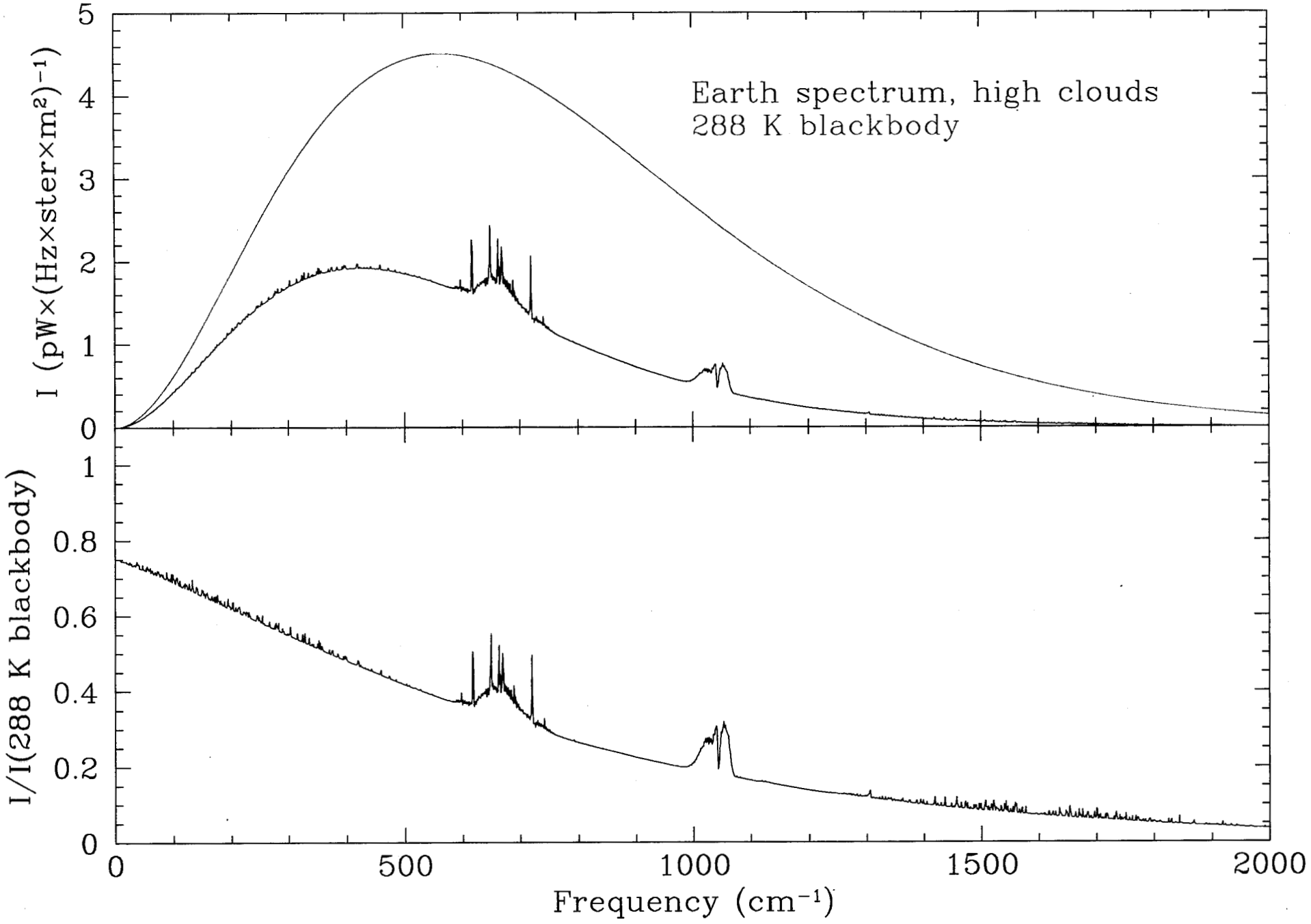
Earth spectrum, high clouds
288 K blackbody
I (pW×(Hz×ster×m²)⁻¹)
I/I(288 K blackbody)
Frequency (cm⁻¹)
0
1
2
3
4
5
0.2
0.4
0.6
0.8
500
1000
1500
2000

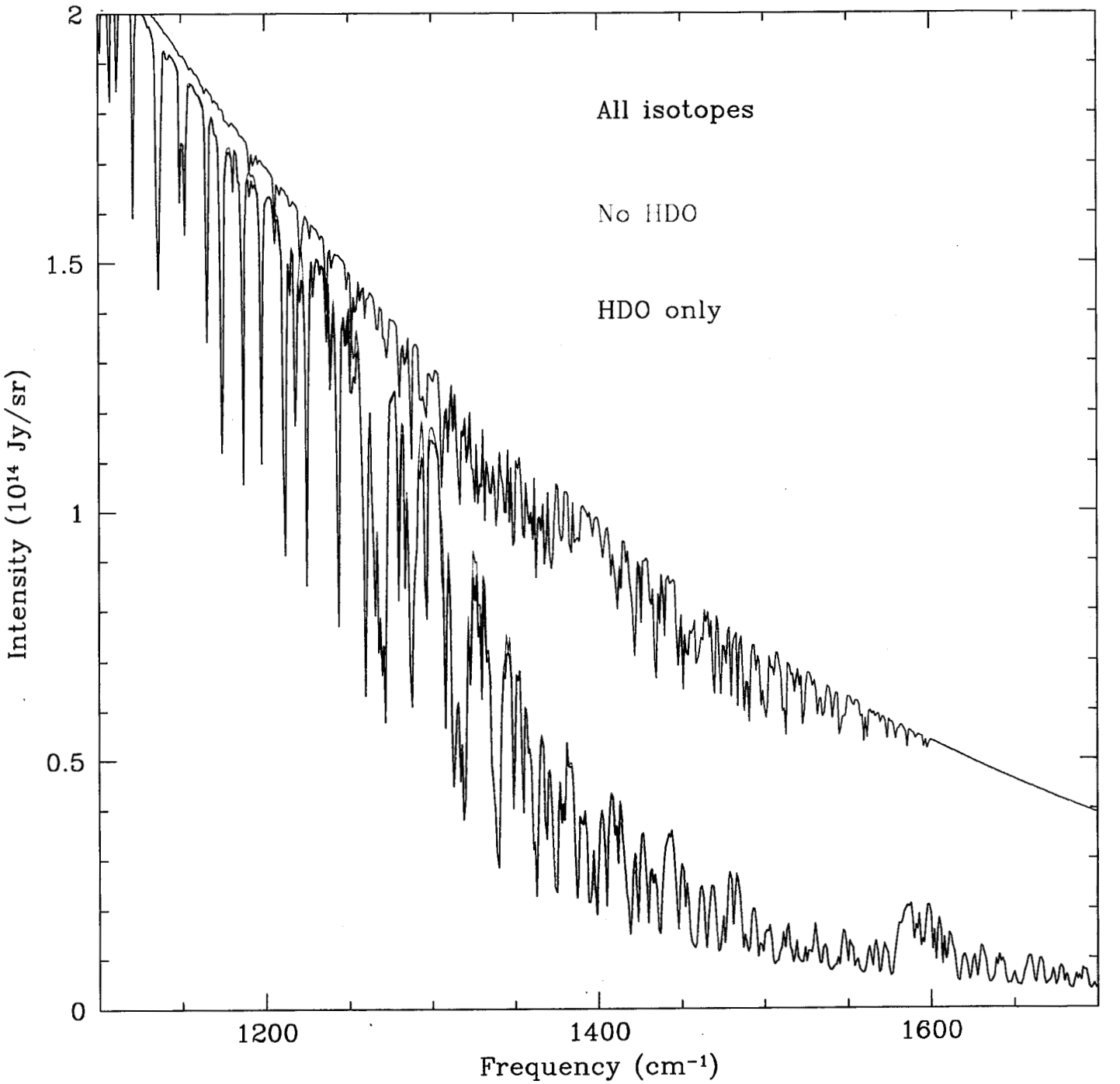
All isotopes
No HDO
HDO only
Intensity (10^{14} Jy/sr)
Frequency (cm^{-1})
0
0.5
1
1.5
2
1200
1400
1600

Emission spectrum from a cloudy area (Hanel *et al.*, 1972*c*).

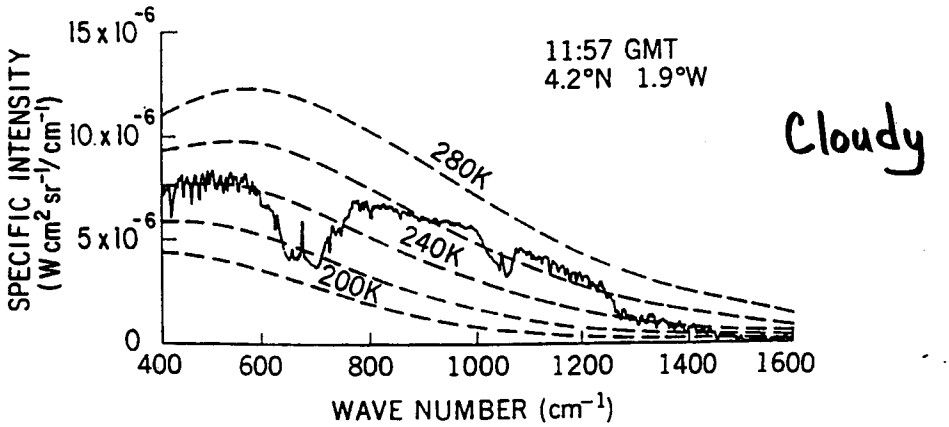

Fig. 6.2.6 Emission spectra from a desert area showing the effect of low emissivity between 1100 and 1250 cm^{-1} caused by residual rays in quartz sand. The comparison spectrum from an area covered by vegetation shows nearly the same brightness temperature on both sides of the ozone band at 1042 cm^{-1} (Hanel *et al.*, 1972*c*).

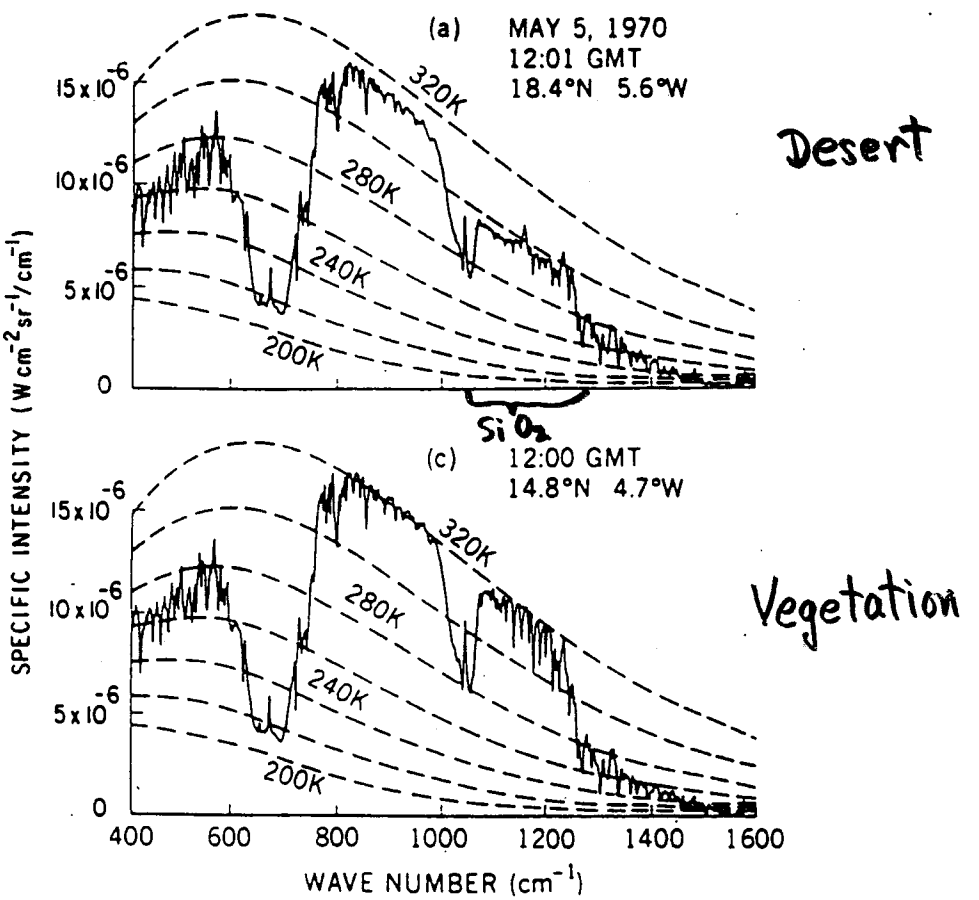

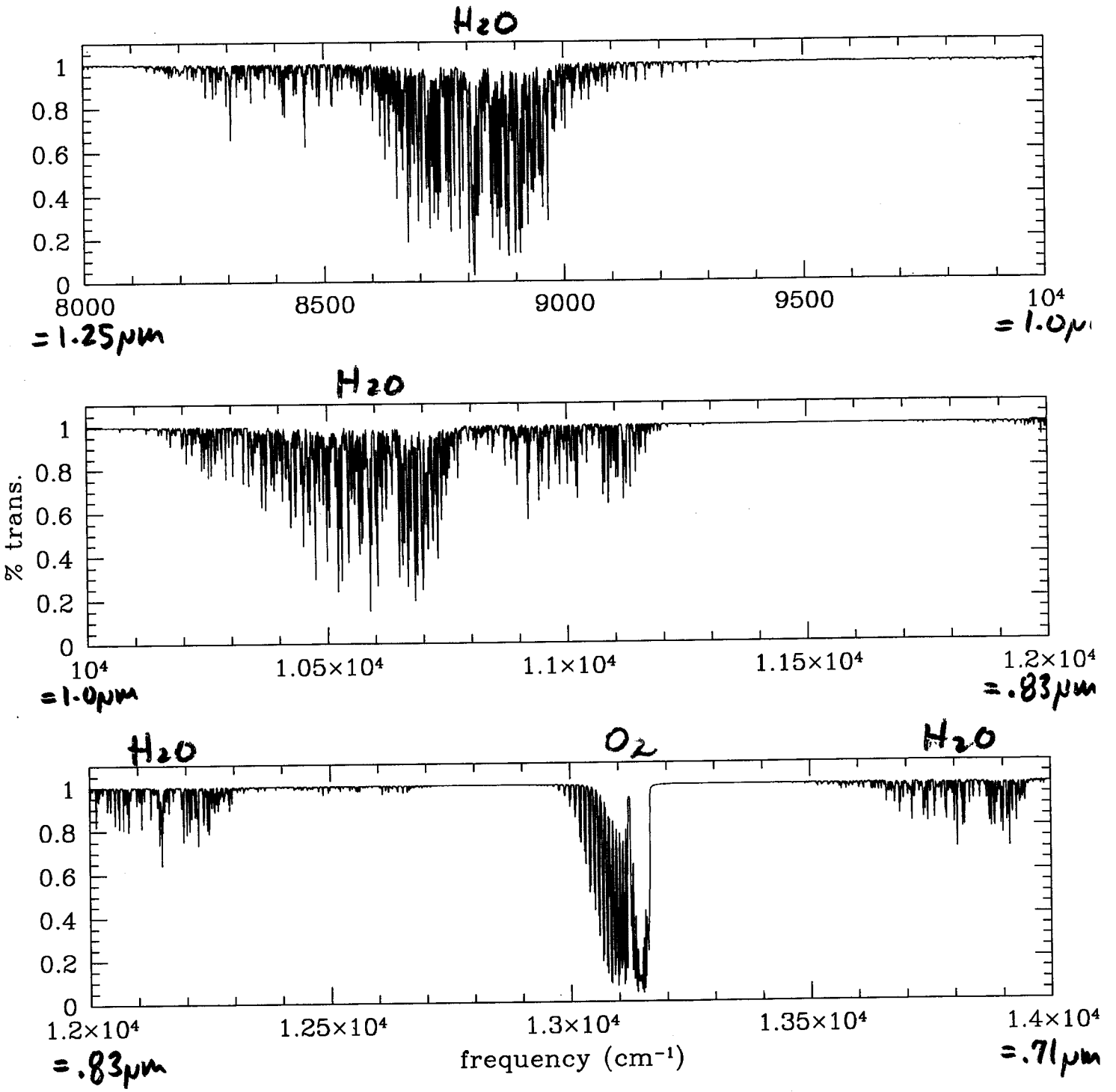
H2O
1
0.8
0.6
0.4
0.2
0
8000
8500
9000
9500
10⁴
=1.25μm
=1.0μ
H2O
% trans.
1
0.8
0.6
0.4
0.2
0
10⁴
1.05×10⁴
1.1×10⁴
1.15×10⁴
1.2×10⁴
=1.0μm
=.83μm
H2O
O2
H2O
1
0.8
0.6
0.4
0.2
0
1.2×10⁴
1.25×10⁴
1.3×10⁴
1.35×10⁴
1.4×10⁴
=.83μm
frequency (cm⁻¹)
=.71μm

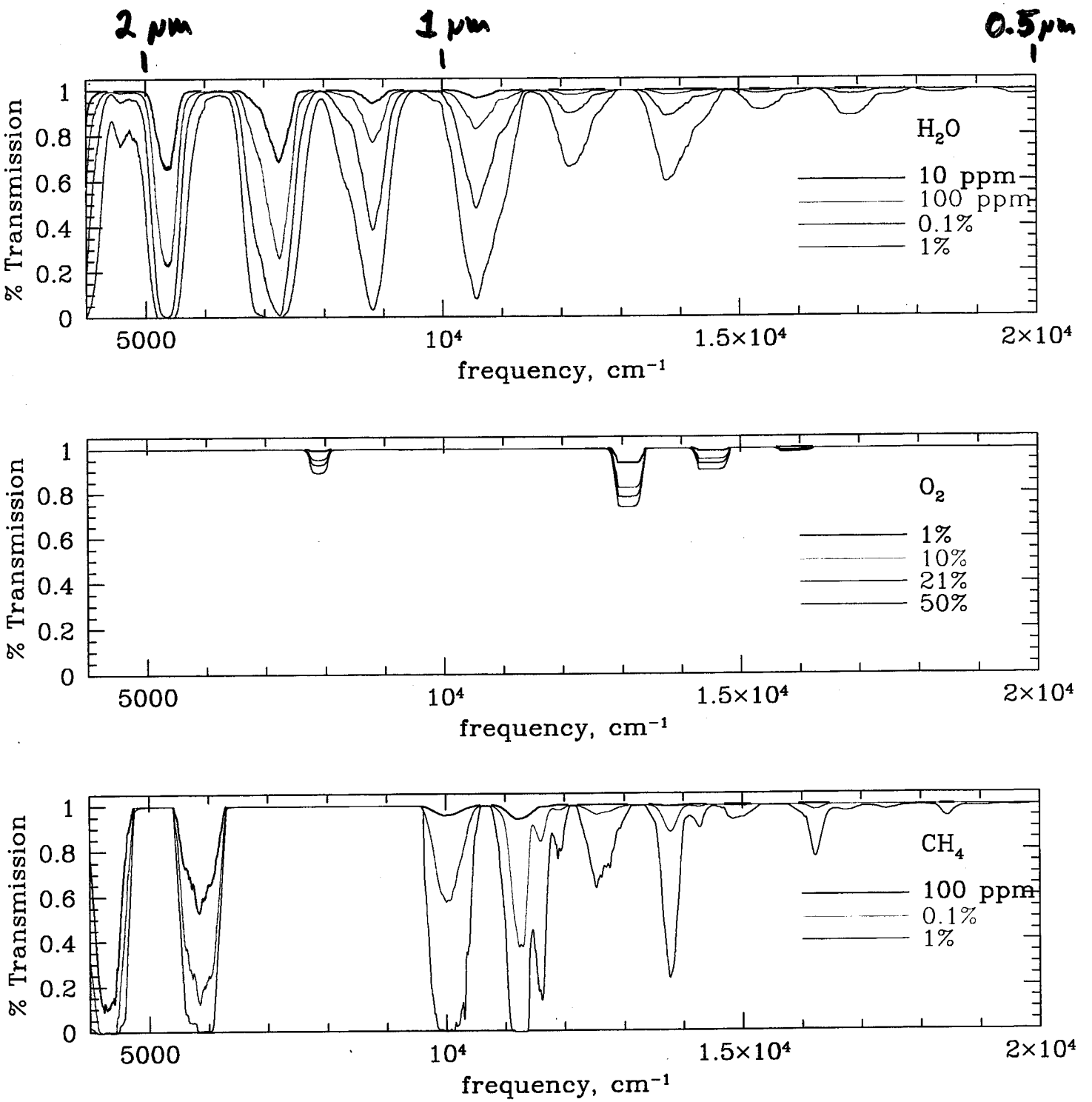
2 μm
1 μm
0.5 μm
% Transmission
1
0.8
0.6
0.4
0.2
0
5000
10⁴
1.5×10⁴
2×10⁴
frequency, cm⁻¹
H₂O
10 ppm
100 ppm
0.1%
1%
O₂
1%
10%
21%
50%
CH₄
100 ppm
0.1%
1%

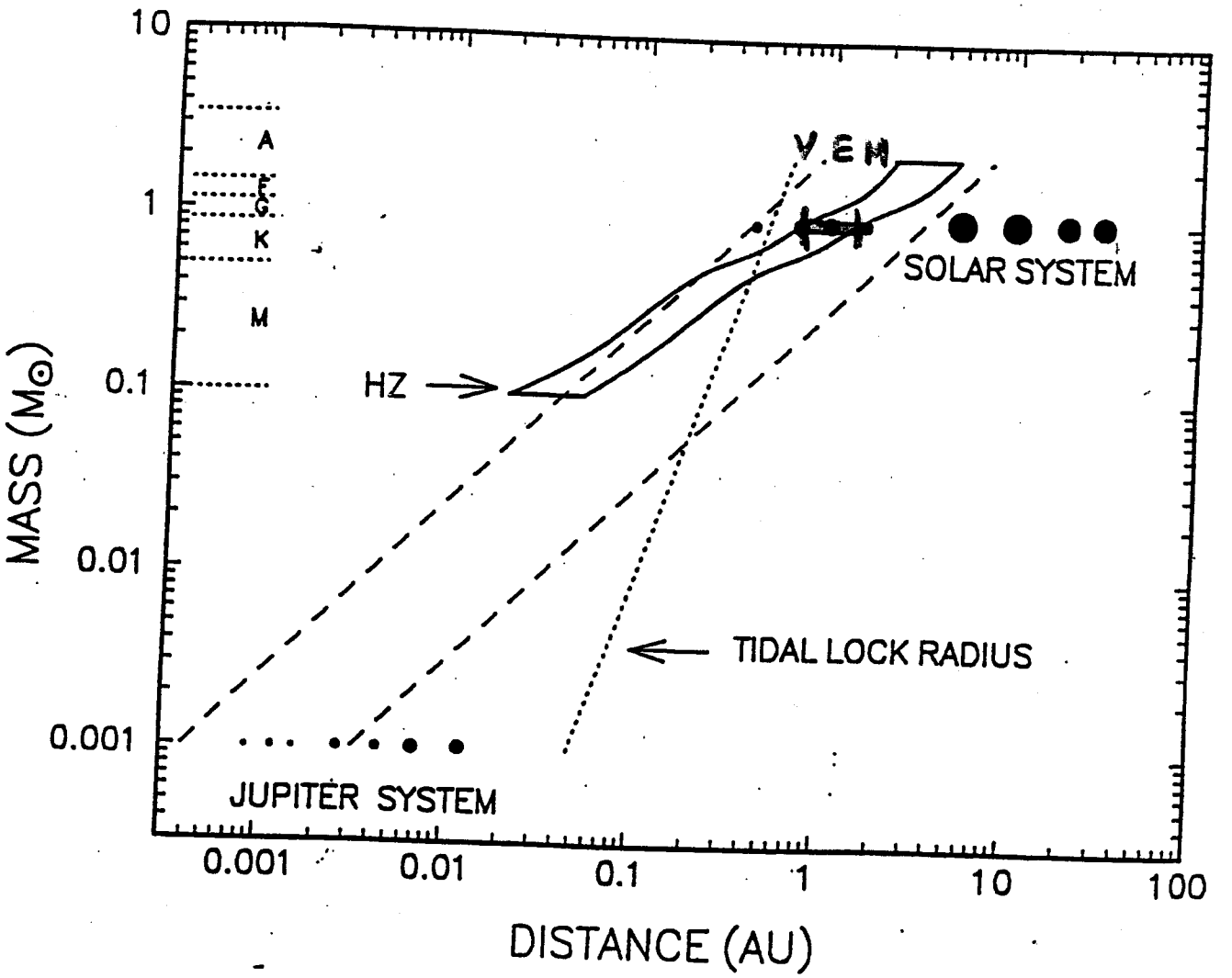

Kasting et al. (1993)

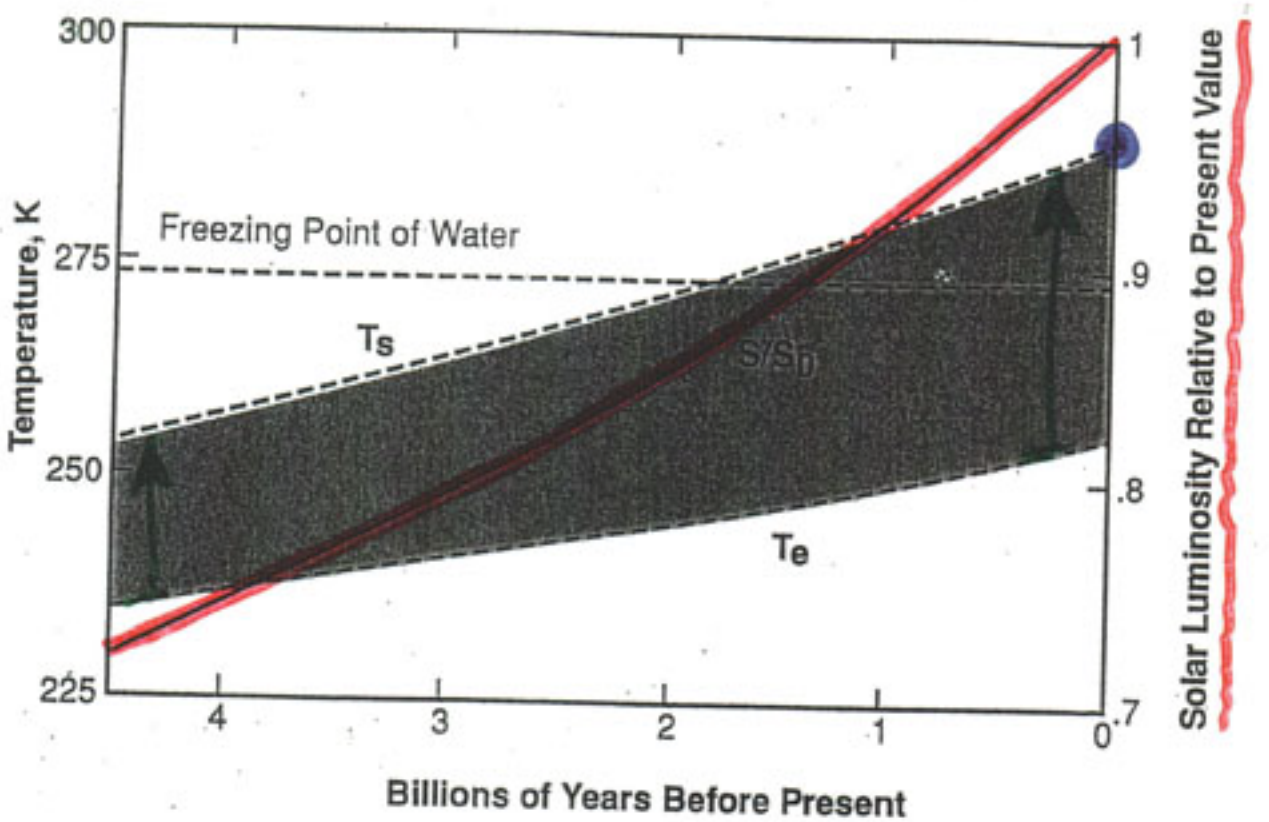

Figure 1. Diagram (Kasting and Toon 1989) illustrating the faint young Sun problem for Earth. Solid curve is solar luminosity relative to today's value, as calculated by Gough (1981). Dashed curves represent effective radiating temperature, T_e, and mean global surface temperature, T_s, as calculated by a one-dimensional climate model, assuming constant atmospheric CO_2 fixed relative humidity, and no cloud feedback.

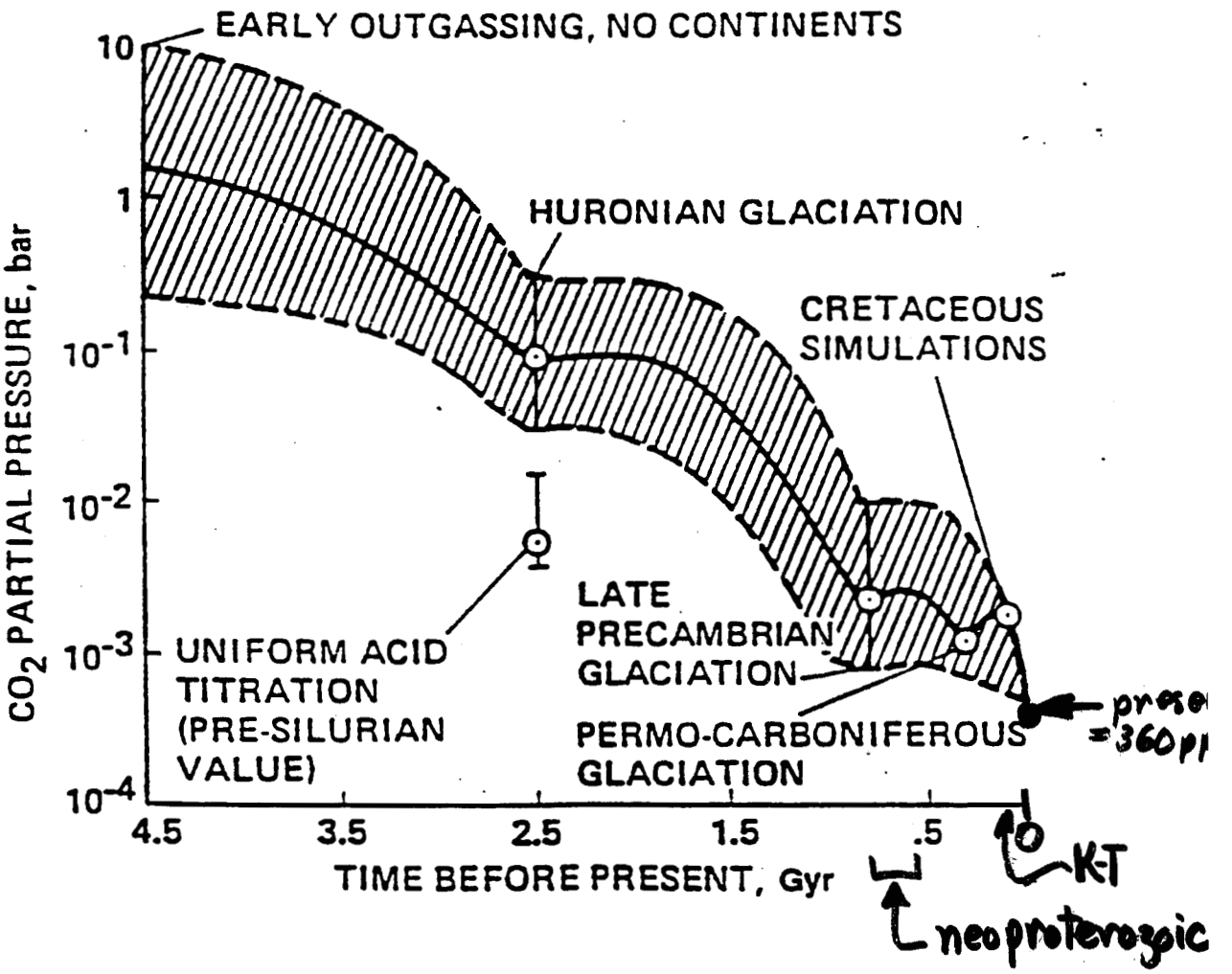

Figure 9.6 Estimated pCO_2 over geologic time. The solid line is a best guess model. The shaded envelope represents the climatologically reasonable range of pCO_2. The point labeled "uniform acid titration" is the pre-Silurian CO_2 pressure estimated by Holland and Zbinden (1986) from paleosol data. After Kasting (1987).

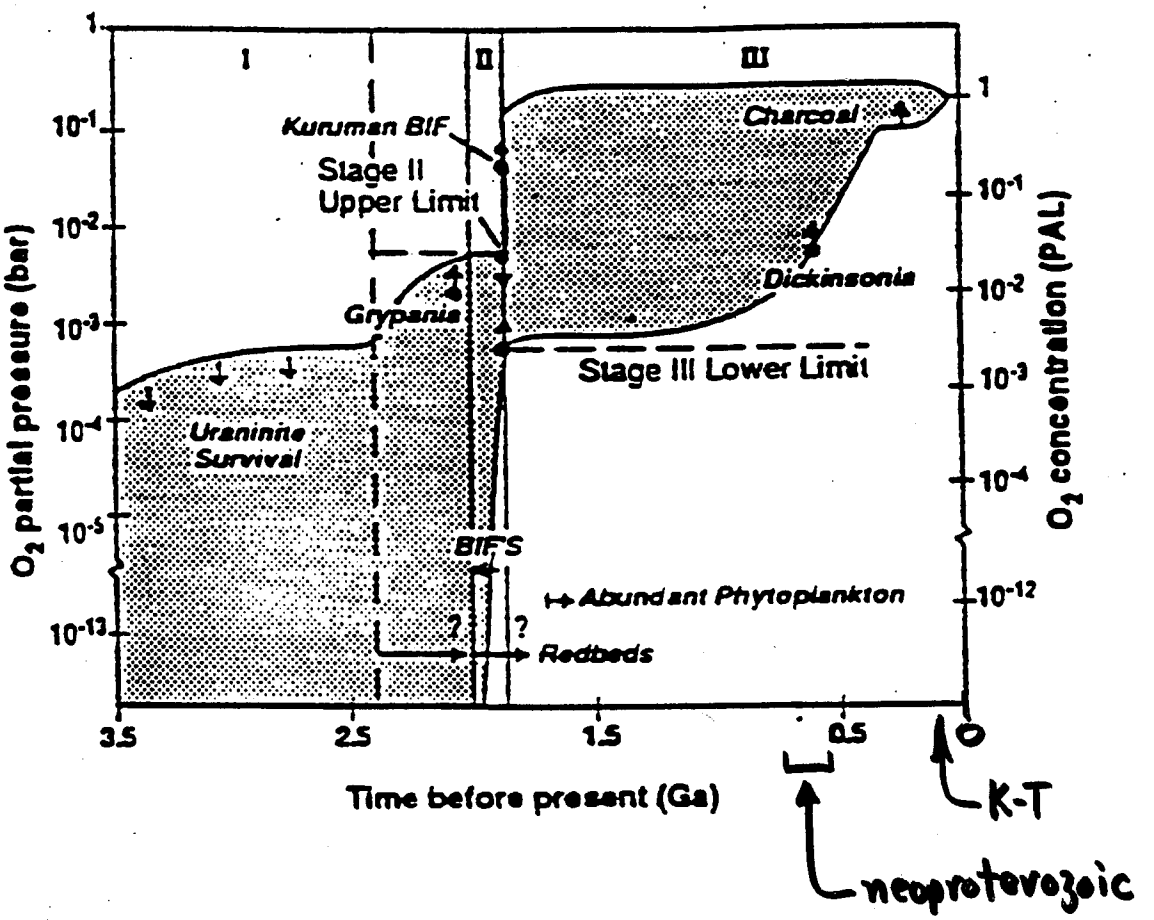

Figure 9.15 Estimated change of oxygen levels over geologic time. The shaded area represents the range permitted by data. The dashed line indicates a possible earlier date for the beginning of stage II. After Kasting (1993).

Troubled youth. Life evolved during the early Earth's extremes.

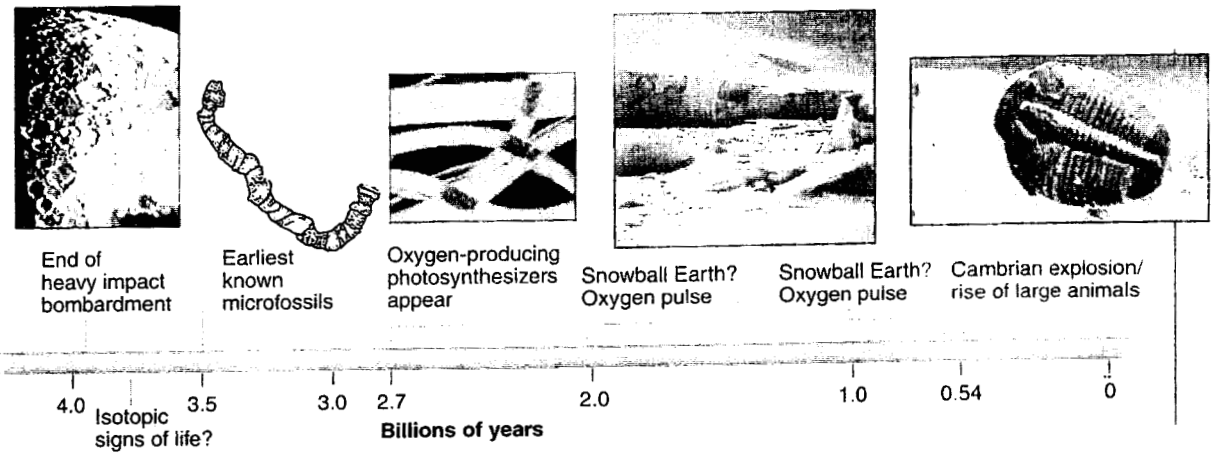

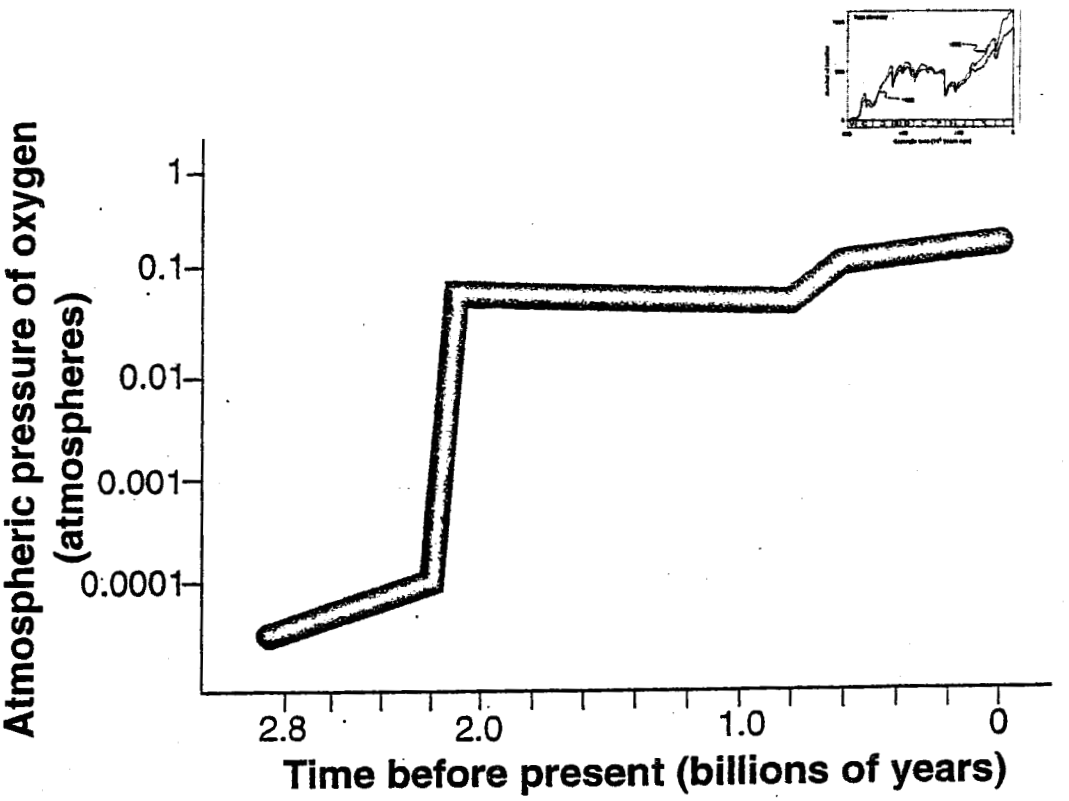

Earth Was Completely Covered by Ice, Geologists Say

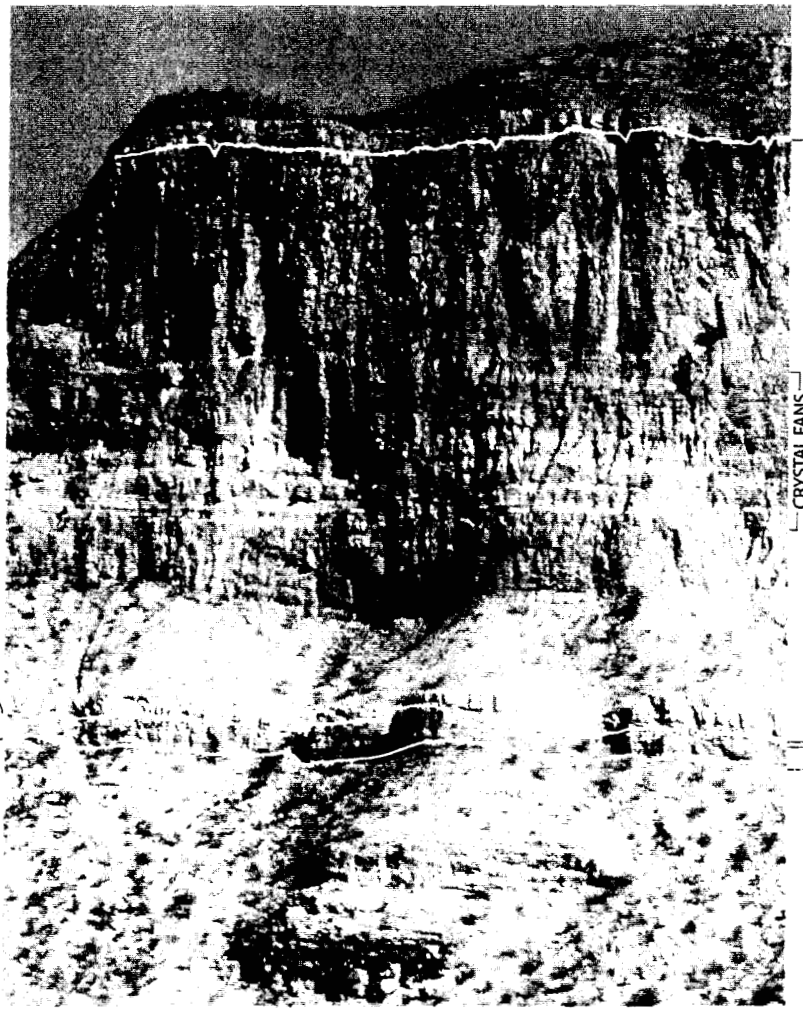

COURTESY OF GALEN PIPPA HALVERSON

150 My before appearance of metazoan life —

Neoproterozoic (730-580 My ago) - shows many signs of glaciation within 3° of equator at sea level:

1. sediments known at equator.

2. ice-smoothed stones dropped into sediment.

3. Fe gone at 1.8 Ga ($\Rightarrow$ no O_2), but reappears at time of glaciation ($\Rightarrow$ O_2 present so Fe^{2+} insoluble & precip. out)

4. $\delta^{13}C$ shows large decreases / increases matching ~4 glacial episodes & ~1 CH_4 burst.

5. rock sequence shows sand dunes & glacial deposits (ice) overlain by thick cap carbonate layer (warm oceans).

6. early animals appear just after oscillations, dramatic increase

Ref: Paul Hoffman & Dan Shrag.

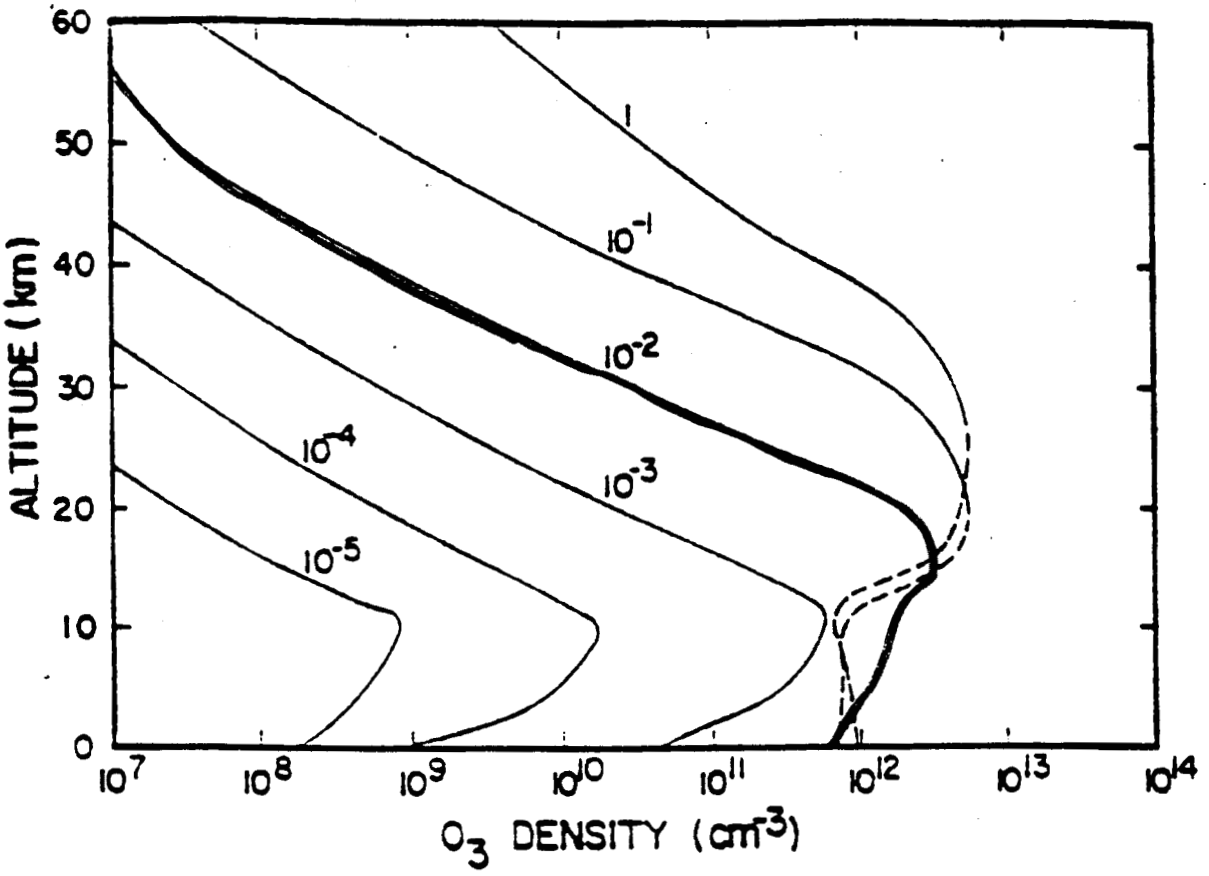

Fig. 1. Ozone profiles at various oxygen levels. The assumed solar zenith angle is 45°.

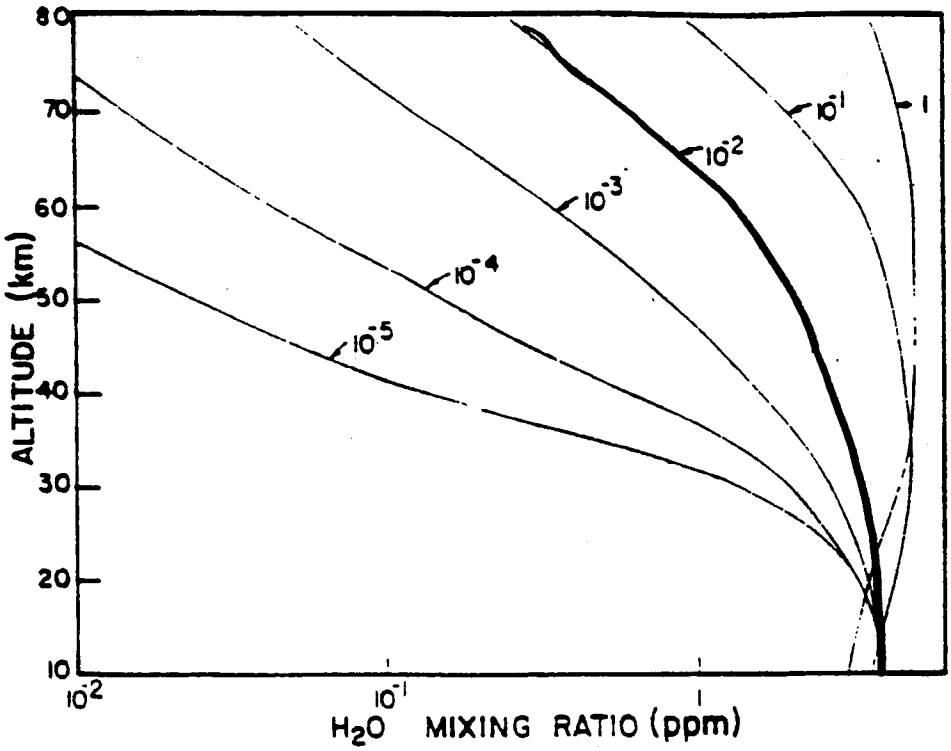

Fig. 4. Water vapor profiles for various oxygen levels. The H_2O density is fixed below 10 km.

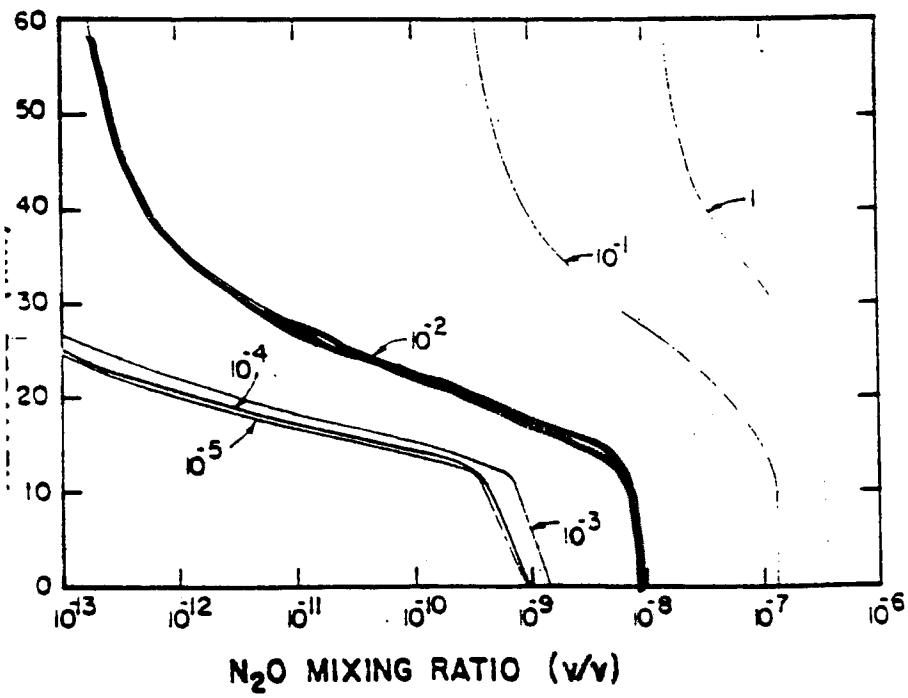

N_2O profiles for various oxygen levels. A constant upward flux at ground level is assumed.

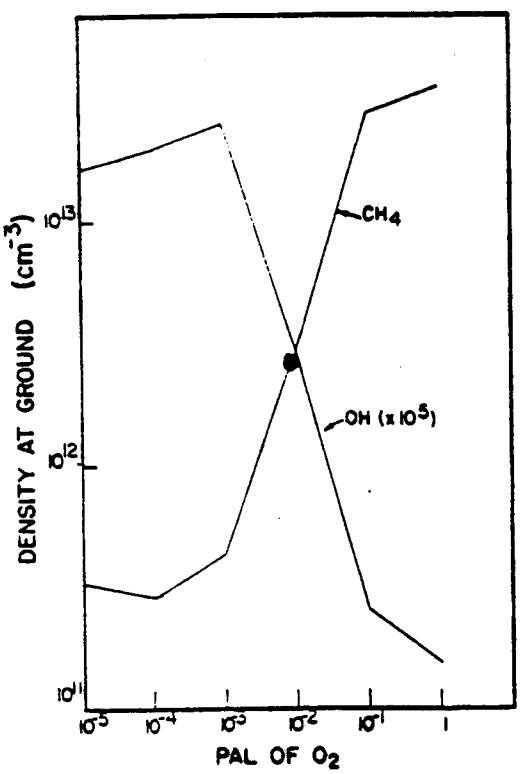

Ground level CH_4 and OH densities at various oxy

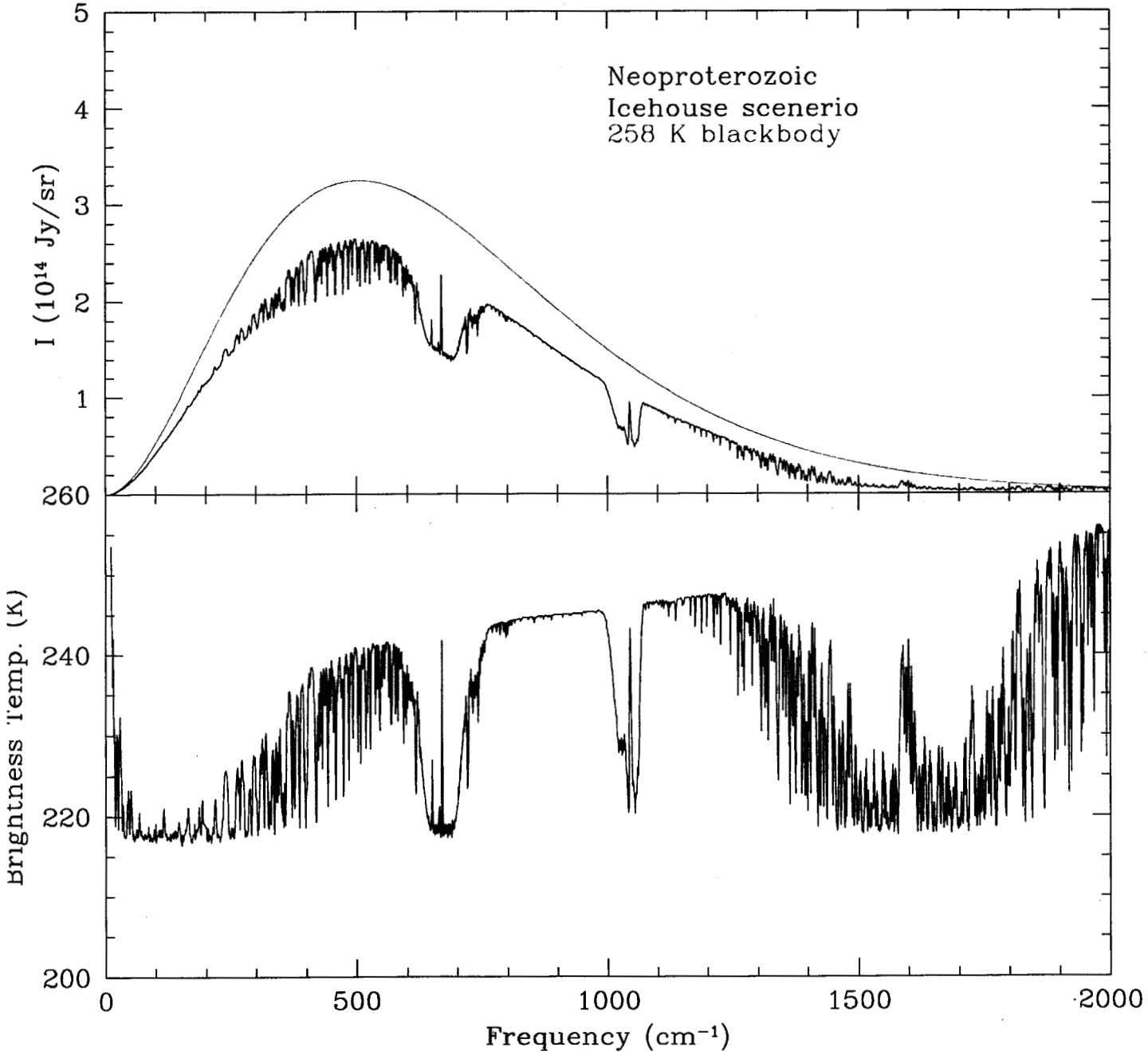
Neoproterozoic
Icehouse scenerio
258 K blackbody
I (10^{14} Jy/sr)
Brightness Temp. (K)
Frequency (cm^{-1})
5
4
3
2
1
260
240
220
200
0
500
1000
1500
2000

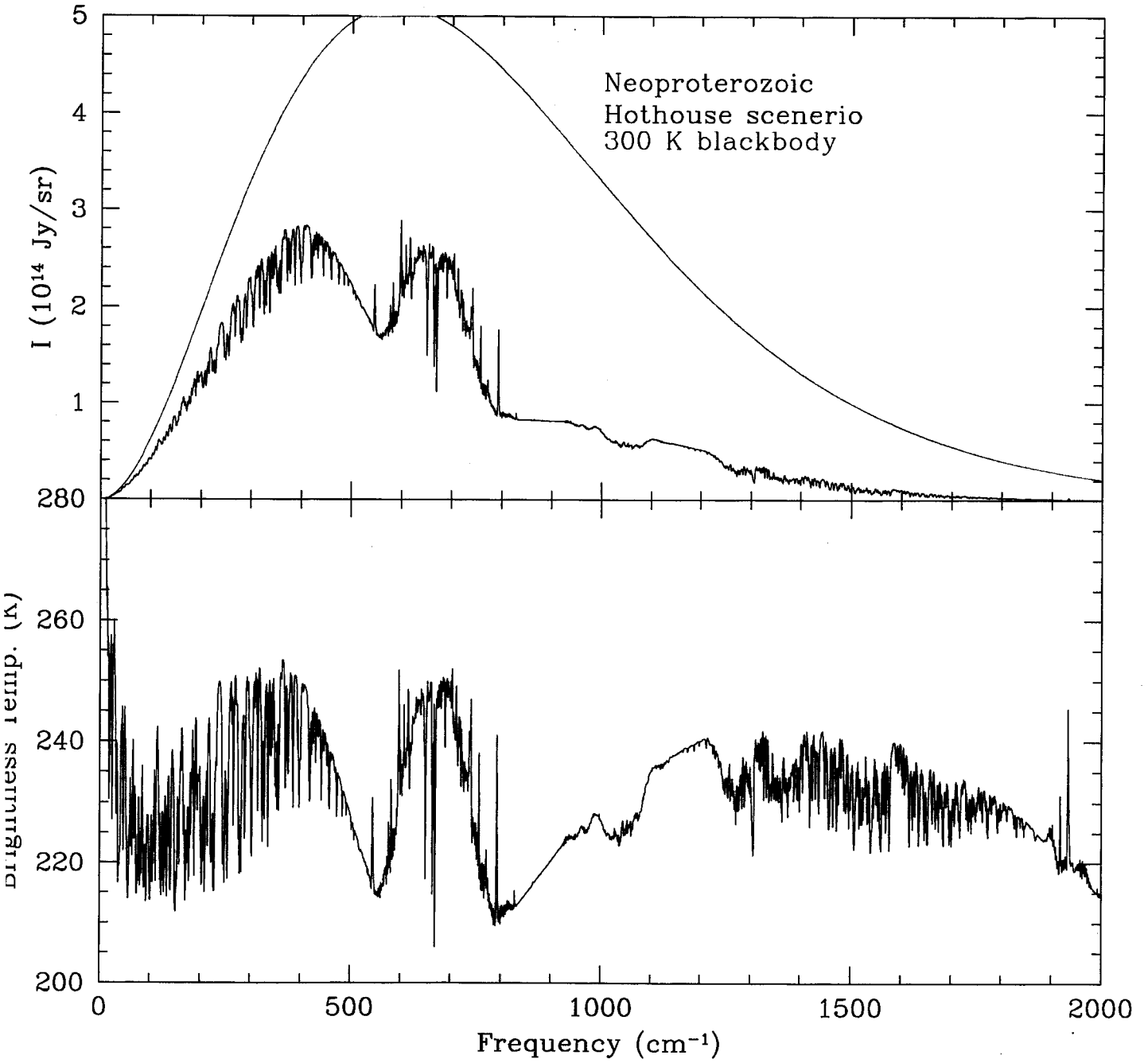
Neoproterozoic
Hothouse scenerio
300 K blackbody
I (10^{14} Jy/sr)
Brightness temp. (K)
Frequency (cm^{-1})
5
4
3
2
1
280
260
240
220
200
0
500
1000
1500
2000

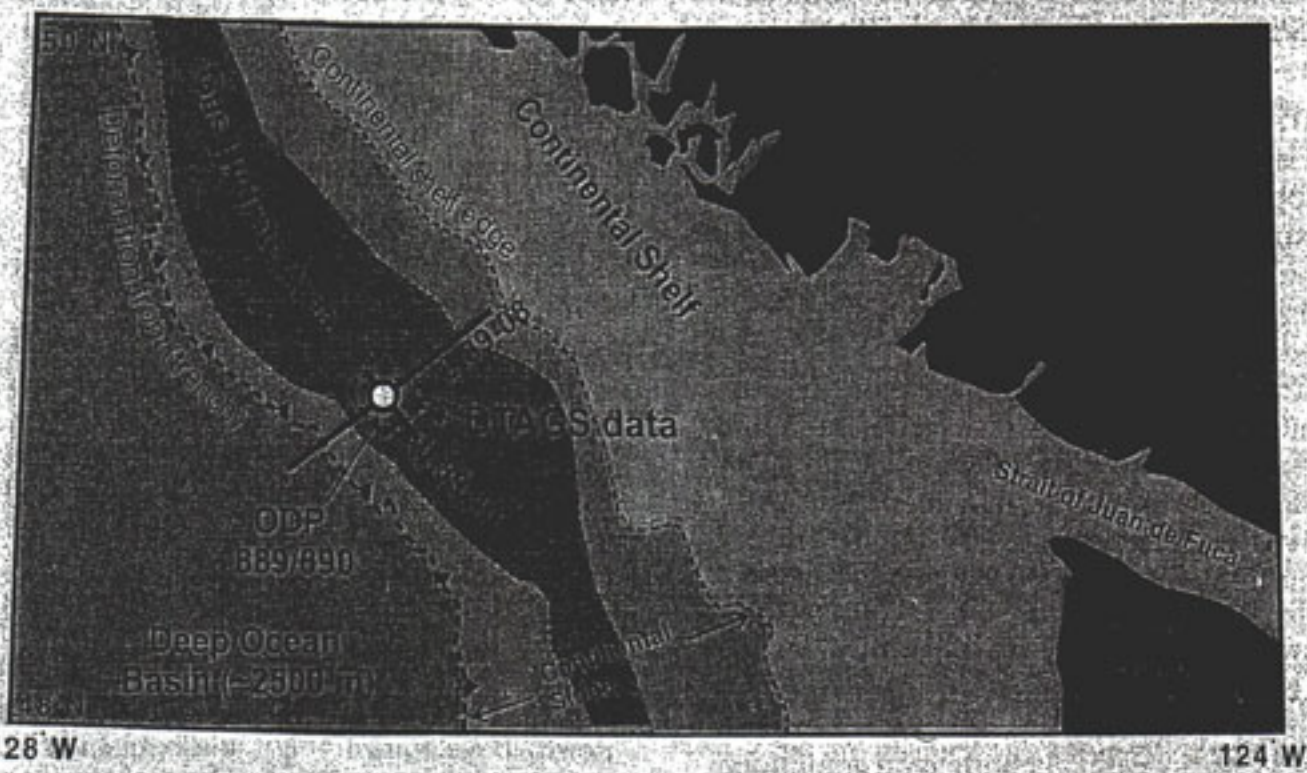

Fig. 1. Area of deep sea gas hydrates off the west coast of Canada with the locations of the DTAGS and conventional multichannel seismic lines and ODP Site 889/890.

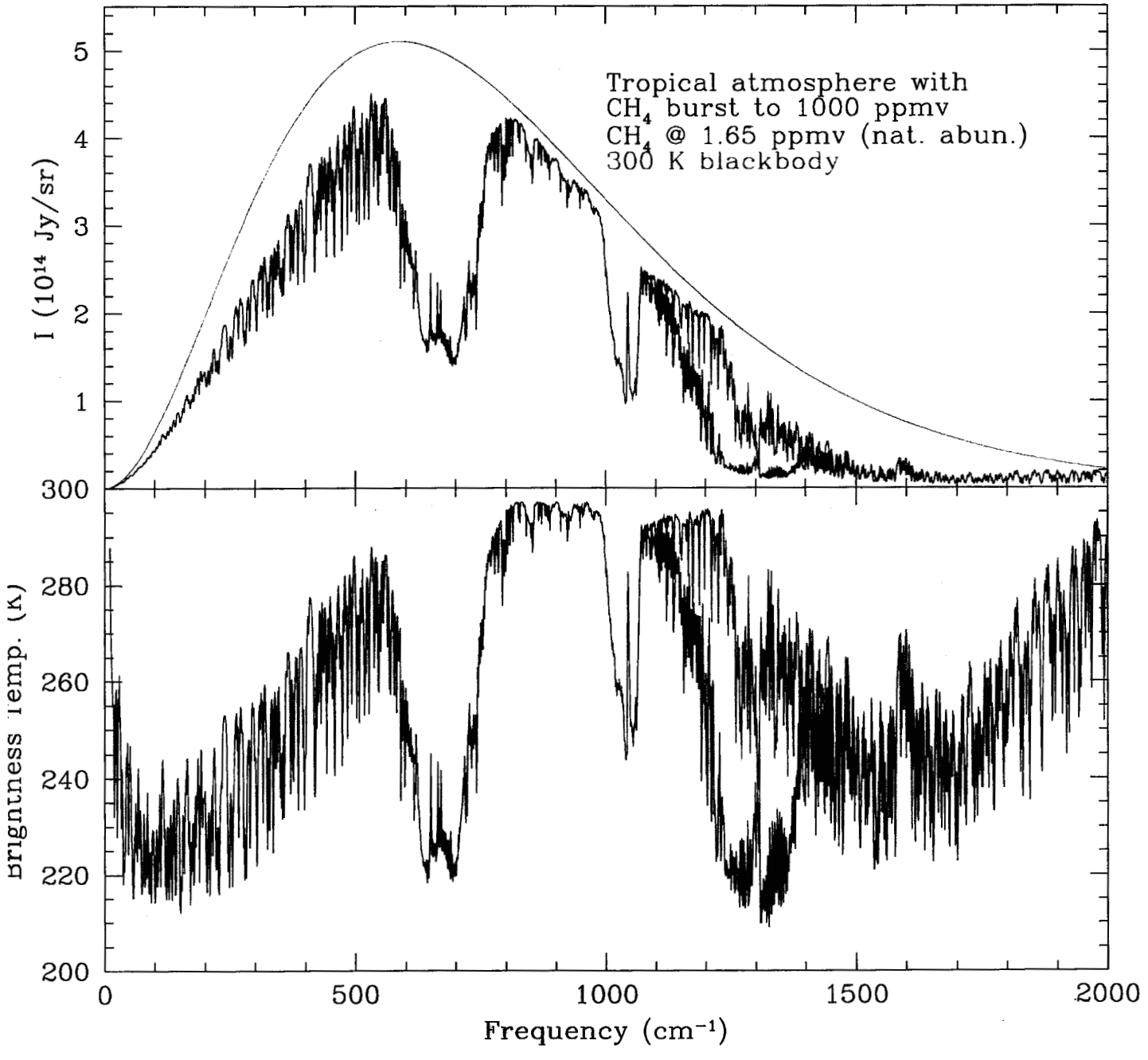
Tropical atmosphere with
CH4 burst to 1000 ppmv
CH4 @ 1.65 ppmv (nat. abun.)
300 K blackbody
I (10^14 Jy/sr)
Brightness Temp. (K)
Frequency (cm^-1)
0
500
1000
1500
2000
1
2
3
4
5
200
220
240
260
280
300

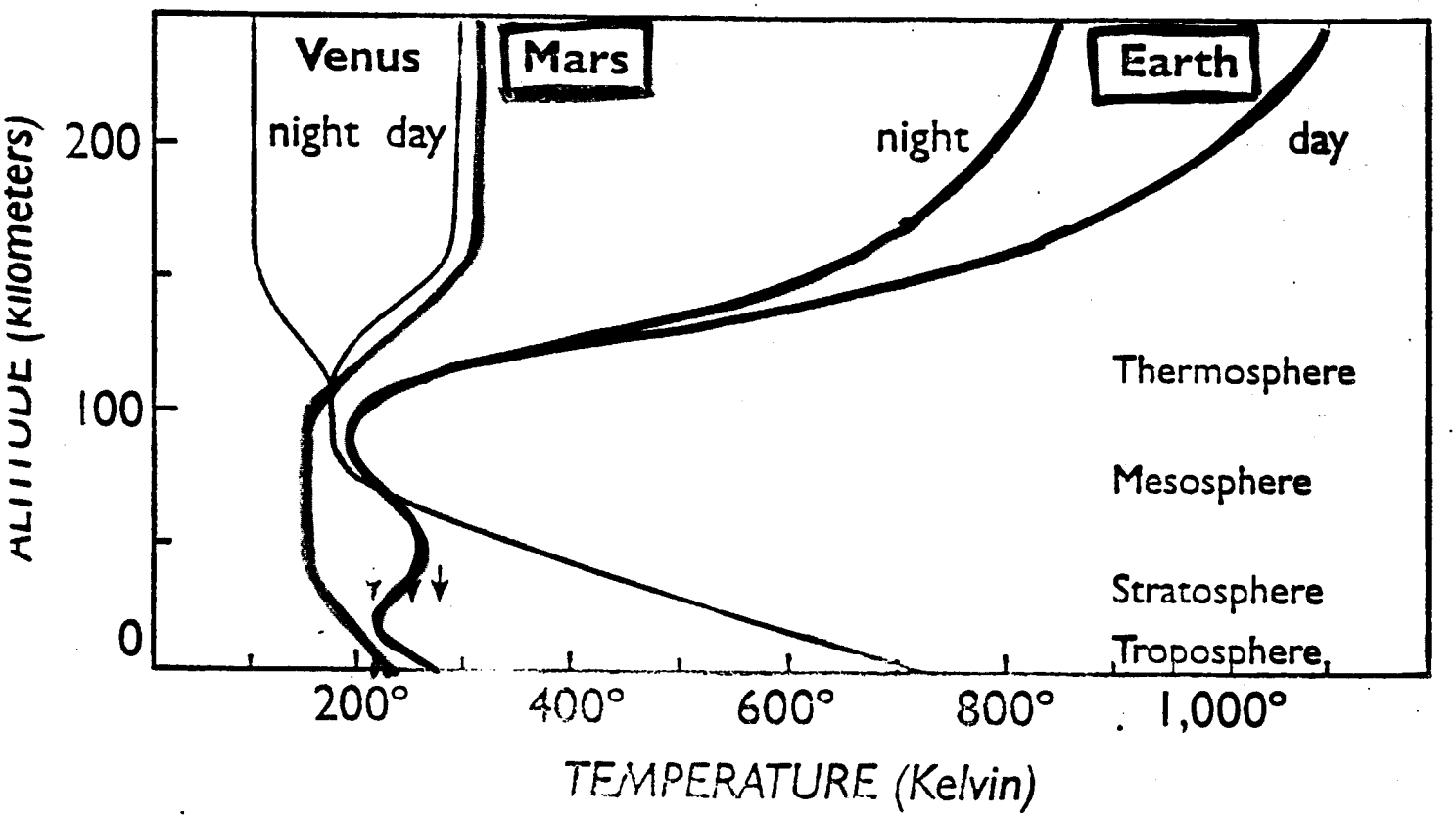
Venus
night day
Mars
Earth
night
day
Thermosphere
Mesosphere
Stratosphere
Troposphere
ALTITUDE (Kilometers)
200
100
0
200°
400°
600°
800°
1,000°
TEMPERATURE (Kelvin)

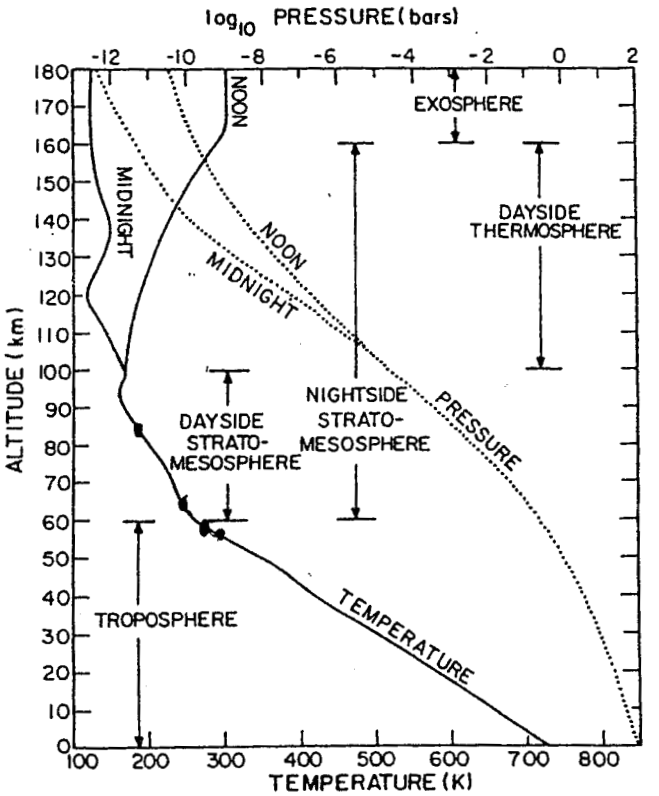

} cloud-tops

Figure 8.1 Altitude profile of temperature and pressure at 30° latitude for the atmosphere of Venus, based on the standard atmosphere. After Seiff, A., 1983, "Models of Venus' Atmospheric Structure," in Hunten et al. (1983; cited in section 8.1), p. 1045, as quoted by Prinn, R. G., 1985, "The Photochemistry of the Atmosphere of Venus," in Levine (1985; cited in section 8.1). p. 281.

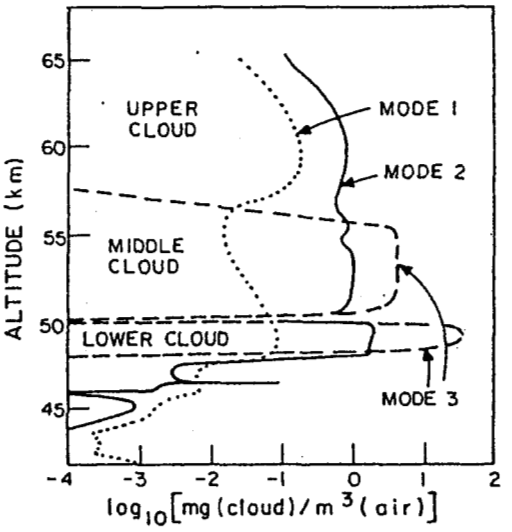

Figure 8.2 Altitude profile of the mass density of three modes of cloud particles in the middle atmosphere of Venus. After Knollenberg, R., and Hunten, D. M., 1980, "The Microphysics of the Clouds of Venus: Results of the Pioneer Venus Particle Size Spectrometer Experiment." *J. Geophys. Res.* **85**, 8039, as quoted by Prinn, R. G., 1985, "The Photochemistry of the Atmosphere of Venus," in Levine (1985; cited in section 8.1). p. 281.

Table 8.2 Composition of the atmosphere of Venus

Species	Mole fraction	References and remarks
CO_2	$96.5 \pm 0.8\%$	
N_2	$3.5 \pm 0.8\%$	
H_2O	2×10^{-5}	surface
	6×10^{-5}	22 km
	1.5×10^{-4}	42 km
Ar	$7 \pm 2.5 \times 10^{-5}$	
CO	$1.7 \pm 1 \times 10^{-6}$	surface
	$3.0 \pm 1.8 \times 10^{-5}$	42 km
	$4.5 \pm 1 \times 10^{-5}$	cloud top
	1×10^{-3}	100 km
		(1)
O_2	$< 3 \times 10^{-7}$	(2); cloud top
He	$12^{+24}_{-8} \times 10^{-6}$	
Ne	$7 \pm 3 \times 10^{-6}$	
HCl	6×10^{-7}	(3); cloud top
COS	3×10^{-7}	(4)
SO_2	$5\text{–}100 \times 10^{-9}$	(5)
Kr	2.5×10^{-8}	
SO	$2 \pm 1 \times 10^{-8}$	(6)
HF	$5^{+5}_{-2.5} \times 10^{-9}$	(3)
Xe	1.9×10^{-9}	

Unless otherwise stated, the composition data is taken from von Zahn et al. in Hunten et al., eds. (1983).

(1) See discussion in Yung and DeMore (1982); (2) Trauger, J. T. and Lunine, J. I., 1983, Icarus 55, 272; (3) Connes, P. et al., 1967, Astrophys. J. 147, 1230; (4) Crisp, D. et al., 1990, Nature 345, 508; (5) Zasova, L. V. et al., 1993, Icarus 105, 92; (6) Na, C. Y. et al., 1990, J. Geophys. Res. 95, 7485.

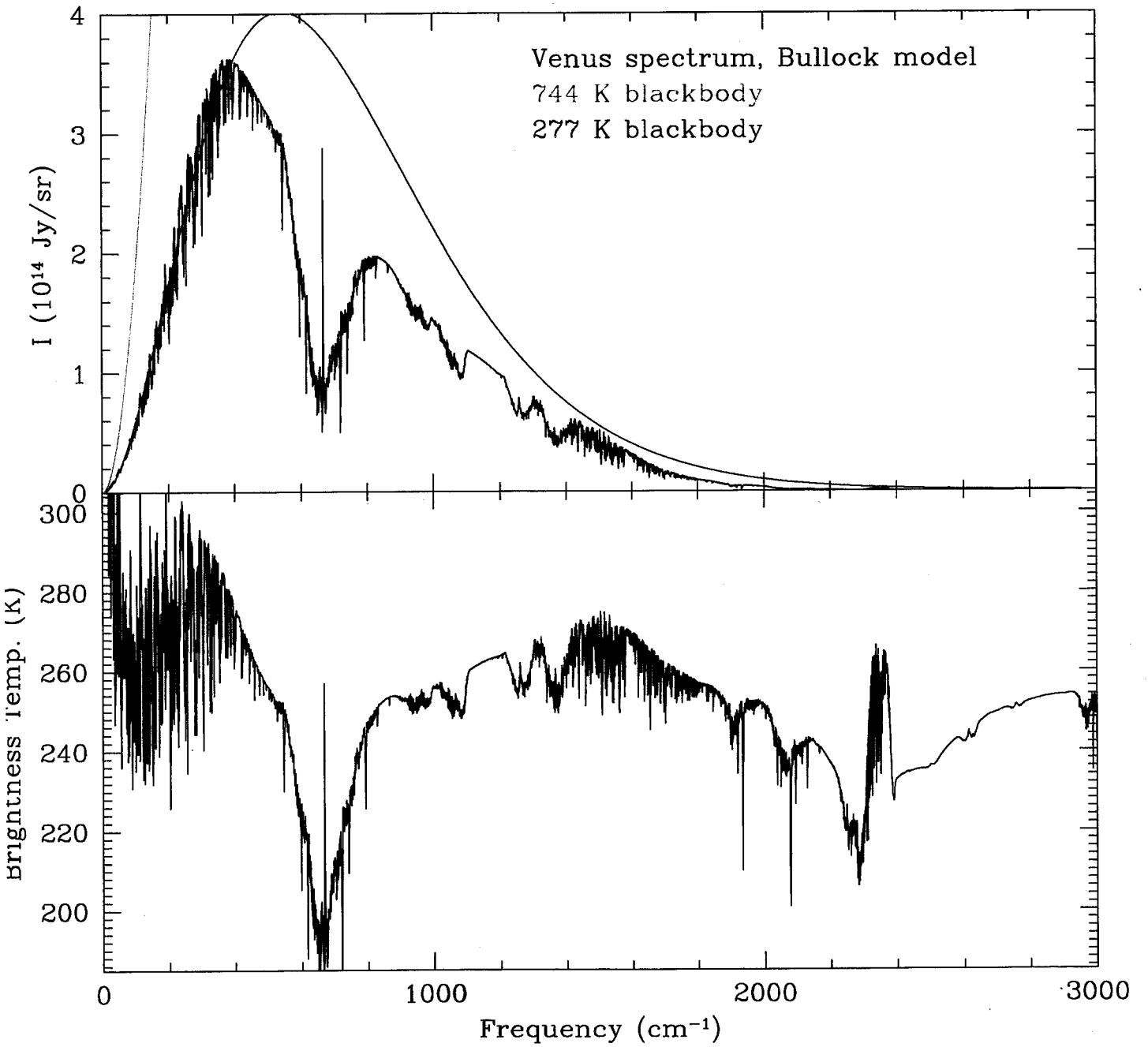
Venus spectrum, Bullock model
744 K blackbody
277 K blackbody
I (10^{14} Jy/sr)
Brightness Temp. (K)
Frequency (cm^{-1})
0
1
2
3
4
200
220
240
260
280
300
0
1000
2000
3000

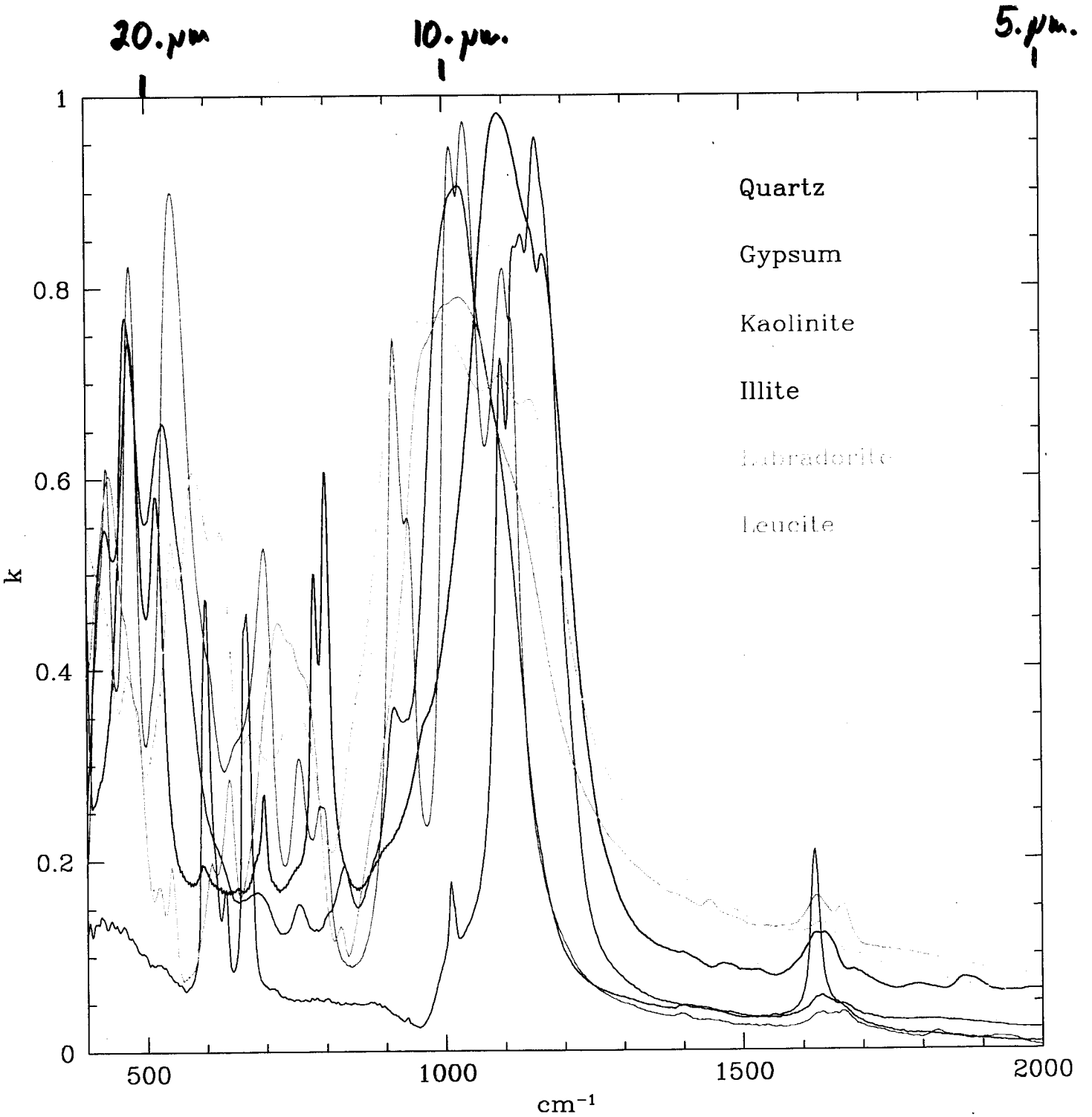
20. μm
10. μm.
5. μm.
Quartz
Gypsum
Kaolinite
Illite
Labradorite
Leucite
k
cm⁻¹
0
0.2
0.4
0.6
0.8
1
500
1000
1500
2000

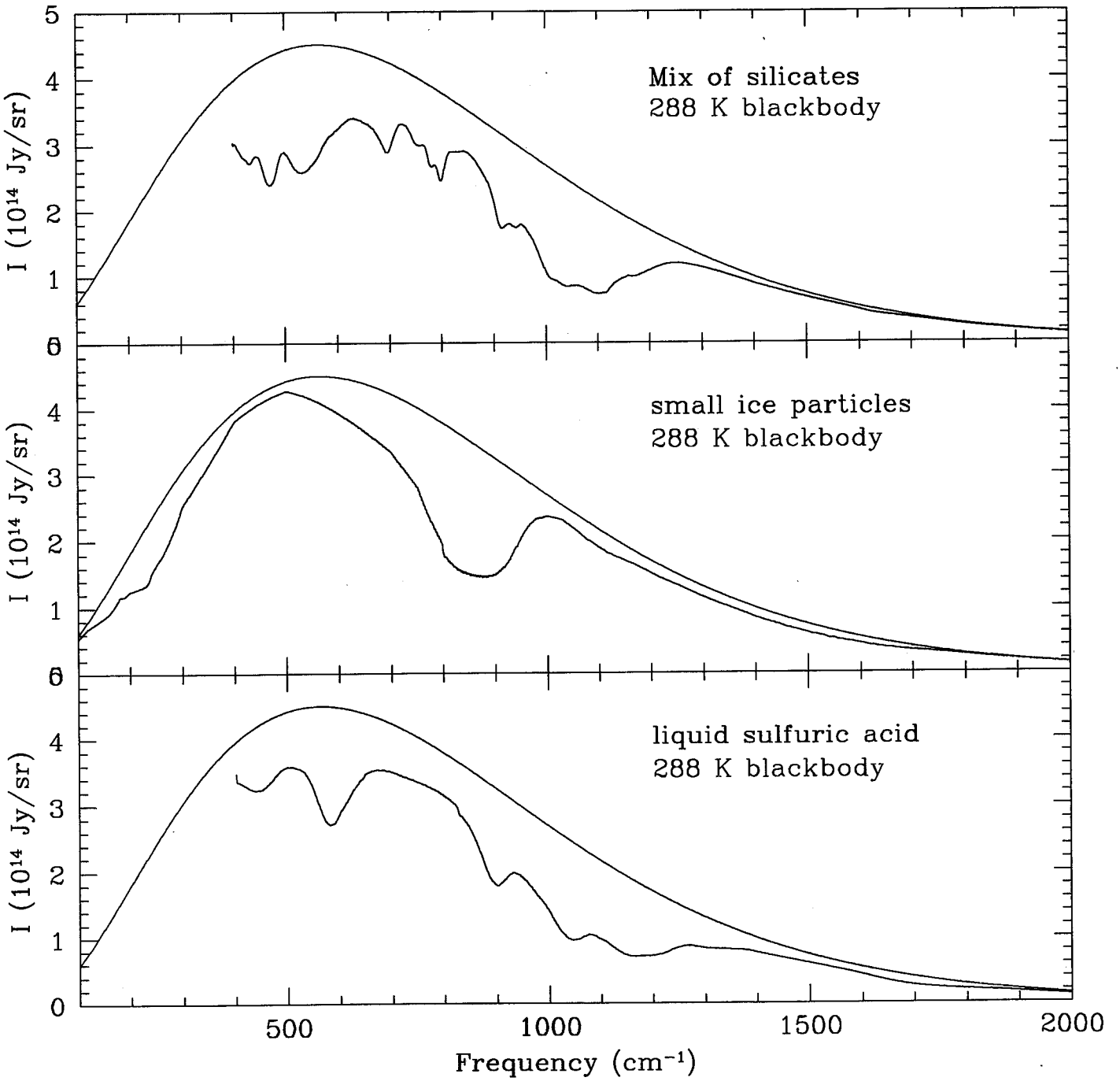
Mix of silicates
288 K blackbody
small ice particles
288 K blackbody
liquid sulfuric acid
288 K blackbody
I (10^{14} Jy/sr)
0
1
2
3
4
5
500
1000
1500
2000
Frequency (cm^{-1})

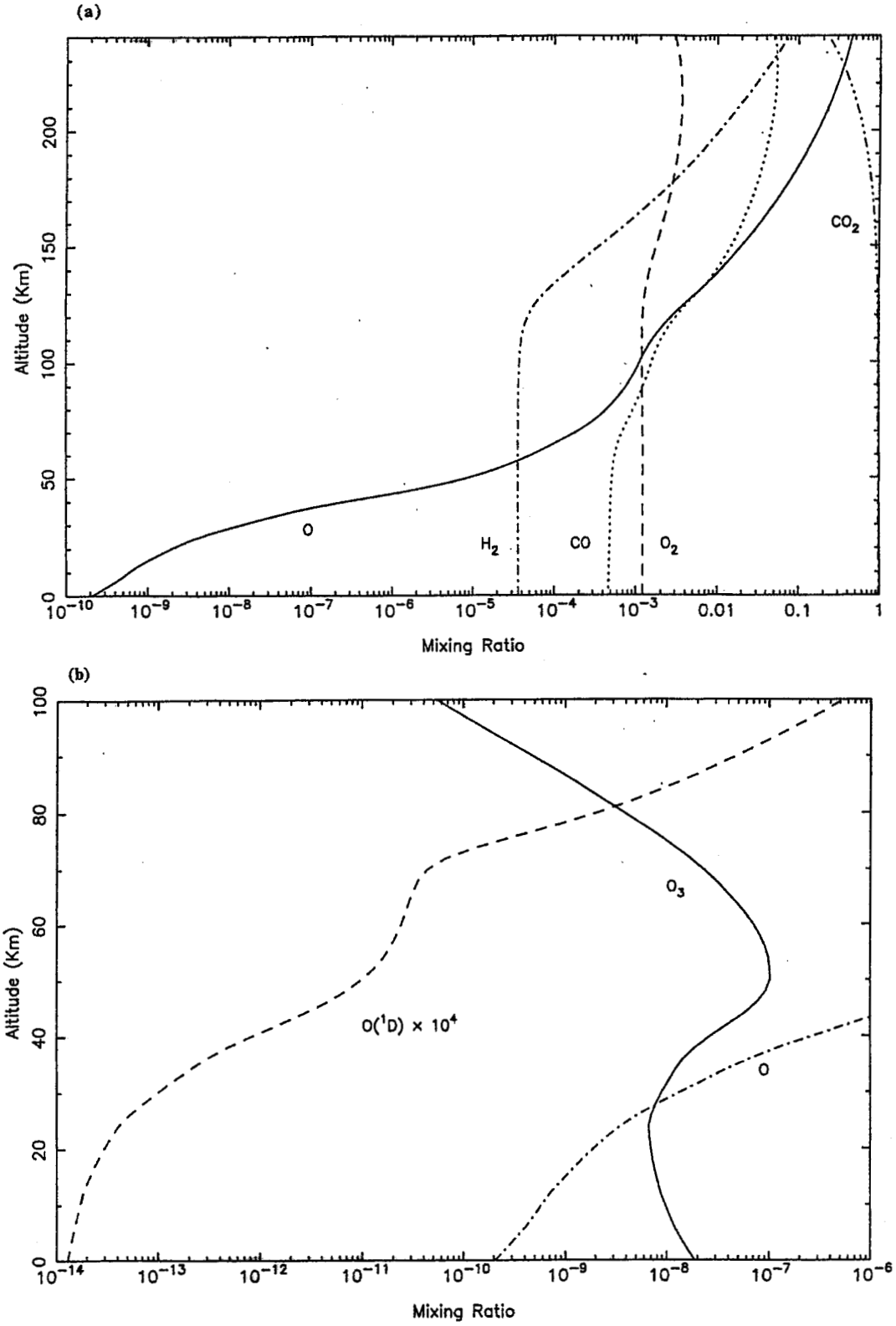

Figure 7.11 (a) Mixing ratios of CO_2, CO, O_2, H_2, and O. (b) Mixing ratios of O_3, O, and $O(^1D)$. From Nair, H., Allen, M., Anbar, A. D., Yung, Y. L., and Clancy, R. T., 1994, "A Photochemical Model of the Martian Atmosphere." *Icarus* **111**, 124.

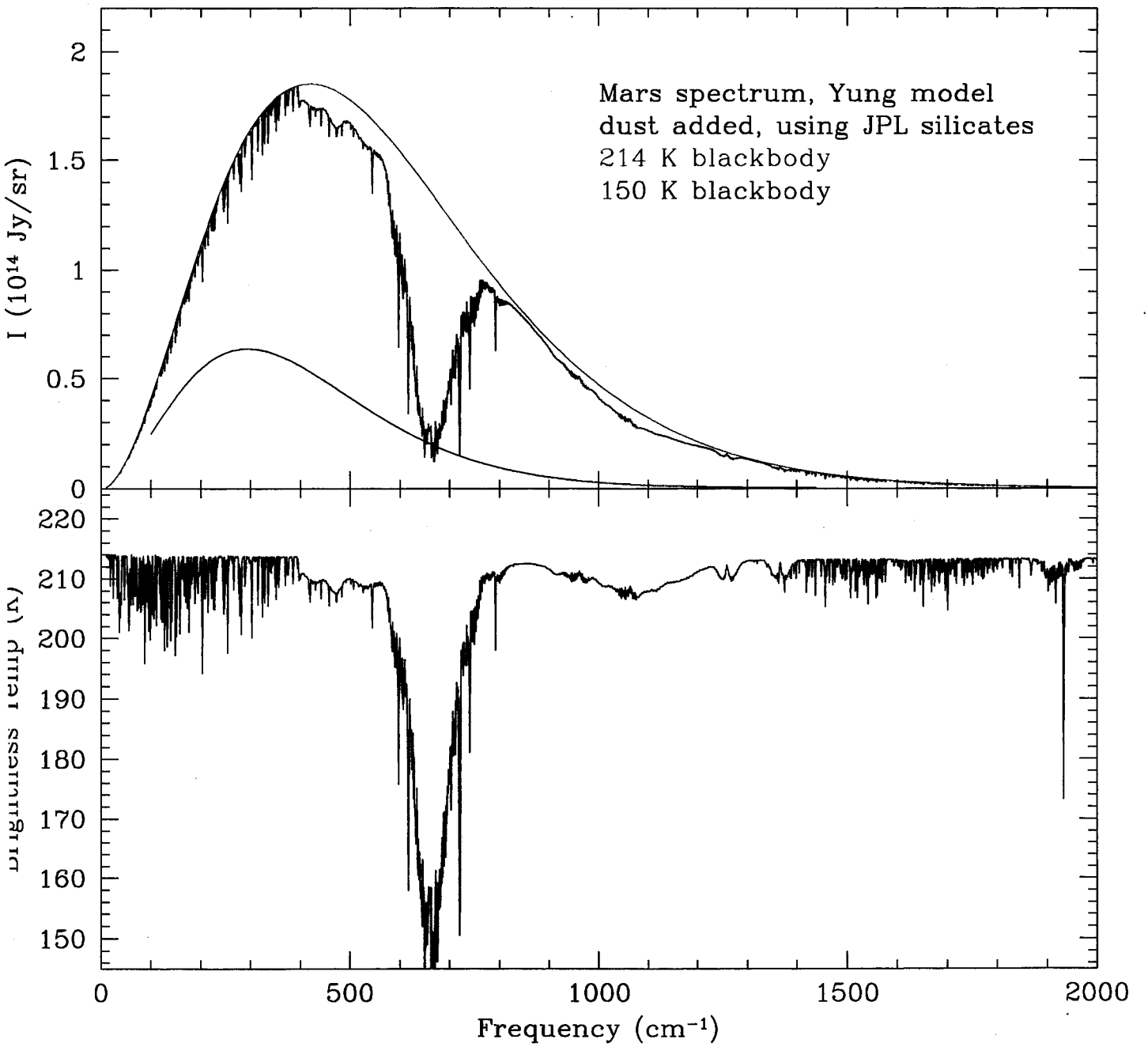
Mars spectrum, Yung model
dust added, using JPL silicates
214 K blackbody
150 K blackbody
I (10^{14} Jy/sr)
0
0.5
1
1.5
2
Brightness Temp (K)
150
160
170
180
190
200
210
220
0
500
1000
1500
2000
Frequency (cm^{-1})

Fig. 6.2.8 Martian emission spectra recorded by Mariner 9 early in the mission with large amounts of dust in the atmosphere (Hanel *et al.*, 1972*a*): (a) mid-latitude spectrum; (b) south polar spectrum.

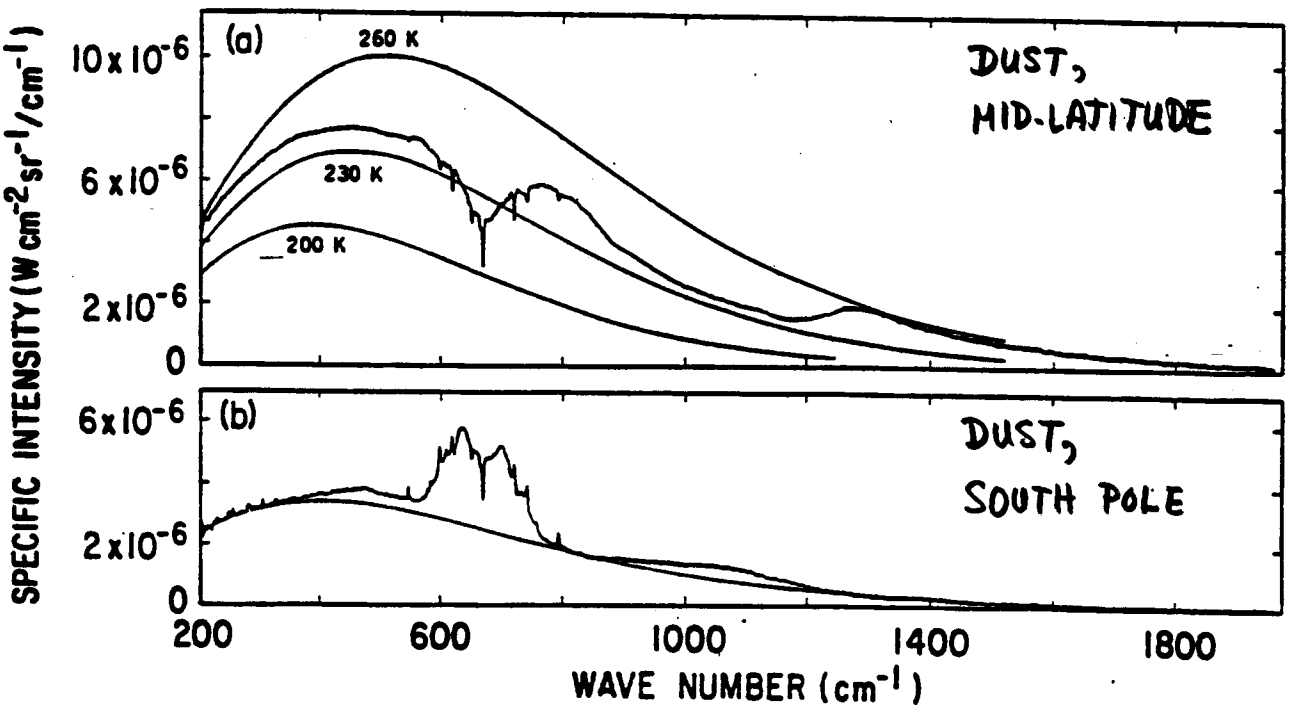

Fig. 6.2.11 Martian spectra over the Tharsis Ridge and over Arcadia. The Tharsis Ridge area contained water ice clouds. The lower spectrum was calculated with such clouds (Curran *et al.*, 1973).

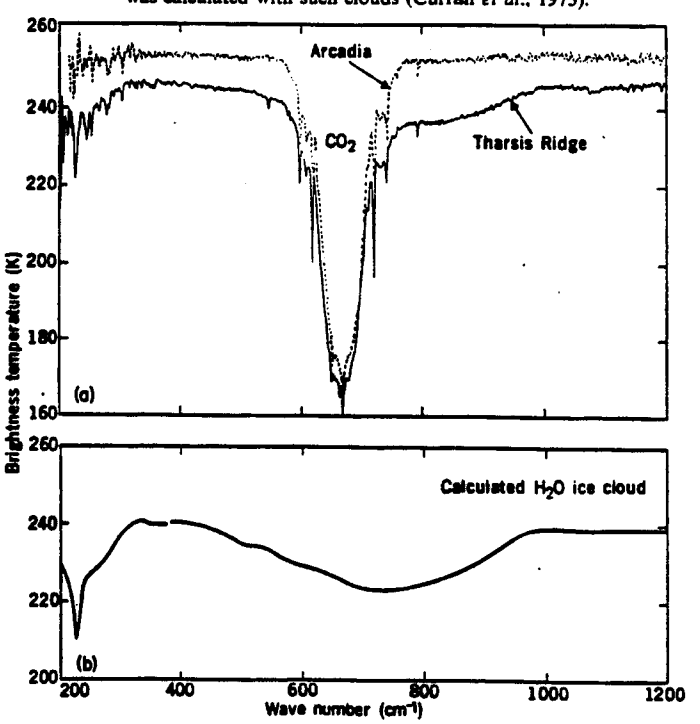

WATER ICE CLOUDS

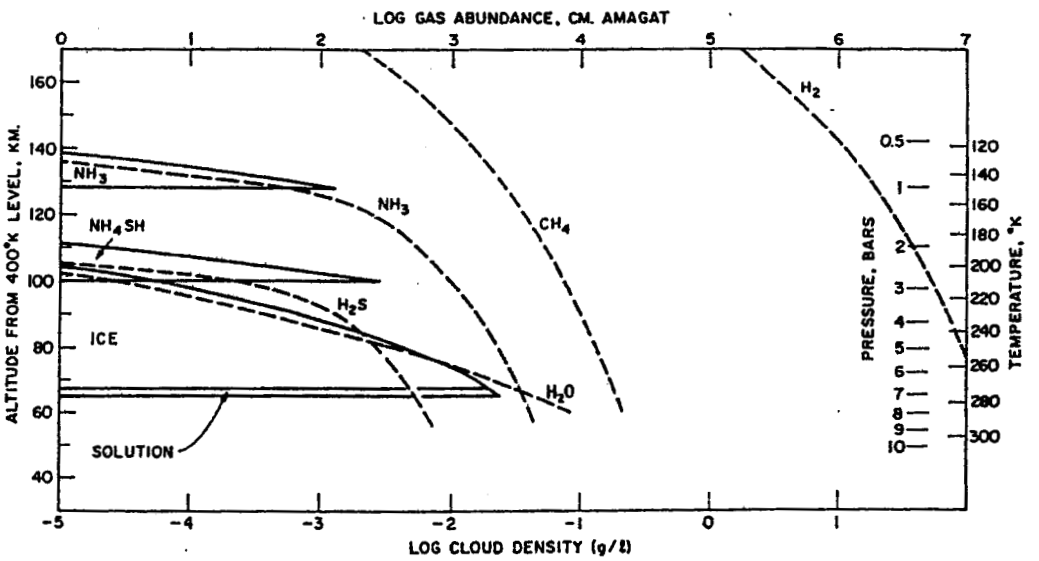

Figure 5.8 A model of the clouds of Jupiter based on cosmic abundances of the elements. The main cloud layers, composed of aqueous NH_3 solution plus H_2O ice, solid NH_4SH, and solid NH_3, are formed by condensation of H_2O, NH_3, and H_2S, which are stable in the lower atmosphere. After Weidenschilling, S. J., and Lewis, J. S., 1973, "Atmospheric and Cloud Structures of the Jovian Planets." *Icarus* **20**, 465.

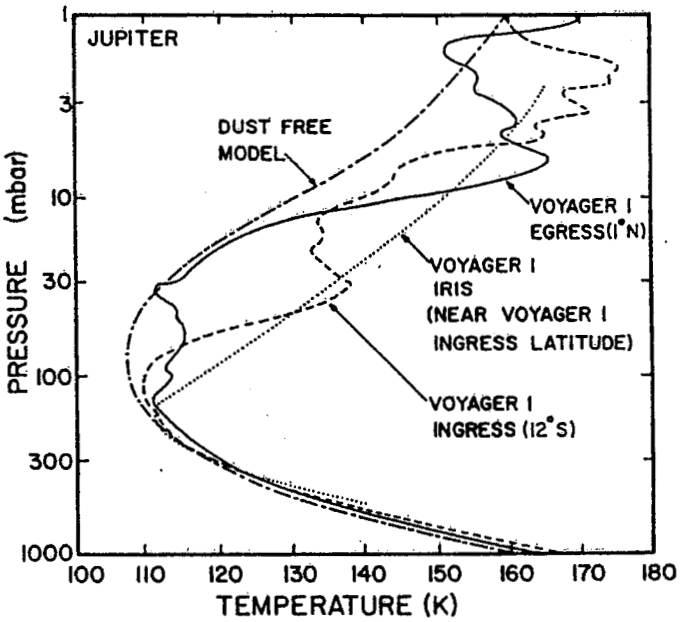

Figure 5.4 Radio science radio occultation measurements of the temperature profile in the troposphere and the middle atmosphere to 1 mbar. After Lindal, G. F. et al., 1981, "The Atmosphere of Jupiter: An Analysis of the Voyager Radio Occultation Measurements." *J. Geophys. Res.* **86**, 8721.

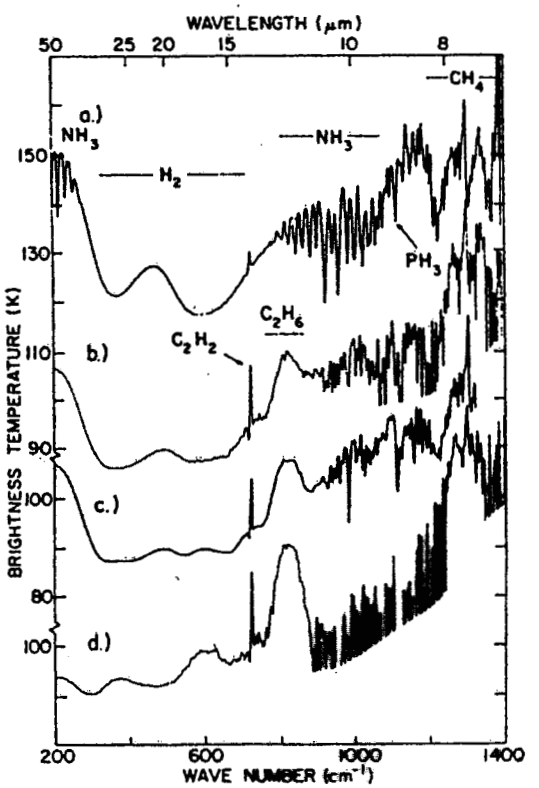

Figure 5.5 IRIS observations of the infrared spectra of Jupiter's atmosphere. After Hanel, R. et al., 1981, "Infrared Observations of the Saturnian System from Voyager 1." *Science* **212**, 192.

nulling interferometer
(Bracewell)

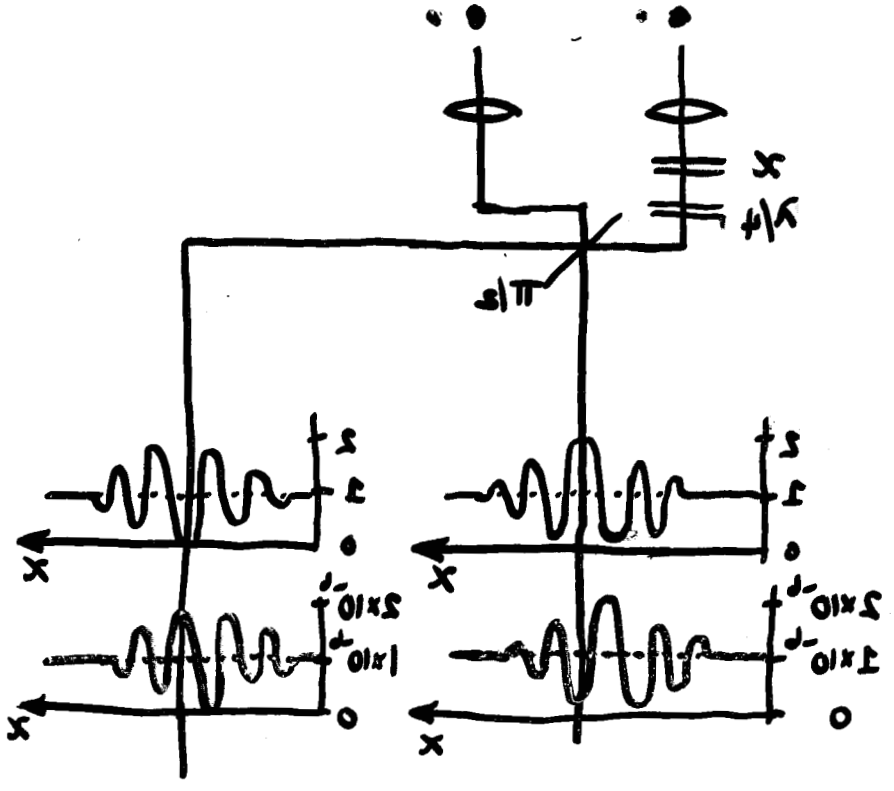

star:
at x=0, I=0.

planet:
at x=0, I≈Ip

---

stellar interferometer
(Michelson)

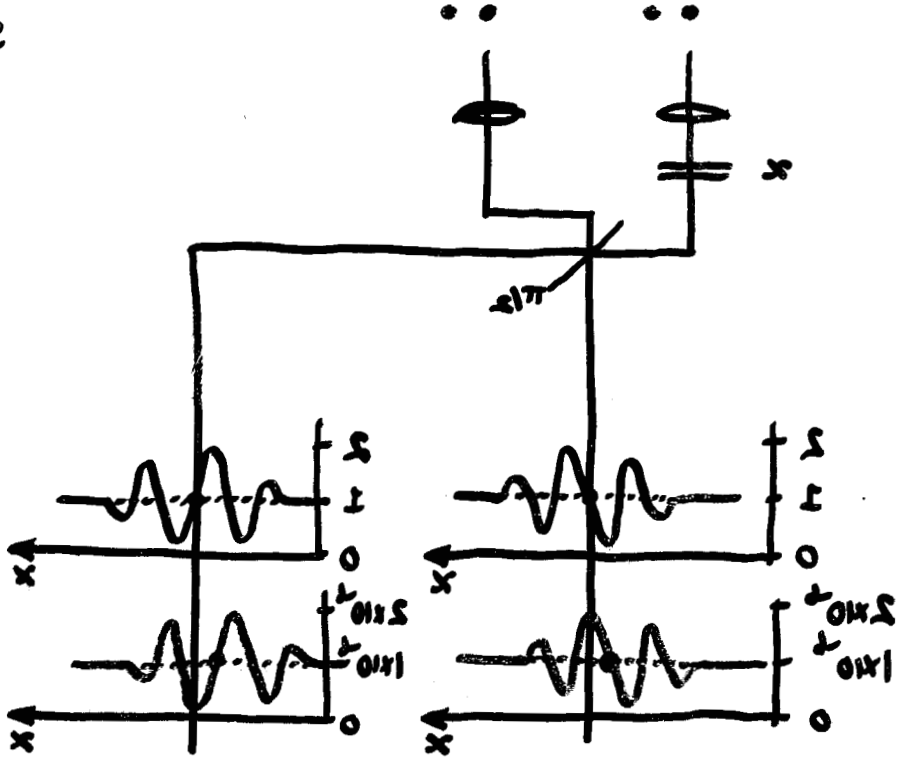

star:
at x=0, I=Is

planet
at x=0, I≈Ip

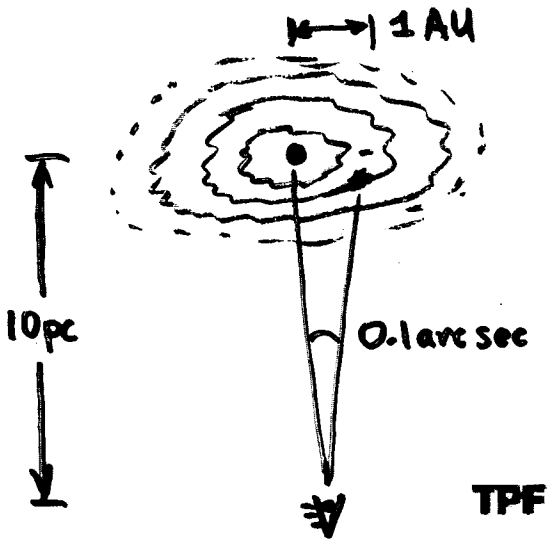

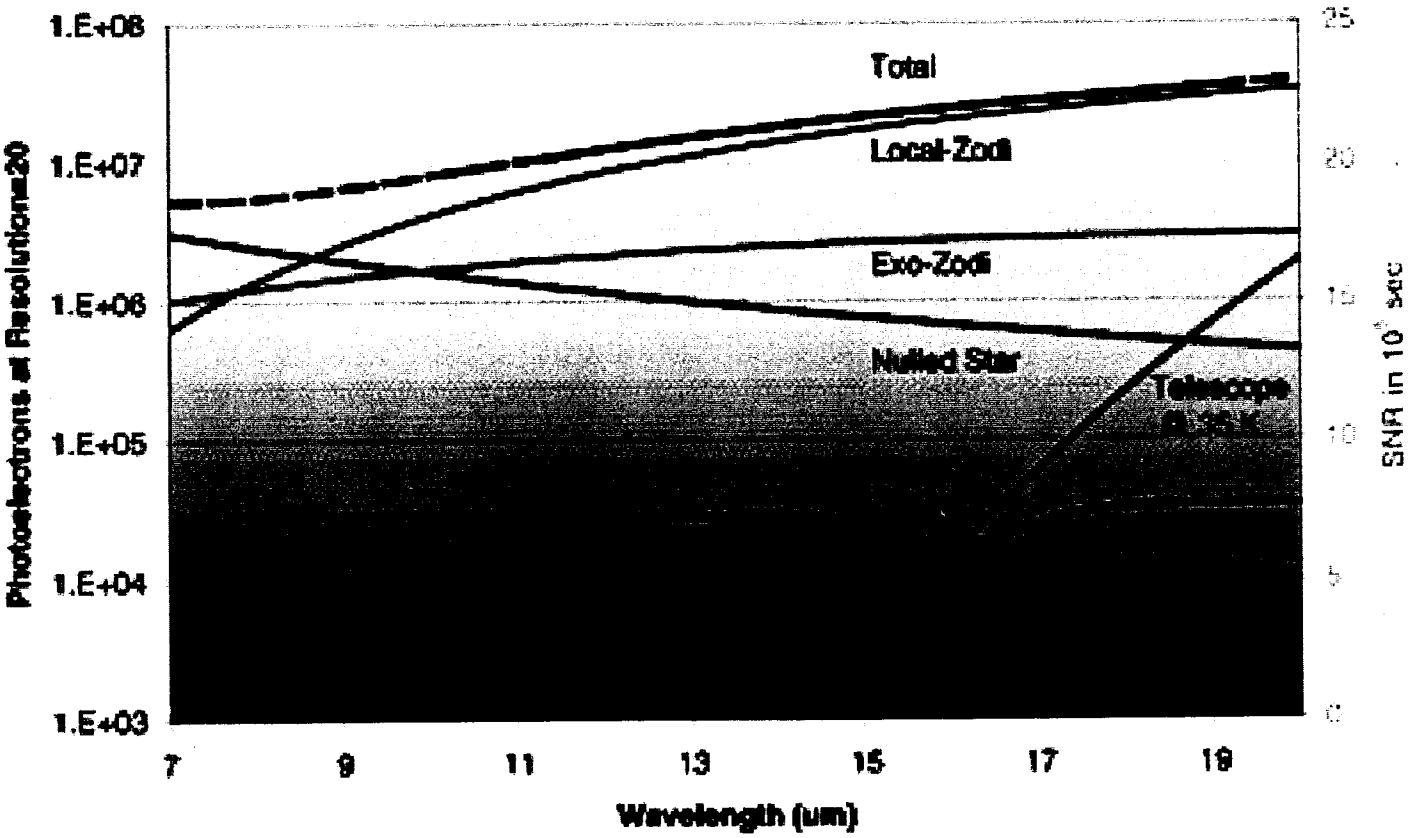

Spectral type	No. target stars (d < 15 pc, not binary)
A: very hot	8
F: hot	21
G: sun-like	58
K: cool	107
M: very cool	282
total	476

TPI

Terra Nova

The Origins Program :The Next Decade and Far Beyond

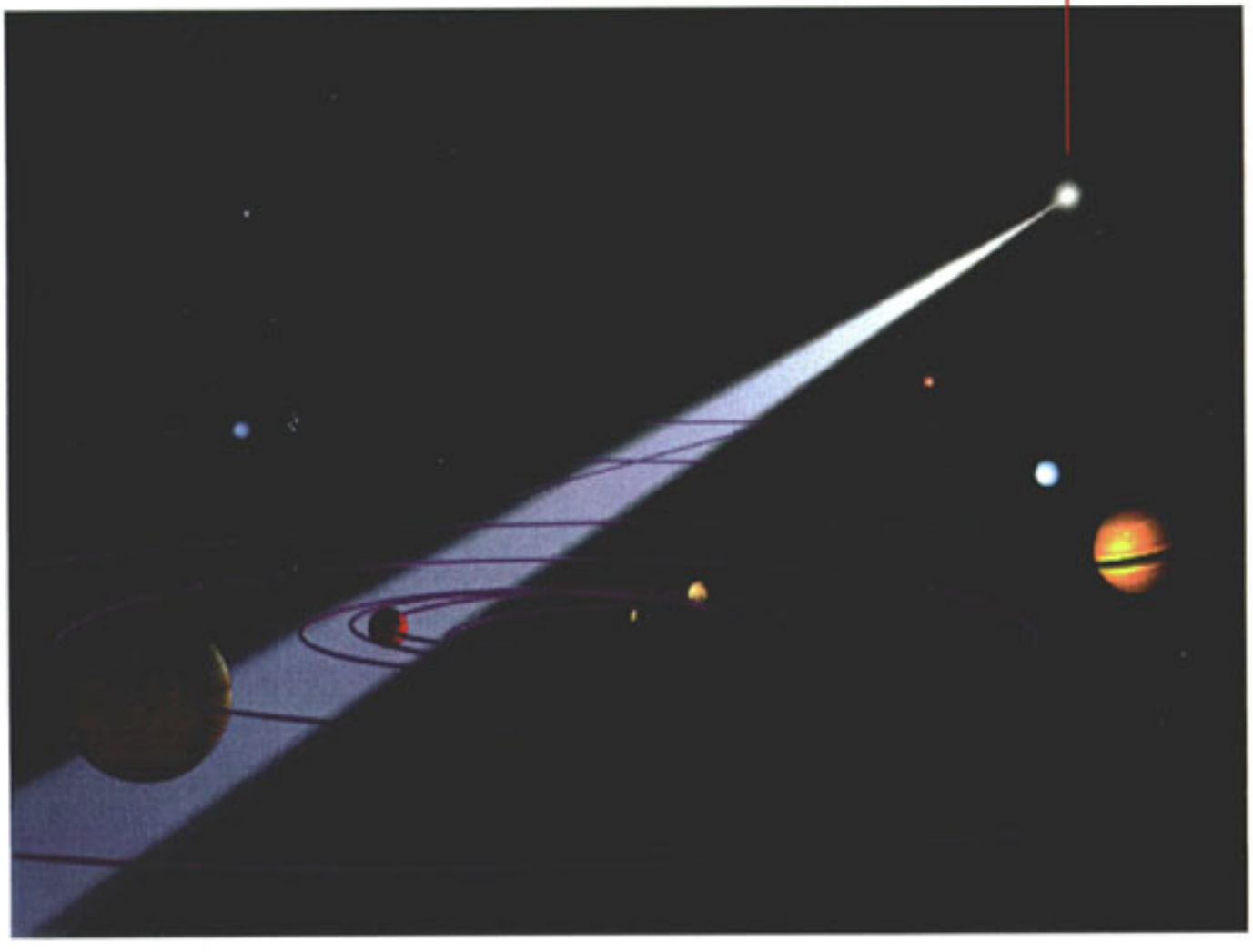

A Systems Strategy for Understanding Origins of Life and its Presence Outside the Solar System

A Presentation to the Administrator
September XX, 98

Fundamental requirements for visible light (0.6 μ) imaging

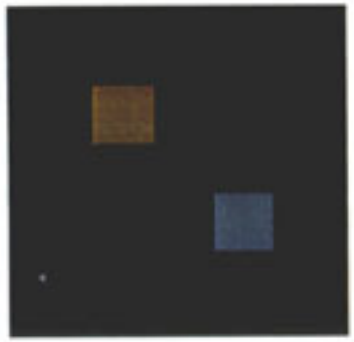

Separate planet from moon
Baseline: 1km

Collecting area:
4-6 10m-telescopes

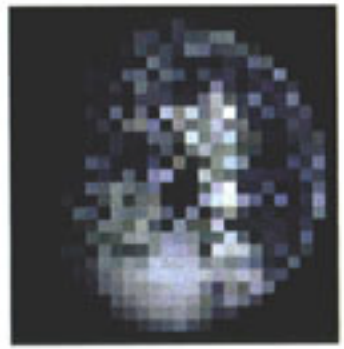

25 by 25 pixels

Baseline: 400km

Collecting area:
25 60m-telescopes

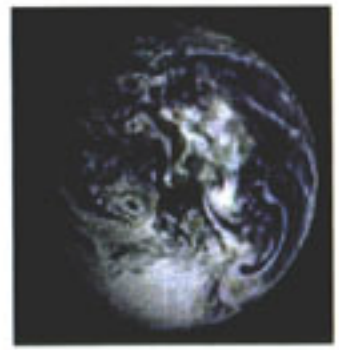

100 by 100 pixels

Baseline:

Collecting Area

Alternate Designs for Array Elements

- thin Fresnel lens with occulter
- large single mirror with coronograph

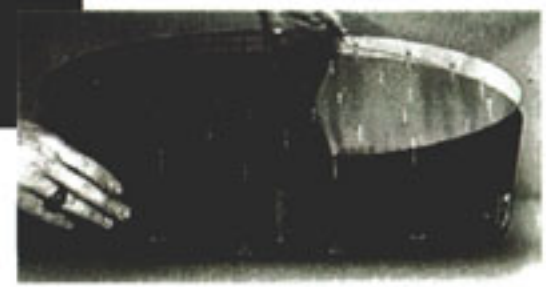

Fundamental Requirements for IR (10 μ) Imaging

Separate planet
from moon
Baseline: 17 km

Collecting area:
4-6 10m-telescopes

25 by 25 pixels

Baseline: 6600 km

Collecting area:
25 60m-telescopes

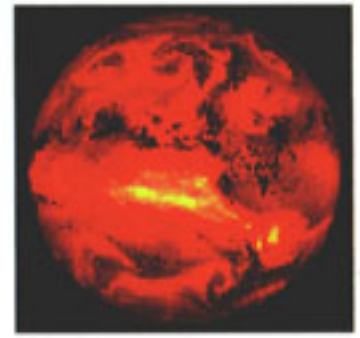

100 by 100 pixels

Baseline:

Collecting area:

Possible Design for a 25 by 25 pixel imager

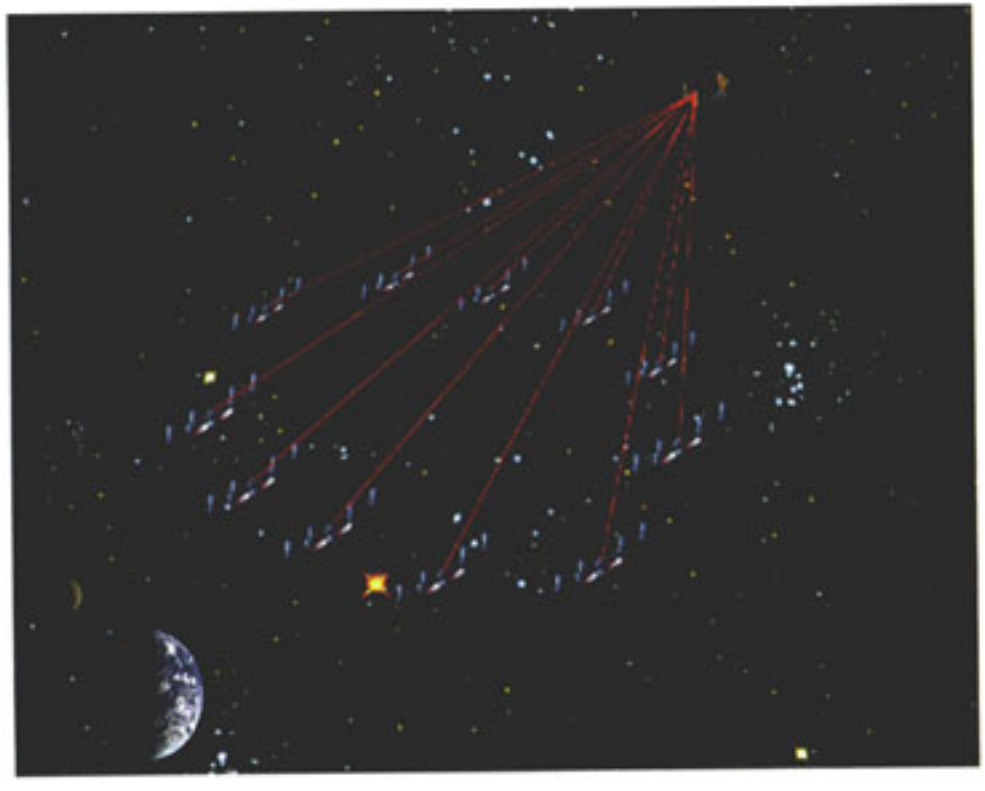

- array of ~25 elements collectors each ~3000 m^2
- baseline ~6000 km
- starlight nulled at each collector
- array configuration independent from design of individual element

Example of possible array element:
Nulling interferometer

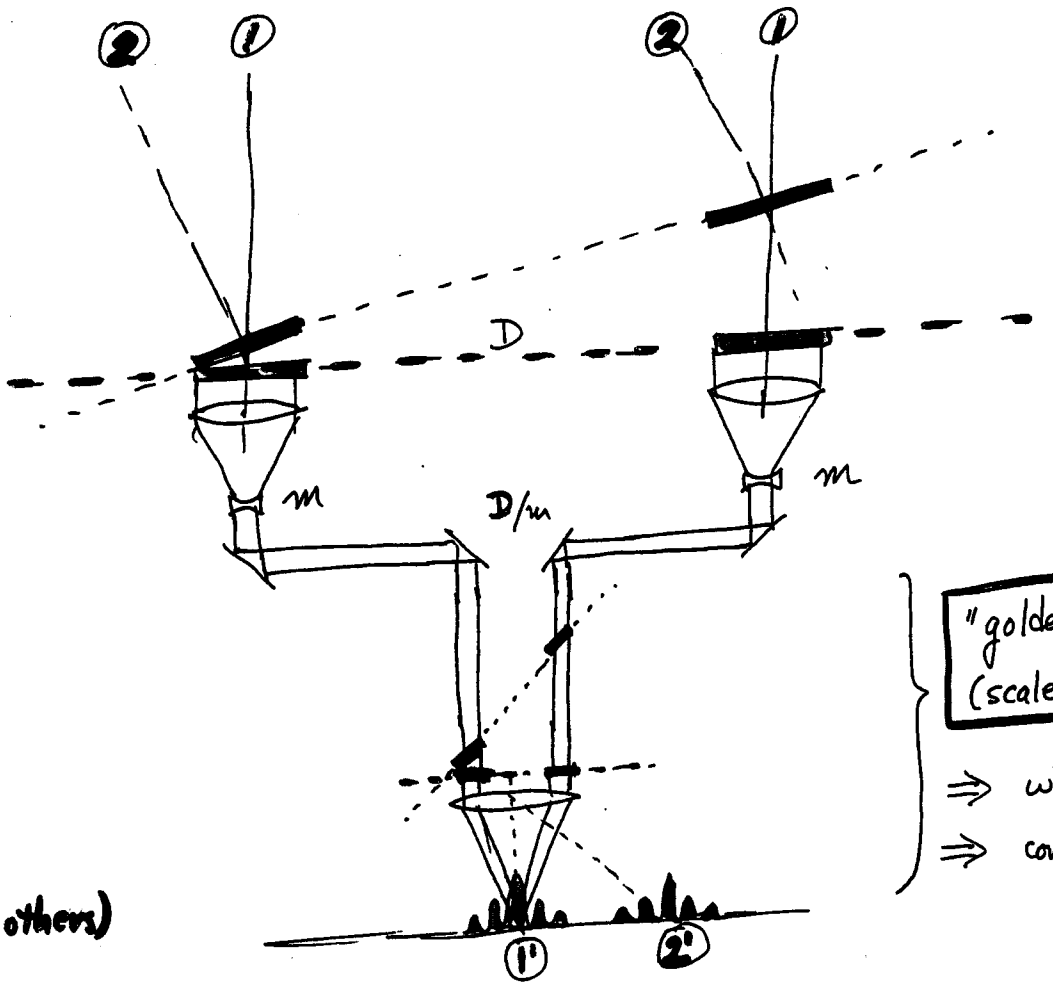

"golden rule"
(scaled pupil)

⇒ wide field.

⇒ complex diffraction pattern.

(Traub, others)

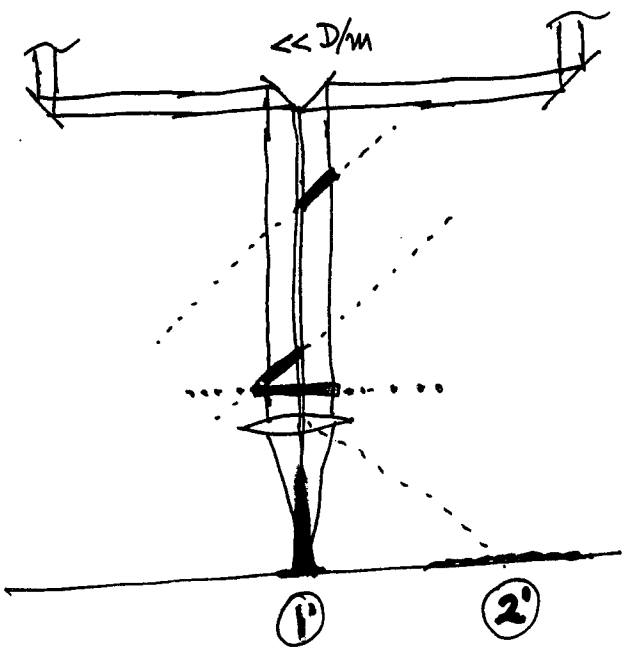

"hyper telescope"
(densified pupil)

⇒ narrow field.

⇒ compact diffraction pattern.

(Labeyrie, Pedretti)

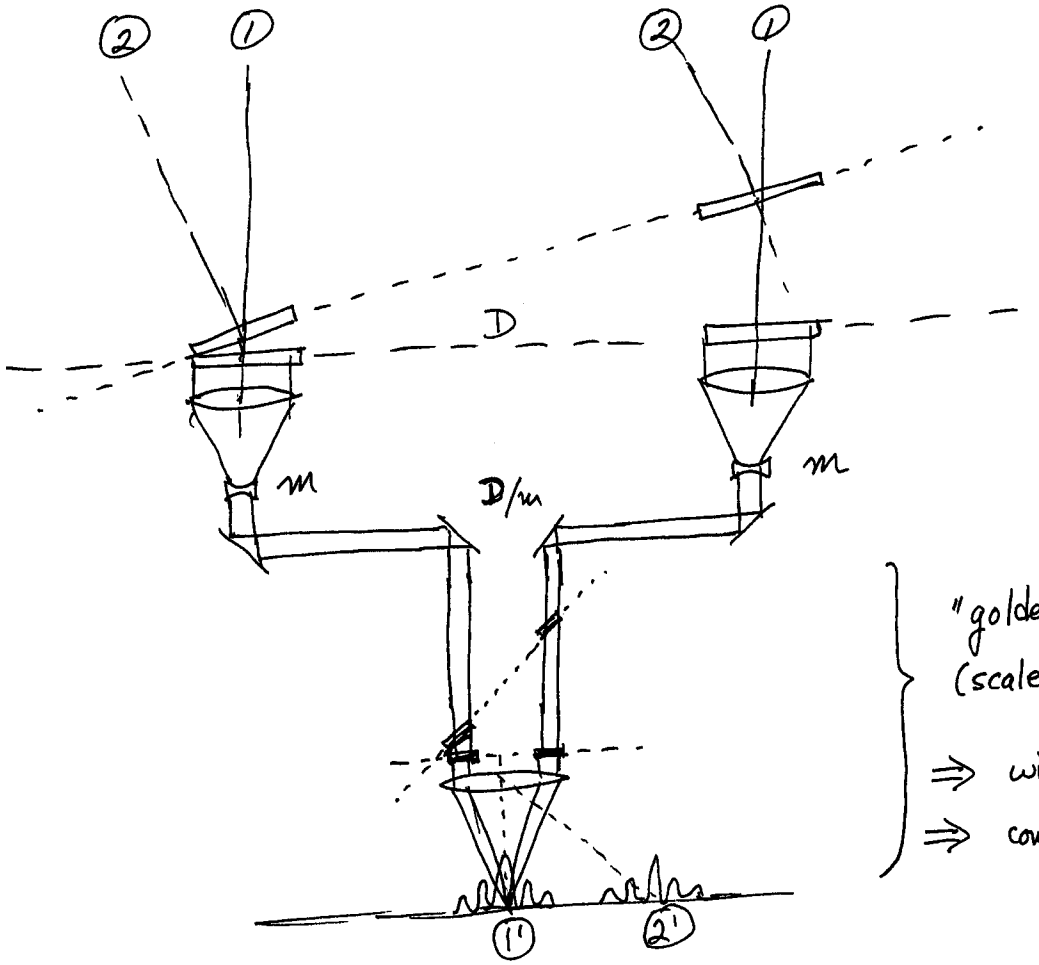

"golden rule"
(scaled pupil)

⇒ wide field.

⇒ complex diffraction pattern.

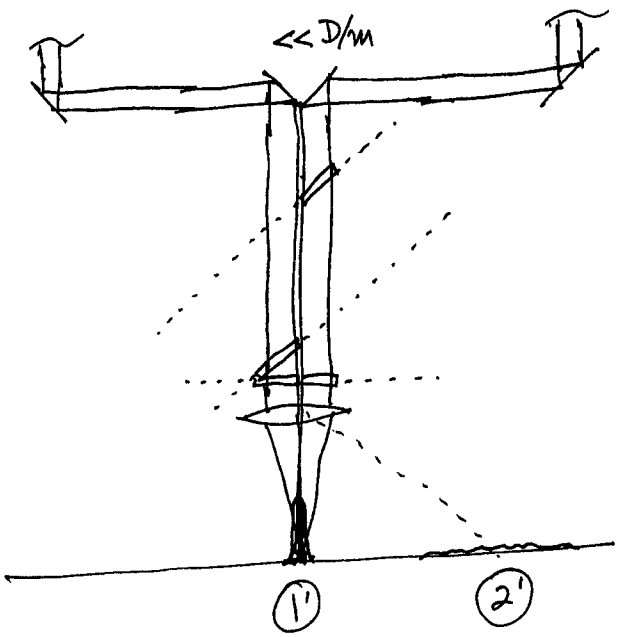

"hyper telescope"
(densified pupil)

⇒ narrow field.

⇒ compact diffraction pattern.

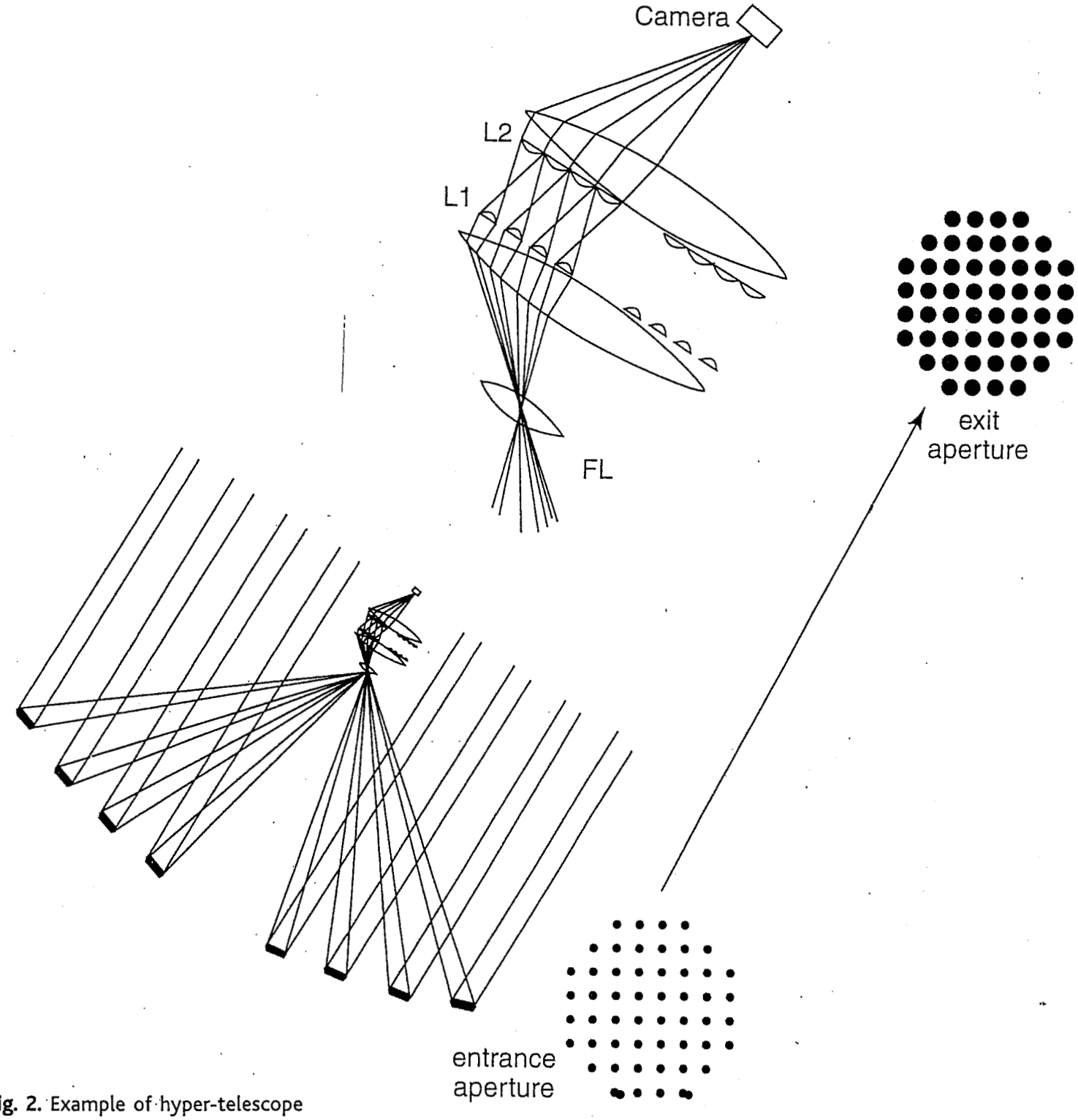

Fig. 2. Example of hyper-telescope optics. Multiple mirrors form a sparse paraboloidal giant mirror, and a lens (FL) in the focal plane forms a pupil image on a pair of lens arrays L1 and L2, having short and long focal lengths, respectively. This setup enlarges the subpupils in the exit aperture compared to those in the entrance aperture, producing a usable image on the camera.

A. Labeyrie, Science, 1999 or 2000

Effect of pupil deformation

Computer simulation (Auillans 1999). The interferometric field of view is reduced whith increased pupil positioning errors.

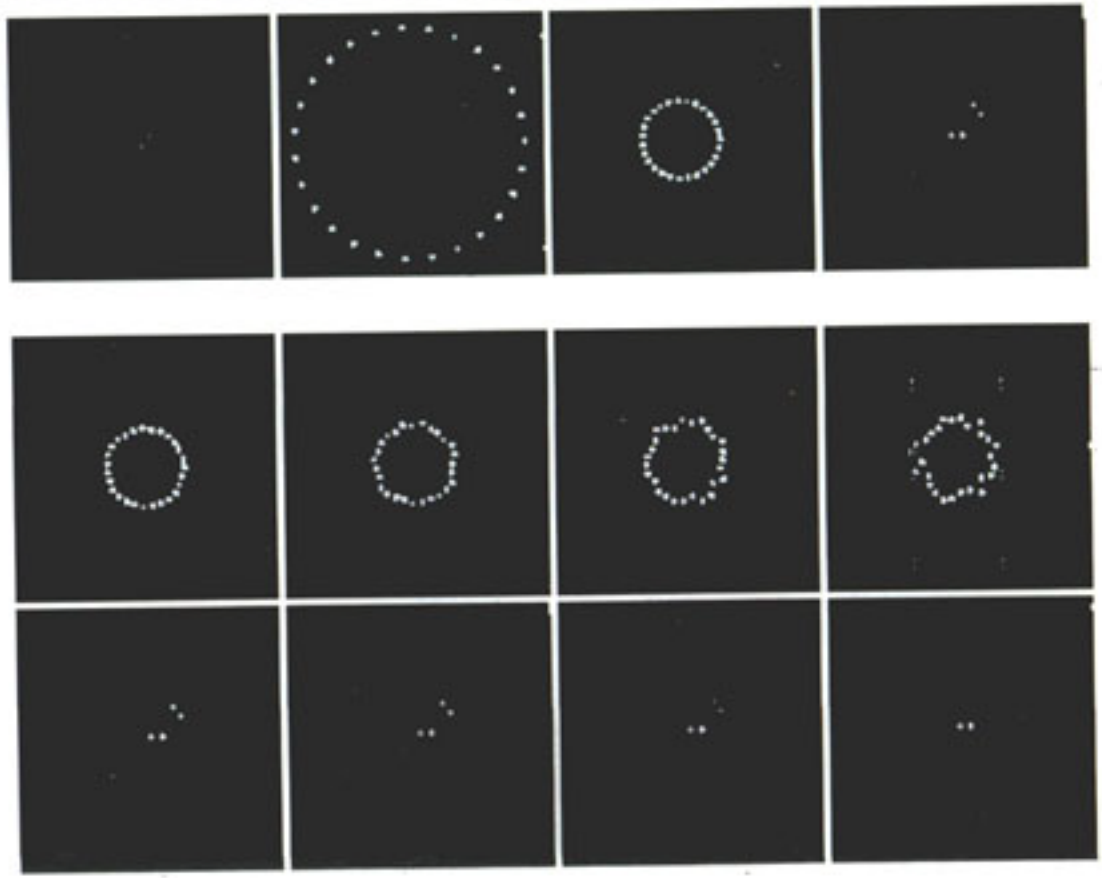

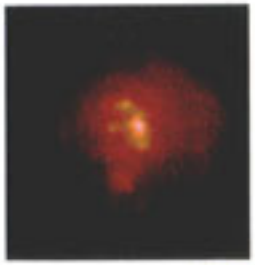

Sky results

Image of double star Castor, Mv=1. Separation = 3.97"

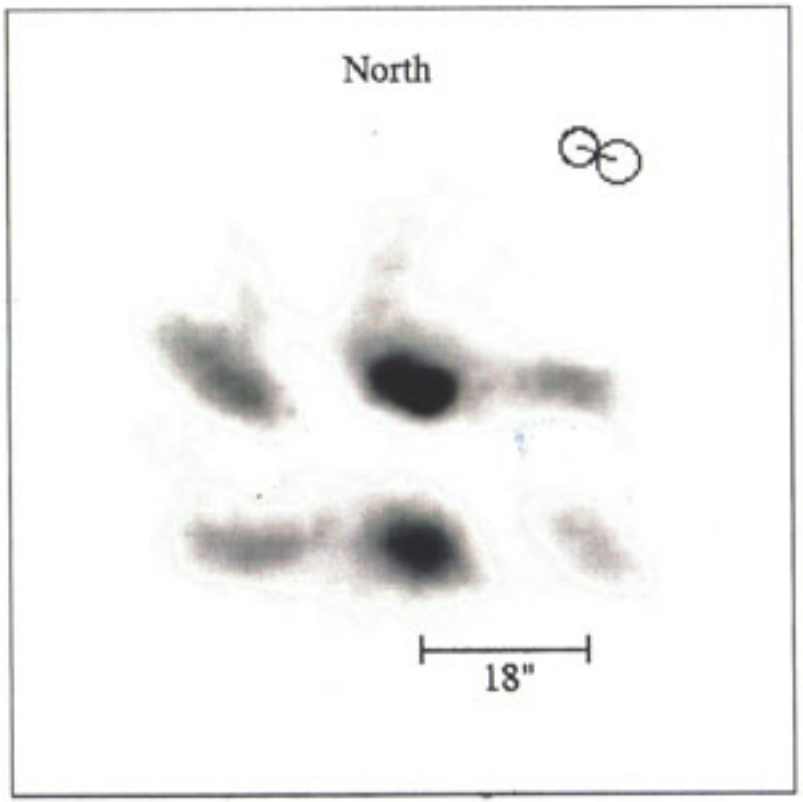

E. Pedretti, 2000